UNIVERSIDAD DE GRANADA

CSIC
CONSEJO SUPERIOR DE INVESTIGACIONES CIENTÍFICAS

UNIVERSIDAD DE GRANADA
PROGRAMA DE DOCTORADO EN BIOMEDICINA

INSTITUTO DE PARASITOLOGÍA Y BIOMEDICINA "LÓPEZ-NEYRA"
CONSEJO SUPERIOR DE INVESTIGACIONES CIENTÍFICAS

DOCTORAL THESIS

Centrosomal defects caused by the Parkinson's disease associated protein kinase LRRK2 and Rab proteins

Jesús Madero Pérez
July 2018

Editor: Universidad de Granada. Tesis Doctorales
Autor: Jesús Madero Pérez
ISBN: 978-84-1306-790-2
URI: http://hdl.handle.net/10481/67459

Acknowledgements/Agradecimientos

Quiero dar las gracias a todas las personas que me han acompañado durante estos casi seis años de investigación doctoral, porque habéis hecho fácil un camino sin recompensas inmediatas ni a medio plazo.

Gracias Sabine, por haberme introducido en el mundo de la ciencia. Gracias por haber entendido y respetado las diferentes etapas que he vivido durante este doctorado. Gracias por haberme devuelto la ilusión y la confianza cada vez que las cosas no salían bien, ¡que fueron unas cuántas! Gracias por haber sacado lo mejor de mí. ¡Gracias por haberme enseñado tantas cualidades como jefa de grupo que espero poder implementar si es que alguna vez llego a tener mi propio lab!

Gracias a todo el lab114 y asociados, ¡por hacer que haya disfrutado de todos los días de trabajo! Gracias Marian por haber estado conmigo todo este largo trayecto, por compartir cafés, música y charlas acerca de todo lo que se puede debatir en esta vida…por compartir los buenos y los malos momentos, por salvar el mundo continuamente, por enseñarme lo que es "*cool"* para no estar "*out"*. Gracias Belén, pequeña Shakira, ¡por poner risas y cordura en este laboratorio! Gracias por estar siempre ahí, como ayuda constante. Gracias Antonio, por acompañarme como componente masculino en este laboratorio. Gracias Mariascen, por ser el mejor fichaje externo del 114. ¡Gracias a los dos por estar siempre con una magnifica sonrisa, dispuestos a ayudar y preparados para hacerme reír con cualquier tontería! Gracias Pilar, por tantos momentos juntos hasta tarde en el laboratorio, y por haber compartido conmigo tantos cotilleos. Gracias Ele, porque me enseñaste al principio en el laboratorio y ¡por haber trabajado para conseguir nuestro artículo! Gracias María, ¡por traer buena música, refranes viejunos y buenas conversaciones al lab! Gracias a todos los antiguos miembros del lab que han estado conmigo en este

periodo, especialmente a Patri y a Mar, ¡por enseñarme tanto de ciencia y por todas las risas!

Gracias a todo el “López-Neyra” por compartir todos esos ratos en la cafetería/cultivos/conserjería/etc… porque me han dado el componente humano/social/afectivo que se necesita para no volverse loco en ciencia.

Gracias Paqui, por todas esas comidas caseras que me permitían no tener que cocinar en casa tras largas horas de trabajo ¡Por esas croquetas de espinacas, el arroz a la campesina y el pisto con huevos!

Gracias a *Sci-Hub* y a su fundadora Alexandra Elbakyan, por permitirme trabajar desde casa accediendo a todos los artículos del mundo.

Gracias a todos mis amigos, por darme tantos buenos momentos y risas. Gracias por ser una parte tan importante de mi vida. Gracias porque hacéis que los problemas del laboratorio desaparezcan al instante cuando nos vemos.

¡Gracias familia! ¡Gracias papá, gracias mamá, gracias Lucía, gracias Carlos, gracias Auri, gracias Luciita! Por quererme y apoyarme siempre. Gracias, porque el modo en el que creéis en mí hace que me supere cada día. ¡Gracias porque me hacéis sentir que puedo con todo! Gracias por ser un ejemplo constante de felicidad y amor. Gracias por ser lo más importante de mi vida y saber que siempre os tendré a mi lado.

Gracias Auri, por alegrarme cada día a la vuelta del laboratorio. Gracias, por apoyarme siempre. ¡Gracias por hacerme sentir genial y especial! Gracias por acompañarme en esta nueva etapa que comenzamos. Gracias por ser mi familia.

Gracias a mis abuelos, por haberme dado tanto a mí y a nuestra familia. A vosotros, y a toda mi familia, os quiero dedicar este trabajo, porque sois mi motivación y mi fuerza para seguir trabajando en este mundo.

¡Gracias con todo mi corazón!

Contents

Abstract / Resumen

Mutations in the *leucine rich repeat kinase 2* (*LRRK2*) gene are the most common cause of familial Parkinson's disease (PD), with autosomal-dominant inheritance, and variants in this gene also confer risk to develop sporadic PD. Whilst the cellular and molecular mechanisms underlying LRRK2-PD remain largely unknown, recent studies have identified a subset of Rab GTPases as physiological LRRK2 kinase substrates.

In the present study, we identify centrosomal alterations caused by pathogenic LRRK2 using different cell lines and confirmed in patient-derived samples. In non-dividing cells, pathogenic LRRK2 causes deficits in centrosome positioning with downstream consequences for cell differentiation, polarity and directional migration. In dividing cells, pathogenic LRRK2 causes centrosomal cohesion defects. Importantly, we demonstrate that these defects are dependent on the LRRK2 kinase activity.

We confirm that Rab8a, a small Rab GTPase with described roles in centrosome-related events, is a LRRK2 kinase substrate, and corroborate that pathogenic LRRK2 increases Rab8a phosphorylation. For the first time, we identify the cellular localization and consequences of LRRK2-mediated Rab8a phosphorylation. We demonstrate that pathogenic LRRK2 causes an abnormal accumulation of phosphorylated Rab8a around the centrosome, which is, at least partially, responsible for the centrosomal cohesion defects.

We also evaluate the effects of *Rab7L1*, a gene that modifies risk for sporadic PD, on the centrosome phenotype. Remarkably, we observe that when increasing Rab7L1 levels, wildtype LRRK2 mimicks the effects of pathogenic LRRK2 on Rab8a phosphorylation and centrosomal cohesion deficits, suggesting that both phenotypes may be a common readout for a broader spectrum of PD.

Whilst the downstream consequences of the centrosomal defects and its relevance for PD remain to be elucidated, the data presented here identify a new role for LRRK2 in the context of centrosomal functioning, and indicate the important role of Rab proteins for understanding PD pathogenesis.

Las mutaciones en el gen *leucine rich repeat kinase 2* (*LRRK2*) son la causa más común de la enfermedad de Parkinson (EP) hereditaria, presentando una herencia autosómica dominante. Además, otras variantes en LRRK2 se han visto asociadas a un mayor riesgo de sufrir EP esporádica, sugiriendo que LRRK2 desempeña un papel importante y general en la EP. Aunque todavía desconocemos los mecanismos celulares y moleculares que subyacen a la EP, recientemente se han descubierto un subgrupo de proteínas de la familia de las Rab GTPasas como sustratos fisiológicos de la actividad quinasa de LRRK2.

En este trabajo, hemos identificado que LRRK2 patogénico causa alteraciones en el centrosoma, usando diferentes líneas celulares y comprobadas en muestras derivadas de pacientes. Por una parte, en células que no se dividen, LRRK2 patogénico causa alteraciones en el posicionamiento del centrosoma, con consecuencias en la capacidad de las células para diferenciarse, polarizarse y migrar. Por otra parte, en células en división, LRRK2 patogénico provoca defectos de cohesión en el centrosoma. De manera significativa, hemos demostrado que dichas alteraciones centrosomales son dependientes de la actividad quinasa de LRRK2.

Conjuntamente, hemos confirmado que Rab8a, una pequeña Rab GTPasa con funciones relacionadas a algunos procesos del centrosoma, es un sustrato de LRRK2, y además hemos comprobado que LRRK2 mutante aumenta dicha fosforilación. Por primera vez, hemos identificado la localización y las consecuencias de la fosforilación de Rab8a. En concreto, LRRK2 patogénico provoca una acumulación de Rab8a fosforilado alrededor del centrosoma, lo que es, al menos en parte, responsable de las alteraciones centrosomales descritas.

Además, hemos evaluado el papel de *Rab7L1*, un gen que modifica el riesgo de desarrollar EP, en los problemas centrosomales. Notablemente, observamos que al aumentar los niveles de Rab7L1, la proteína LRRK2 silvestre se comporta como las versiones patogénicas de LRRK2, causando un aumento en la

fosforilación de Rab8a y alteraciones en el centrosoma, lo que sugiere que ambos fenotipos pueden ser habituales en un espectro más amplio de la EP.

Aunque las consecuencias y la relevancia para la EP de las alteraciones en el centrosoma tienen que ser estudiadas en detalle, este trabajo describe nuevas funciones de la proteína LRRK2 en relación con el centrosoma, y demuestran la importancia de las proteínas Rab en el estudio y comprensión de la EP.

Abbreviations

γ-TuRCs: γ-tubulin ring complexes

BAC: bacterial artificial chromosome

BBB: blood-brain barrier

COR-domain: C-terminal of ROC

DA: Dopamine

DBS: Deep-Brain Stimulation

HEK293: Human embryonic kidney 293 cells

In-1: Inhibitor-1 LRRK2 inhibitor

iPSC: induced pluripotent stem cells

GAK: Cyclin-G–associated kinase

GAPs: GTPase-activating proteins

GBA: β-Glucocerebrosidase

GEFs: Guanine nucleotide exchange factor proteins

GDI1/2: GDP dissociation inhibitor 1/2

GGTII: geranylgeranyl transferase type II

GSK: GSK2578215A LRRK2 inhibitor

GWAS: Genome Wide Association Studies

KI: Knock-in

KO: Knockout

LRRK2: *leucine-rich repeat kinase 2*

L-DOPA: L-3,4-dioxyphenylalanine or Levodopa

LB: Lewy body/bodies

MAPT: *microtubule associated protein tau*

MEFs: murine embryonic fibrosblasts

MP6R: mannose 6-phosphate receptor

MTs: Microtubules

MTOC: Microtubule-Organizing Center

NHP: non-human primates

PCM: Pericentriolar material

PINK1: PTEN-induced putative kinase 1

PD: Parkinson's disease

RE: Recycling endosomes

REP: Rab escort proteins

ROC domain: Ras of complex domain

RILPL1/2: Rab interacting lysosomal protein like 1/2

SNpc: *substantia nigra pars compacta*

SNCA: α-synuclein

SNPs: Single nucleotide polymorphisms

TGN: Trans-Golgi Network

VPS35: *Vacuolar protein sorting-associated 35*

List of figures

I. INTRODUCTION

1. PARKINSON'S DISEASE

At the beginning of the 19th century, an English doctor called James Parkinson thoroughly described for the first time the symptoms and progression of a disease known as "*paralysis agitans*". Although different sources along history partially described some clinical symptoms of the disease, James Parkinson´s work "An essay on the shaking palsy" was seminal to give it a disease entity [1]. Two hundred years later, and after being renamed as Parkinson's disease (PD) in honor of its discoverer, important progress has been achieved to understand the disease.

Being the second most prominent neurodegenerative disease, PD affects 0.3 % of the total population of industrialized countries, increasing to 1 % of the population older than 60, and up to 4 % older than 80 [2]. Due to the severity of the disease and the inability of the patients to live a normal life at advanced disease stages, patients' relatives tend to take care of them, making the global number of people directly or indirectly affected to be counted by millions. Patients' health care costs represent an economic burden for families and government economies. As life expectancy increases in developed countries, PD will soon become a major problem for society. Because of the impact of the many different aspects on social welfare, finding a cure for the disease is, or should be, a top priority for occidental countries.

1.1 Clinical manifestations

PD is clinically characterized by motor and non-motor symptoms. The motor symptoms, considered the cardinal and most characteristic signs of the disease, include tremor at rest, bradykinesia (slow movement), rigidity and postural instability. At later stages of the disease, flexed posture, freezing of gait and falls are common features that complicate patients' lives. PD is also associated with various non-motor symptoms which are frequently underestimated, that appear at early and late stages of the disease. These include cognitive and neurobehavioral

abnormalities (including dementia, depression, apathy and anxiety in more than 50 % of the patients), autonomic failure (urinary incontinence, sweating and orthostatic problems), sleep disorders and sensory abnormalities (mostly pain and lack of smell) [3].

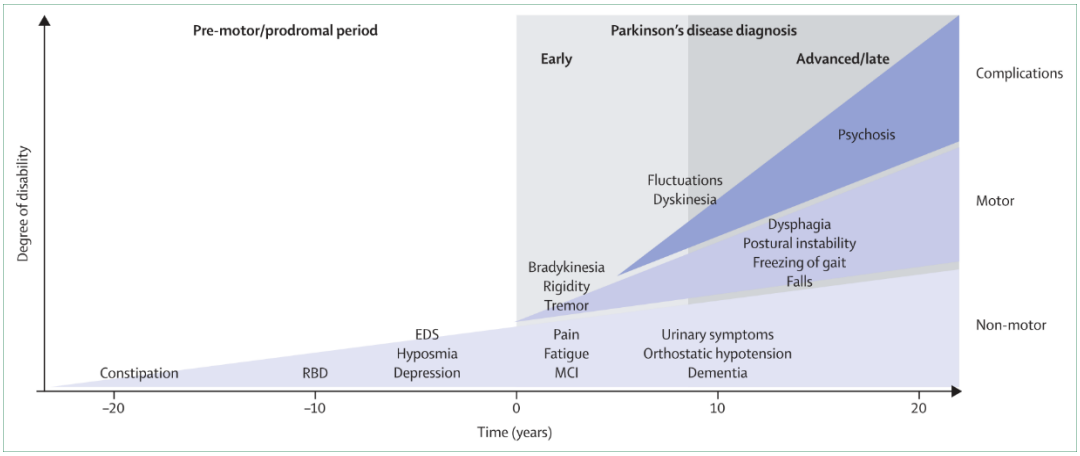

Fig. 1. Clinical manifestations over the course of the disease. From [4]

1.2 Pathology

Pathological examinations of post-mortem PD patient brains show two hallmarks of the disease. On the one hand, patients show a loss of dopaminergic neurons in the *substantia nigra pars compacta* (SNpc). Most of the motor complications associated with PD come from a reduced dopaminergic transmission from the SNpc to the striatum due to the death of dopaminergic neurons, resulting in an increased inhibition of the thalamo-cortical projections, and subsequent repression of the initiation and fine control of movements [5].

The second pathological hallmark of the disease is the appearance, in surviving neurons, of dense intraneural deposits originally described in 1912 by Friedrich Lewy [6]. Lewy bodies (LB) are mainly composed of aggregated and non-soluble α-synuclein, but other proteins including ubiquitin and sometimes even tau [7, 8] can also be found in these inclusions [4, 5]. When localized in neural processes with filamentous morphology they are called Lewy neurites.

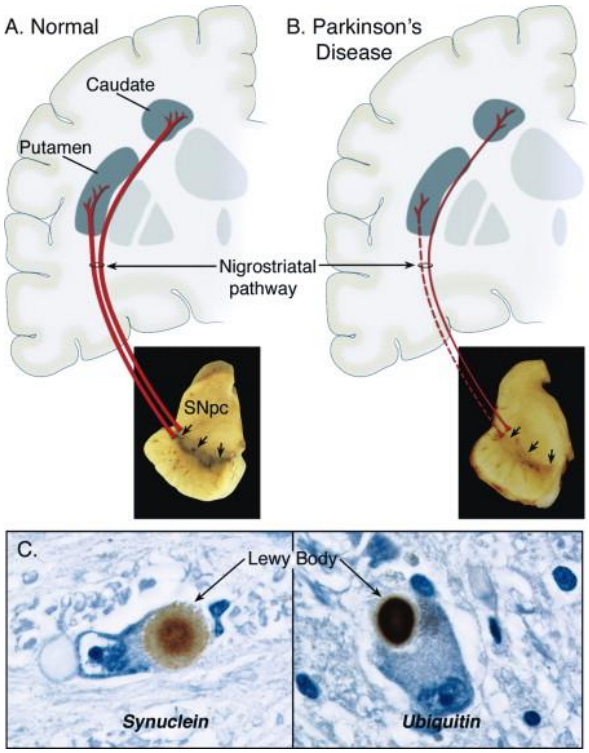

Fig. 2. Pathological hallmarks of Parkinson's disease. a) Nigrostriatal pathway under normal conditions. **b)** Nigrostriatal pathway affected by the loss of dopaminergic neurons in the Substantia nigra pars compacta (SNpc) in PD and consequent dopamine deficiency in the striatum (putamen and caudate nucleus) **c)** Immunostaining of intracellular Lewy bodies with α-synuclein and ubiquitin antibodies. Adapted from [9].

Braak and colleagues proposed a model where LB pathology progresses through six different stages in PD in a temporal and spatially defined pattern [10]. Interestingly, this model correlates with the appearance of clinical symptoms of PD. Specifically, stages 1 and 2 correlate with the appearance of premotor symptoms, stage 3 is related to the first appearance of motor symptoms, and stages 4 to 6 correspond to the more advanced stages of the disease, which include non-motor features [4]. Even though much effort had been put into understanding LB pathobiology, it is unclear whether LB are toxic by themselves, if they reflect a protective mechanism, or simply comprise a cellular waste product [11]. In either case, the presence of LBs implicate abnormal protein aggregation in the disease process.

1.3 Treatment

Current treatments for PD show symptomatic benefits for some motor manifestations, but have little, if any, effect on non-motor symptoms. Unfortunately, there is currently no treatment to prevent or stop disease progression.

i) Dopamine replacement strategies

Since it was originally tested in 1961 [12], L-3,4-dioxyphenylalanine (L-DOPA or levodopa) treatment has been the best choice to treat some of the motor symptoms of PD. Being the metabolic precursor of dopamine, L-DOPA is administered to revert the dopamine reduction in the striatum of PD patients [13]. In contrast to dopamine, L-DOPA can cross the blood–brain barrier, and once internalized by dopaminergic neurons of the SNpc, it is metabolized to dopamine by the enzyme DOPA decarboxylase, and can later be released to replenish dopamine input into the striatum. Additional advances in the field have been achieved in order to get more sustained L-DOPA dosage over time, thereby reducing dopamine peaks that provoke motor response oscillations and dyskinesia (involuntary movements) [14]. In this sense, new L-DOPA formulations and continuous delivery strategies have decreased, but not eradicated, the problems associated with L-DOPA administration. Pursuing the same goal, L-DOPA is now usually co-administered with other drugs that prevent peripheral L-DOPA degradation (Catechol-O-methyltransferase (COMT) inhibitors) and prevent synaptic dopamine clearance by glial cells (Monoamine oxidase type B (MAOB) inhibitors) [14].

Dopamine agonists that activate dopamine receptors in the striatum are another choice to treat the motor symptoms of PD. Their longer half-life and the reduced motor complications compared to L-DOPA make them another attractive option to treat PD. However, dopamine agonists show reduced overall effects as

compared to L-DOPA, and they can also provoke side-effects, including sleepiness and loss of impulse control [14].

In spite of the improvements of dopamine substitution strategies with respect to some motor problems, symptoms like postural instability, dysphagia (difficulty in swallowing) and falls are usually resistant to the above-mentioned treatments.

ii) Non-dopamine related strategies

Therapies are available to treat some of the non-motor symptoms of PD, and some of the adverse effects of dopamine treatments. In this sense, some drugs are used to ameliorate rapid eye movement sleep behavior disorder (RBD), depression, nauseas, orthostatic hypotension, dyskinesia or hallucinations caused by the disease or by the dopamine-related treatments [15]. For example, cholinesterase inhibitors can be useful to treat cognitive defects, and clozapine is the best option for the psychotic symptoms in PD, although the exact mechanisms by which they act are not completely understood [4, 15]. However, much more effort needs to be done in understanding the causes of the non-motor symptoms of the disease and in finding strategies that ameliorate those disabling problems.

iii) Deep-Brain Stimulation (DBS)

Introduced first in 1995 [16], DBS is based on high-frequency electrical stimulation of determined areas (subthalamic nucleus in the case of PD) with an internal electrode. It is a well-established method to treat the motor fluctuations and dyskinesia, generally used in patients with advanced PD. Several recent clinical trials also highlight the benefits of earlier DBS surgical treatments in patients who respond well to L-DOPA treatment, recommending intervention at earlier stages of the disease [17]. However, DBS is a complex treatment due to surgery and posterior complications which include rare intracranial bleedings and device complications.

1.4 Etiology

Despite extensive work during past decades, the precise causes underlying PD remain unknown. Current knowledge suggests that PD is a complex disease, with different causes contributing towards disease development. Importantly, PD has a clear genetic component that is helping the scientific community to understand the disease.

i) Age and gender

Statistical analysis points out to aging as the major established risk factor to develop PD. A recent meta-analysis of epidemiological studies of PD performed between 2001 and 2014 shows that incidence rates increase constantly over time, in both males and females [18]. When looking at gender differences, significantly higher PD incidence rates were found in males than in females at all ages, indicating that gender is also a risk factor for PD [18].

ii) Genetics

Genetic studies (traditionally linkage analyses, and more recently Genome Wide Association Studies (GWAS)) have discovered mutations and variations that associate with PD. Importantly, all these findings are helping the scientific community to model and understand the molecular mechanisms underlying the disease and to find possible therapeutic targets.

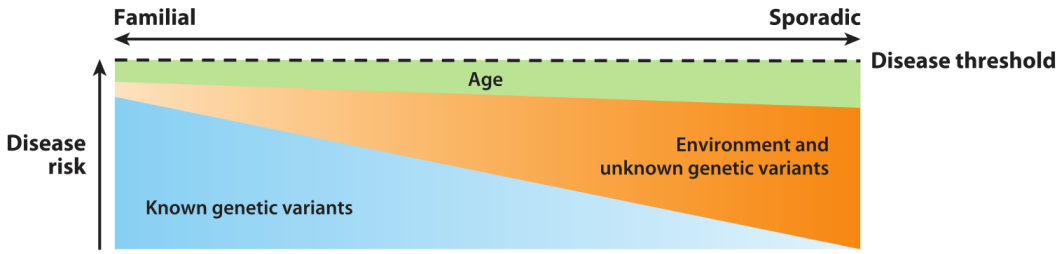

Fig. 3. Etiology of Parkinson's disease. Adapted from [5]

a) Autosomal-dominant mutations

α-synuclein

Mutations in the *α-synuclein* (*SNCA*) gene were the first identified causative genetic component of PD. Polymeropoulos et al. discovered the A53T-*SNCA* mutation in a large Italian family with PD [19], and this was quickly confirmed in three other Greek families [20]. Additional mutations (A30P, E46K, H50Q and G51D) were subsequently found to cause autosomal-dominant PD, but all of them (including A53T) are rare and only observed in few families throughout the world [21]. Duplications, and in some cases triplications of the gene locus are a more common cause of familial PD, but still only account for ~1–2 % of autosomal-dominant familial PD [21, 22]. There seems to exist a direct correlation between the levels of *α*-synuclein and the age of onset and severity of the disease. Given that α-synuclein is the main component of LBs [23], much effort has been put on understanding α-synuclein biology. The protein is found in presynaptic nerve endings, and has been reported to interact with Rab proteins and with different components of the SNARE family, which play primary roles in different vesicle trafficking events [24, 25]. These observations, together with the fact that α-synuclein forms aggregates and fibrils within LBs, point towards clear roles for the protein in intracellular membrane trafficking events and protein homeostasis, deficits of which may underlie PD pathogenesis.

LRRK2

Mutations in the *leucine-rich repeat kinase 2* (*LRRK2*) gene are the most common cause of familial PD, with autosomal-dominant inheritance. LRRK2 mutations affect 1% of patients with sporadic PD and 4 % of patients with hereditary PD worldwide [26], but there are different prevalences amongst populations, with the highest frequencies at 10–30 % of PD cases in Ashkenazi Jewish and 35–40 % of PD cases in North African Berber populations, respectively

[26, 27]. Two additional reasons make the study of LRRK2 biology and pathobiology especially relevant for the whole spectrum of PD. On the one hand, variations in the LRRK2 locus are associated with increased risk to develop sporadic PD [28, 29]. On the other hand, the clinical and neuropathological features of LRRK2 PD patients are similar to those occurring in most sporadic PD patients [26, 30].

VPS35

Mutations in *vacuolar protein sorting-associated 35* (*VPS35*) gene cause a rare form of late-onset, autosomal-dominant PD, accounting for just 0.1-1 % of autosomal-dominant PD [31, 32]. VPS35 is a core protein of the retromer, a complex of proteins required for the retrograde trafficking from late endosomes to the Golgi complex, highlighting and further supporting the implication of altered membrane trafficking associated with PD pathobiology.

b) Autosomal-recessive mutations (PARKIN/PINK1)

PARKIN

Mutations in the *PARKIN* gene cause severe autosomal-recessive juvenile onset parkinsonism (ARJP), and are the most common cause of early-onset PD, accounting for 15-50 % of the cases [33-35]. Interestingly, in most cases, parkin mutant carriers lack LBs in postmortem brain examination, which may be at least in part be due to the early cell death in affected areas. Parkin is a E3 ubiquitin ligase which is recruited to damaged mitochondria upon PINK1-mediated phosphorylation, where it ubiquitinates mitochondrial membrane proteins to promote mitophagy [36, 37].

PINK1

Around 2-9 % of early-onset, autosomal-recessive PD cases are caused by mutations in the *PTEN-induced putative kinase 1* (*PINK1*) gene [22, 38]. PINK1 is a kinase localized to mitochondria, where it is activated upon mitochondrial membrane potential depolarization [39] to phosphorylate parkin and thereby regulate the autophagic degradation of defunct mitochondria [37]. These findings highlight the mechanistic link between mitochondrial homeostasis and PD pathomechanisms.

Mutations in other genes (e.g. DJ-1, FBXO7, PLA2G6, ATP13A2, DNAJC6 and SYNJ1) have been shown to segregate with PD but represent rare forms of the disease. Interestingly, they have been linked to autophagic and endocytic pathways, mitochondrial health and synapse homeostasis, highlighting the role of those mechanisms in PD [40].

c) Risk variants

GWAS have identified several variants that confer risk to develop PD [21]. Although the actual risk of most of these variants is relatively low, ranging from 1.2-1.5 times the risk to develop PD as compared to non-carriers, the identified genes give clues as to the cellular and molecular pathways that may contribute to disease development. Interestingly, there are four genes which have been continuously detected as risk factors in these studies: *SNCA*, *LRRK2*, *GBA* and *MAPT* [21, 22].

The fact that mutations in SNCA and LRRK2 cause autosomal-dominant PD and variants also modulate risk to develop sporadic PD [28, 29] highlights the key role of both proteins for the entire disease spectrum. Interestingly, homozygous loss-of-function mutations in GBA are known to cause Gaucher disease (GD), an autosomal recessive lysosomal storage disorder [41]. GBA is a lysosomal enzyme that cleaves glucocerebroside to ceramide and glucose [42]. Heterozygous GBA

mutations increase PD risk by around 20-fold [43], again pinpointing towards an important link between endolysosomal dysfunction and protein dyshomeostasis and PD pathogenesis. The fact that variants in the *microtubule associated protein tau* (*MAPT*) gene, associated with Alzheimer's disease and other tauopaties with dementia also increase PD risk [29], has suggested a common link between these apparently different diseases. Tau is involved in the assembly and stabilization of the microtubular network [44], suggesting that improper microtubule organization and membrane trafficking contributes to cellular dyshomeostasis in PD.

During the past few years, many other susceptibility genes have been described. *Rab7L1* is one of the five genes within the *PARK16* locus identified to modify risk for PD in several GWAS [28, 29]. Due to the fact that Rab7L1 interacts with LRRK2, and both of them form a complex with GAK (Cyclin-G-associated kinase) [45], a protein involved in clathrin-dependent endocytosis and in clathrin-dependent cargo traffic from the Golgi to the lysosome [46], and another risk factor for PD [47], the study of Rab7L1-LRRK2 biology has become a subject of intense study.

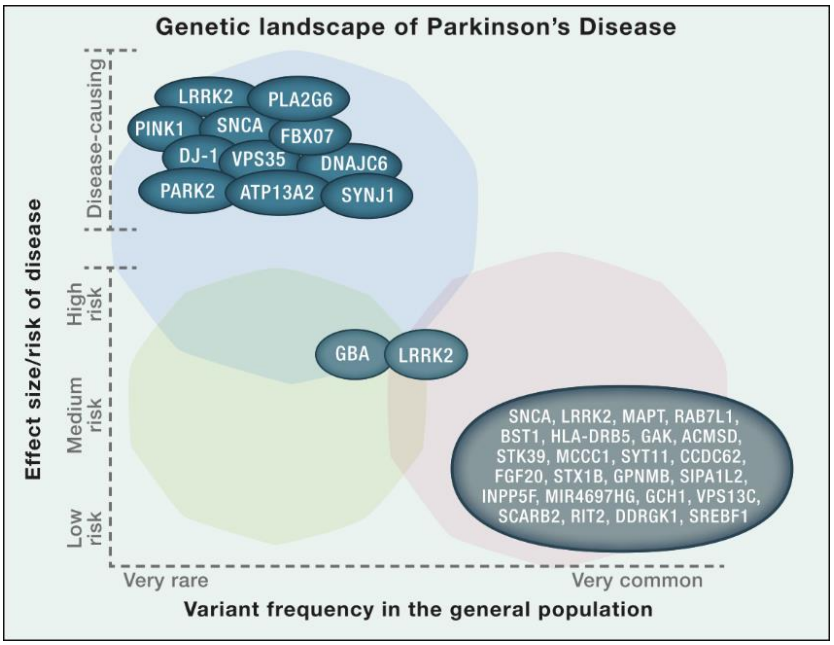

Fig. 4. Genetics of Parkinson's disease. From [48]

1.5 Molecular mechanisms

Different and not mutually exclusive mechanisms have been proposed to underlie neurodegeneration in PD patients. A wealth of evidence indicates that membrane trafficking in general, and the autophagy/endolysosomal system in particular, may be compromised in PD. The presence of LBs, mainly consisting of aggregated α-synuclein, indicates a defect in the autophagic clearance of protein aggregates. In support of this, an increased number of autophagosomes and reduced number of lysosomes has been observed in the *SNpc* of postmortem samples from PD patients as well as animal models of the disease [49, 50]. In addition, and as mentioned above, many of the genes linked to PD, either through Mendelian inheritance (*SNCA*, *LRRK2, VPS35*) or via polymorphisms conferring risk (*GBA*, *RAB7L1*, *GAK*), have established roles in the autophagy/endolysosomal pathways [51, 52].

Mitochondrial dyshomeostasis and oxidative stress are also associated with PD mechanisms [53-55]. This is supported by the known mitochondrial functions of the gene products involved in autosomal-recessive PD such as PINK1 and Parkin [21]. In addition, some drugs which affect the proper functioning of the mitochondrial respiratory chain, like MPTP, cause parkinsonism, which further points towards the importance of mitochondrial health in the context of PD [56]. Mitochondria dysfunction caused by genetic mutations or by environmental exposure to drugs leads to increased oxidative stress [57], which combined with the already high levels of oxidative stress in DA neurons due to the generation of ROS during DA metabolism [58], may explain the relatively selective death of DA neurons.

Apart from such cell-autonomous processes, non-cell autonomous mechanisms have been proposed to contribute to PD development. On the one hand, different studies have shown α-synuclein-positive LBs in fetal grafted neurons in PD patients [59, 60], suggesting that the pathology can spread from one

cell to another in a "prion-like" fashion. On the other hand, increasing evidence coming from post-mortem analysis of PD patient brains, genetic analyses and epidemiological studies support the importance of inflammation and immune responses in PD [61]. Chronic neuroinflammation accompanied by active microglia is a common process in the *SNpc* and other regions affected in PD [62, 63]. In addition, several proteins causative for PD like α-synuclein or LRRK2 have been reported to regulate microglia and T-cell functions [64, 65], and LRRK2 is highly expressed in immune cells [66]. Finally, GWAS have identified genetic variations in the human leukocyte antigen (HLA) region associated with altered risk [67], suggesting an important role of the immune system in PD.

2. LRRK2

The initial finding of autosomal-dominant mutations in the *PARK8* locus segregating with late-onset familial PD [68] was followed by the identification and cloning of the *LRRK2* gene [69, 70]. Patients carrying LRRK2 mutations show a clinical and neuropathological phenotype similar to sporadic PD patients. Importantly, LRRK2 mutations show an incomplete age-dependent penetrance, varying from around 50 % at age 50 to approximately 75 % at age 79 [26, 71, 72], but penetrance can also be as low as 26 % at age 80 when analyzing Ashkenazi Jewish populations carrying the LRRK2 G2019S mutation [73]. Therefore, it seems that the genetic background and/or environmental factors seem to play an additional role in in the development and manifestation of LRRK2-PD.

2.1 Structure and activity

LRRK2 is a 280 kDa, multidomain protein with a catalytic core consisting of a kinase domain and a ROC (Ras of complex) GTPase domain linked to a COR-domain (C-terminal of ROC). In addition, LRRK2 encompasses protein-protein interacting domains (armadillo, ankyrin and leucine-rich repeat

(LRR) domains) and a WD40 domain [74]. Most of the autosomal-dominant mutations in LRRK2 are clustered within the catalytic domains of the protein. The most frequent mutation, G2019S, and a less common I2020T mutation are within the kinase domain, while R1441C/G/H and N1437H mutations are located in the GTPase domain and the Y1699C mutation in the COR domain, respectively. Interestingly, although only the most prominent G2019S mutation displays enhanced kinase activity when assessed *in vitro*, recent *in vivo* studies indicate that all pathogenic mutants show increased kinase activity [75, 76]. Importantly, such kinase activity seems to mediate LRRK2-induced neuronal toxicity [77, 78].

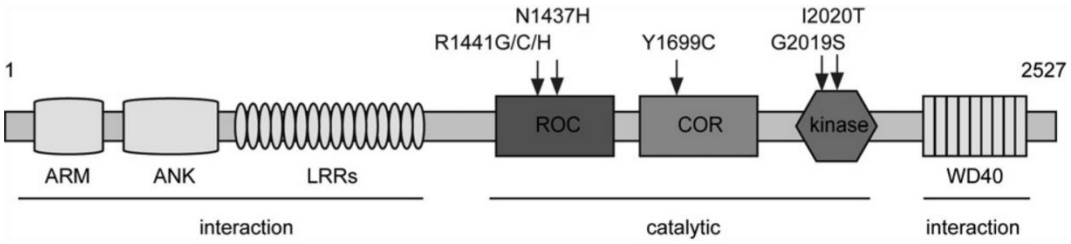

Fig. 5. Domain structure of LRRK2. Full-length LRRK2 is indicated with its distinct domains, and clearly pathogenic mutations indicated above. ARM, armadillo repeats; ANK, ankyrin repeats; COR, C-terminal of ROC domain; LRR, leucine-rich repeats. From [79]

Kinases are ideal drug targets, and important effort has been made towards developing specific, potent and brain-permeable LRRK2 kinase inhibitors as disease-modifying strategies to treat LRRK2-related PD. Drug development has led to several generations of compounds with increased selectivity and brain permeability. Various compounds have been generated, including Inhibitor-1 and GSK2578215A (GSK), which displays higher selectivity against LRRK2 kinase, even though neither one of those is blood-brain barrier (BBB) permeable. Newer compounds with exquisite potency, selectivity and BBB permeability have been generated, including MLi-2 from Merck, PF-06447475 and PF-06685360 from Pfizer, and GNE-7915 and GNE-0877 from Genentech, respectively [80]. Preclinical trials using animal models have raised issues associated with fully

inhibiting LRRK2 kinase activity. The use of this recently-developed kinase inhibitors in non-human primates (NHP) has shown the presence of histological changes in the lung (lamellar body accumulation in type II pneumocytes) with very high doses [81, 82], that have also been observed with other less specific LRRK2 kinase inhibitors in rodent and NHP studies [82, 83]. However, these abnormal histological lung changes are not associated with deficits in lung functions, and are quickly reversible after drug intake [81].

There has been intense debate on the crosstalk between the GTPase and kinase domain of LRRK2 [84, 85]. In vitro studies have shown increased GTP binding [86-88] and/or decreased GTP hydrolysis [87, 89-91] for all pathogenic mutations in the ROC and COR domain. These mutants do not seem to display increased kinase activity when assessed *in vitro* [92], but do so towards select substrates when assessed *in vivo* [75]. A possible explanation for this apparent discrepancy has recently been suggested. Mutations in the ROC-COR domain, possibly mediated by enhanced GTP binding and a resulting conformational change, make them especially prone to Rab7L1-mediated kinase activation by currently unknown mechanisms [93], whilst in the *in vitro* studies, the absence of such cellular LRRK2 activators would impede kinase activation.

Several aminoacids within LRRK2 are subject to phosphorylation. LRRK2 phosphorylates itself on S1292, making this site an autophosphorylation site. However, since autophosphorylation of protein kinases usually occurs at very low stoichiometry, detection of S1292 phosphorylation does not serve as a sensitive measure of LRRK2 kinase activity [94]. A set of other residues, including S910, S935, S955 and S973, are phosphorylated at much higher stoichiometry, but not by LRRK2 itself [95, 96], but rather by other cellular kinases [97]. These so-called cellular phosphorylation sites, especially S935, have been used as a readout of the efficacy of LRRK2 kinase inhibitors [97], likely because the binding of kinase inhibitors causes a conformational change within LRRK2, which inhibits the

binding of LRRK2 to 14-3-3 proteins, leading to dephosphorylation of these residues [97].

2.2 LRRK2 expression

LRRK2 is ubiquitously expressed amongst different tissues and cell types [98, 99]. Kidney and lung are the organs with the highest LRRK2 expression, which may explain the abnormalities observed in those organs in mice and monkeys upon LRRK2 kinase inhibition or knockout, respectively, and which also suggests an important physiological role for LRRK2 in those tissues [82]. LRRK2 is expressed in the brain [100], showing high levels in dopamine-receptive areas, especially in the striatum and cortex [101, 102]. There is controversy on the actual levels of LRRK2 within *SNpc*, with some studies suggesting that the levels are comparable to other brain areas [103, 104], but many others suggesting that they are considerably lower [101, 102, 105, 106].

LRRK2 is also highly expressed in many different cells of the immune system, including peripheral blood mononuclear cells, lymph nodes, spleen and primary microglia [66, 82, 99, 107]. Interestingly, LRRK2 expression is robustly upregulated upon stimulation with pro-inflammatory signals (including IFN-γ and LPS (Lipopolysaccharide, an outer membrane component of bacteria) suggesting that LRRK2 may play an important role in the immune system [66, 107]. In support of this, variations around the LRRK2 locus have been identified as risk factors for autoimmune diseases such as Crohn's disease [108, 109], systemic lupus erythematosus [110] and leprosy [111], further highlighting its importance in immunity and inflammation.

2.3 LRRK2 disease models

i) Animal models

A vast array of genetic animal models aimed at recapitulating the pathological and clinical symptoms of PD have been generated, but most models show none or only modest alterations in DA neuron survival [112].

LRRK2 knock-in (KI) mice with either the G2019S or R1441C mutation display no overt PD-relevant histopathological or behavioral abnormalities, although kidney irregularities have been observed [83, 113]. Although no DA neuron degeneration is observed in LRRK2 KI mice, dopamine D2 receptor function is partially impaired in the LRRK2-R1441C KI mice [113], and the extracellular release of dopamine in the LRRK2-G2019S KI mice is also deficient [114], which results in a DA deficiency in the striatum, similar to some extent to the one observed in PD patients.

Various human bacterial artificial chromosome (BAC) transgenic rodent models overexpressing pathogenic LRRK2 have been generated. Human G2019S-LRRK2 BAC transgenic mice were reported to display mild but selective SNpc DA neuron death, with abnormalities in autophagy, mitochondria and neurite complexity, but without effects on striatal DA levels or behavioral alterations [115, 116]. In contrast, a rat model overexpressing G2019S-LRRK2 showed mild behavioral modifications and impaired dopamine reuptake, but no reduction in the number of DA neurons or of striatal DA levels [117]. Human R1441G-LRRK2 BAC transgenic mice overexpressing LRRK2 5-10 fold above endogenous levels showed age-dependent and progressive hypokinesia, and these mice also showed impaired DA release and dendritic abnormalities in SNpc DA neurons, without a reduction in the number of these neurons [118]. A recent study showed that inducible and selective overexpression (5-fold increase above endogenous) of G2019S-LRRK2 driven by the tyrosine hydroxylase (TH) promoter causes age-dependent DA neurodegeneration and accumulation of high molecular weight

α-synuclein [119]. Whilst independent validation of this model is required, it represents a substantial advance in the genetic modelling of PD in mice, and at the same time suggests that LRRK2 pathology can occur in a cell-autonomous manner.

In vivo delivery of LRRK2 through recombinant viral vectors has allowed to target specific neuronal populations and to obtain PD related phenotypes, likely because of the non-physiological levels of protein expression. Targeting the DA neurons of the SNpc in mice through Herpes simplex virus (HSV)-pathogenic LRRK2 injection caused a 50 % neuronal loss which was not observed with the kinase-dead LRRK2 mutant [120]. Similarly, an adenovirus-pathogenic LRRK2 rat model showed progressive loss of DA neurons in the SNpc [121], and effect which was later shown to be kinase dependent [122].

Taken together, the research carried out in rodent models indicates that perhaps due to the short lifespan of these animals, overexpression of pathogenic LRRK2 (using BAC transgenic or viral vector-based systems) is the only way to obtain a PD-related phenotype.

ii) Cellular models

Although lacking the complexity of the intact brain network and the crosstalk between different neuronal populations, *in vitro* cellular models offer the opportunity to test the implications of pathogenic LRRK2 for various intracellular mechanisms and allow for the discovery and validation of molecular pathways. At the same time, the use of distinct drugs to modulate specific steps of cellular homeostasis, enable insights into the precise function(s) of LRRK2 within a specific pathway.

Primary patient-derived dermal fibroblasts, induced pluripotent stem cells (iPSC) and differentiated iPSC have been instrumental in characterizing LRRK2 functions [123-126]. In addition, overexpression of LRRK2 in several immortalized cell lines (especially the human neuroblastoma, neuronal-like

SH-SY5Y cell line) have led to primary findings for the LRRK2 field [127], which have later been corroborated in other disease models. Other cell lines, including HEK293 (human embryonic kidney) cells have been routinely used for proteomics and interactor analyses as well.

The most common phenotype described in these studies is the reduction of neurite length and complexity upon pathogenic LRRK2 expression, similar to the dystrophic neurites found in PD brains [128]. Using primary cortical cultures transduced with LRRK2, Macleod et al., first described the implications of LRRK2 on regulating neurite process morphology, showing that pathogenic LRRK2 causes a reduction in neurite length and branching with an accumulation of autophagic structures [129]. Autophagy defects were proposed to be underlying the neurite shortening phenotype observed under mutant LRRK2 overexpression in differentiated SH-SY5Y cells [127]. In agreement with these data, one of the earliest studies using iPSC-derived DA neurons from PD patients showed that endogenous LRRK2-G2019S neurons present altered morphology with fewer and shorter neurites, accompanied by autophagy deficits caused by autophagosome maturation defects [126]. These data were corroborated by another group that corrected the LRRK2-G2019S mutation in iPSC-derived neurons and reverted the neurite outgrowth problems [130].

2.4 Cellular and molecular pathways

Due to its ubiquitous expression, the presence of several protein-protein interaction domains and a vast array of reported interactors (see below), LRRK2 has been implicated in many different cellular functions and pathways. In addition, the use of a wide variety of model systems, the use of endogenous versus overexpression or knockout approaches, and the study of both physiological LRRK2 versus pathogenic LRRK2 mutants, have increased the complexity of trying to integrate results and obtain a clear idea of the intracellular role(s) of

LRRK2. Data coming from different model systems consistently indicate that wildtype and pathogenic LRRK2 play important roles at different stages of several membrane trafficking events which are highly interconnected and interdependent, including autophagy, endocytosis, lysosomal biology and the retromer complex.

i) Autophagy

Autophagy is a cellular catabolic process by which proteins and defunct organelles are transported to the lysosome for degradation [131]. Autophagy can be classified into three distinct subtypes depending on the mechanisms by which the distinct components are delivered to the lysosome. Macroautophagy (hereafter autophagy) is the most common form of autophagy, and it involves the engulfment of proteins or organelles by a double-membrane vesicle called the autophagosome which later fuses with the lysosome. Chaperone-mediated autophagy (CMA) is the most selective type of autophagy, in charge of specific protein degradation which requires the identification of a signal peptide within the protein with the help of chaperones, followed by translocation of proteins into the lysosome. Finally, microautophagy occurs when the lysosome membrane itself engulfs small cytoplasmic components [131].

Evidence for a physiological role of LRRK2 in autophagy comes from studies involving LRRK2-KO (knockout) research. Different studies have shown that LRRK2-KO mice have autophagic alterations in kidney cells, with increased levels of the autophagy marker LC3-II which could be explained by either increased autophagosome formation and/or diminished clearance [132-134]. Pharmacological LRRK2 kinase inhibition in cellular models also leads to accumulation of LC3-II positive autophagosomes [135, 136], although another study reported the opposite effect, with LRRK2 kinase inhibition causing deficits in the induction of autophagy [137]. In either case, most current data suggest an important role for endogenous LRRK2 in controlling autophagy.

Pathogenic LRRK2 also alters the autophagy/endolysosomal system. Mice overexpressing human LRRK2-G2019S and R1441C show increased number of enlarged autophagosomes within neurons from the cerebral cortex and striatum [115]. Fibroblasts from pathogenic LRRK2 PD patients show alterations in autophagy as compared to healthy controls, and autophagic alterations have also been described in SH-SY5Y cells overexpressing LRRK2-G2019S [127, 138, 139]. Finally, iPSC-derived dopamine neurons from LRRK2-G2019S PD patients show accumulation of autophagic vacuoles caused by a decrease of autophagosome clearance [126].

Under overexpression conditions, Gomez-Suaga et al., proposed that the increase in autophagosome accumulation observed upon LRRK2-G2019S kinase domain expression is through an increase in cytosolic Ca^{2+} that activates the CaMKK/AMPK pathway. At the same time, mutant LRRK2 expression produced a partial alkalinization of lysosomal pH, thus reducing the number of lysosomes with acidic pH. These events were mediated by endolysosomal calcium channels (such as TPC2) which are directly or indirectly regulated by LRRK2 to modulate Ca^{2+} release important for endolysosomal trafficking [140]. A later study confirmed that expression of pathogenic LRRK2 (R1441C, Y1699C and G2019S) causes enlarged, non-functional lysosomes, but contrary to the previous report, lysosomal pH was found to be more acidic [141]. Altogether, evidence points towards pathogenic LRRK2 causing autophagic deficits, probably by blocking the autophagic flux, and mediated by alterations in endolysosomal functioning.

ii) Endocytosis

Endocytosis is the process by which the cell incorporates components from the extracellular space [142]. There are different forms of endocytosis, including clathrin-mediated endocytosis, clathrin-independent endocytosis, pinocytosis and phagocytosis. These processes usually involve vesicles budding off from the

plasma membrane, fusion with an early endosome, and subsequent protein sorting that directs the endocytosed components to the late endosome and then the lysosome for degradation, or to the recycling endosome to recycle receptors back to the cell surface.

LRRK2 interacts with different components of the endocytic pathway, and mutations in LRRK2 have been reported to affect both early and late steps of this pathway. Interestingly, LRRK2 interacts with different members of the Rab GTPase family, small proteins that control specific vesicle trafficking events. Rab5b, a protein localized to early endosomes, has been proposed to interact with LRRK2 using a yeast two-hybrid screen [143]. In this study, pathogenic LRRK2 was also shown to impair synaptic vesicle endocytosis, which was rescued by Rab5b overexpression. Rab7 is localized to late endosomes, and has also been suggested to interact with LRRK2 [144]. Furthermore, pathogenic LRRK2 was reported to regulate endocytic vesicle trafficking in a Rab7-dependent manner [145]. Gómez-Suaga et al. found that pathogenic LRRK2 caused a pronounced delay at late stages of the endocytic pathway, causing abnormally elongated late endosomes and concomitant accumulation of proteins to be degraded. Interestingly, overexpression of active Rab7 rescued these deficits caused by pathogenic LRRK2 [145].

iii) Retromer-mediated trafficking

The retromer is a complex of different proteins including membrane-associated sorting nexins and a trimer composed of VPS26, VPS29 and VPS35 [146]. It is important for recycling of transmembrane receptors from endosomes to the trans-Golgi network and the plasma membrane [146]. The D620N mutation in VPS35 causes autosomal-dominant PD, affecting 0.1-1 % of patients with familial PD [147, 148], making the study of retromer biology an important topic in the PD field.

Several pieces of evidence point towards a link between LRRK2 and retromer-mediated trafficking. VPS35 overexpression ameliorates the pathogenic LRRK2-induced locomotor phenotype in a *Drosophila* model, suggesting that retromer deficiencies may underlie such LRRK2-mediated defects [149]. In addition, overexpression of VPS35 in rat primary neuronal cultures rescues the endolysosomal defects observed upon pathogenic LRRK2 expression, and overexpression of VPS35 in G2019S LRRK2 mutant-expressing flies rescues dopaminergic neuron loss [150]. In addition, co-immunoprecipitation of LRRK2 and VPS35 suggest a possible physical interaction between these two proteins [150]. Additional possible links between LRRK2 and retromer-mediated trafficking pathways are indicated by its reported interaction with Rab7L1 and Rab9 [45, 150, 151], both of which are involved in the same endosome-to-Golgi retrograde pathway [152, 153]. On the one hand, Rab7L1 has been implicated in the trafficking of the cation-independent mannose 6-phosphate receptor (MP6R) from the endolysosome compartment to the Golgi apparatus, as knockdown of Rab7L1 provoked a significant reduction in lysosomal and Golgi accumulation of MP6R [150, 152] similar to VPS35 knockdown or pathogenic LRRK2 effects [150]. In addition, knockdown of Rab7L1 caused a reduction in the levels of VPS35 and VPS29 [150], suggesting that Rab7L1 is required for proper retromer complex formation. On the other hand, Rab9 overexpression rescued the endolysosomal abnormalities observed in LRRK KO Drosophila models, suggesting possible deficits in retromer-mediated endosome-to-Golgi retrieval pathways [151].

iv) Golgi apparatus

At the intersection of the secretory, endocytic and lysosomal pathways, the Golgi apparatus is in charge of the classification and delivery of newly synthesized proteins coming from the endoplasmic reticulum (ER), but also acts as an acceptor compartment from the retromer pathway to later re-distribute proteins that avoid

lysosomal degradation back to their original compartments [154]. In addition to its function as a sorting station, the Golgi apparatus also plays important roles in post-translational modification of proteins, can act as a microtubule-nucleating center as well as a calcium store [154]. The trans-Golgi network (TGN) is the tubular reticular membrane at the trans face of the Golgi, and it is a specialized sorting machinery to deliver cargo molecules to different cellular compartments [155].

Interestingly, the Golgi apparatus is located next/around the centrosome in most vertebrate cells, and its structure and positioning partially depend on microtubules (MTs) originating from the centrosome [156], the major Microtubule-Organizing Center (MTOC) of the cell. The centrosome, together with the Golgi apparatus define the polarity of many different cell types, and are important for polarized secretion, cell migration and cell differentiation [157]. In addition, the MT-nucleating capacity of the Golgi apparatus (rather than the centrosome) seems to contribute towards maintaining MT polarity in neuronal dendrites [158, 159].

Early studies indicated that both endogenous and overexpressed LRRK2 can localize to the Golgi apparatus [160-162]. In addition, fragmentation of the Golgi apparatus was observed in cortical neurons from wildtype and G2019S-LRRK2 transgenic mice, which was more severe in neurons from A53T α-synuclein and LRRK2 double-transgenic mice, suggesting a synergistic effect of both PD-related proteins on Golgi morphology [163]. Additional evidence for a link between LRRK2 and Golgi integrity has emerged from the finding that overexpressed Rab7L1 recruits LRRK2 to the Golgi complex resulting in Golgi fragmentation and autophagy-mediated Golgi clearance and/or aberrant Golgi clustering [45, 150]. Whilst further work is necessary to determine the precise molecular mechanism(s), current data indicate that pathogenic LRRK2, especially

in conjunction with α-synuclein or Rab7L1, can cause structural and/or functional deficits of the Golgi complex.

v) Cytoskeleton

Three main classes of filaments compose the eukaryotic cytoskeleton: microfilaments or actin filaments, intermediate filaments and MTs. They provide structural support for the cell, and are essential for establishing cellular shape, compartmentalization, and cell polarity. They play pivotal roles in the intracellular transport of molecules and organelles, and are crucial for axon and dendrite formation as well as cellular migration [164].

MTs are highly dynamic, hollow cylindrical structures, typically formed by 13 protofilaments composed of heterodimers of α- and β-tubulin [165]. Generally, MT polymerization originates at the centrosome, the major MTOC. Increasing evidence points towards MT dysfunction as a common phenotype for several neurodegenerative diseases. For example, mutations in *MAPT* cause familial frontotemporal dementia with parkinsonism linked to chromosome-17 (FTPD-17), progressive supranuclear palsy, and mild, late-onset parkinsonism [166]. In addition, tau aggregates form neurofibrillary tangles, a common hallmark of Alzheimer's disease [167], and tau pathology may also be observed in PD patients [7, 168-170]. Tau proteins are expressed in neurons, where they bind to and stabilize MTs. Interestingly, LRRK2 has been reported to interact with and phosphorylate MT-associated tau, but not free tau, thereby interfering with its ability to bind MTs and decreasing MT stability [171, 172]. Whilst such phosphorylation seems to occur at low stoichiometry, other scaffold-type mechanisms by which LRRK2 may regulate tau phosphorylation by other kinases have been proposed as well [173].

LRRK2 has also been reported to interact with actin [174], and most prominently with MTs. *In vitro* data indicate that both endogenous as well as

overexpressed LRRK2 can interact with different tubulin isoforms [175]. Importantly, all pathogenic LRRK2 mutants except for G2019S show co-localization with MTs under overexpression conditions [88, 176]. Blanca Ramirez et al. demonstrated that the association of pathogenic LRRK2 to MTs depends on LRRK2 GTP binding rather than on the kinase activity [88]. Other studies indicate that LRRK2 may regulate posttranslational MT modifications which contribute to altered MT stability [177-179]. In either case, altered MT stability could contribute to the well-established neurite shortening phenotype observed in different mutant-LRRK2 neuronal cell models. In addition, enhanced interactions of pathogenic LRRK2 with MTs may interfere with select vesicular trafficking events, further aggravating the membrane trafficking defects caused by additional LRRK2-mediated modulation of Rab proteins.

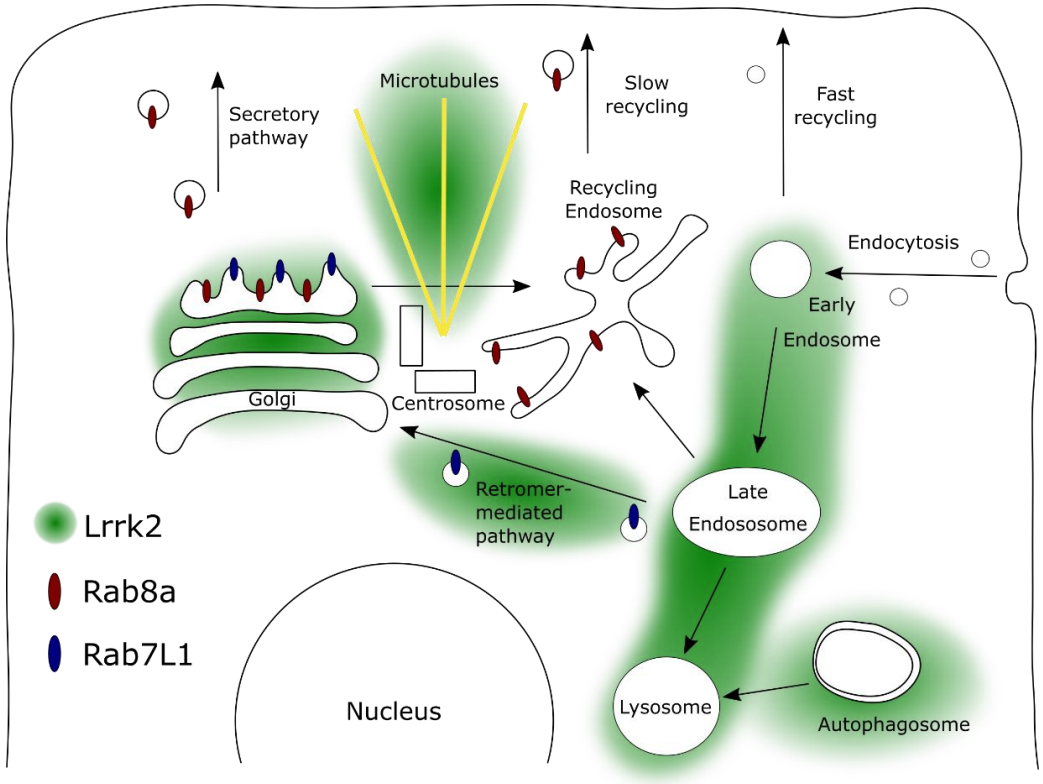

Fig. 6. The role of LRRK2 in membrane trafficking. LRRK2 distribution represented as a green shadow. In red, the small GTPase Rab8a and its cellular distribution. In blue, the small GTPase Rab7L1 and its cellular distribution.

2.5 LRRK2 interactors

LRRK2 has been described to interact with a large set of different proteins. Filtering for independent data replication, the number of interactors becomes reduced to 62 [180]. At least two reasons may account for such a high number of interactors. The many distinct protein-protein interaction domains may make LRRK2 prone to interact with a variety of distinct proteins in a scaffold-type manner. In addition, given the ubiquitous tissue expression, LRRK2 could interact with small subsets of those proteins in a tissue- and cell type-specific manner. Here, I will summarize the ones that have been independently validated, corroborated by different techniques, and which are more relevant for this dissertation.

These interactors include a set of Rab proteins such as Rab5b, Rab7L1, Rab8, Rab10 and Rab32 [75, 143, 150, 181]. Colocalization of LRRK2 with those different Rab proteins in distinct cell types has been reported, most prominently with Rab7L1, which is able to relocalize LRRK2 from the cytosol to a Rab7L1-positive Golgi compartment [45, 76, 150]. Similarly, Rab32 also interacts and recruits LRRK2 to different transport vesicles [181]. Rab32 is highly expressed in melanocytes, acts on the transport of key enzymes for melanogenesis [182], and plays a role in the formation of lysosome-related organelles (LRO). As mentioned above, LRRK2 also interacts with other proteins important for membrane trafficking events, including VPS35, and with MTs, either via direct interactions or via interaction with tau [88, 171, 176].

Another set of consistently reported LRRK2 interactors are 14-3-3 proteins [183, 184], which usually bind phosphorylated proteins protecting phosphorylation sites from dephosphorylation, or can mediate dimerization of two distinct target proteins [185]. Phosphorylation at LRRK2 S910 and S935 residues is needed for the binding of LRRK2 to 14-3-3 proteins [183, 184]. Interestingly, most pathogenic LRRK2 mutations show decreased S910 and S935 phosphorylation and a

concomitant reduced binding to 14-3-3 proteins, which leads to a decrease in cytosolic LRRK2 [183, 184]. Similarly, treatment with LRRK2 kinase inhibitors provokes S910 and S935 dephosphorylation, most likely because of a conformational change in LRRK2 that inhibits the binding to 14-3-3 proteins and leaves S910 and S935 accessible to phosphatases [97].

2.6 LRRK2 kinase substrates

During the past 13 years of LRRK2 research, much effort has been directed towards identifying LRRK2 kinase substrates, as detection of their phosphorylation status is crucial towards measuring on-target effects of LRRK2 kinase inhibitors in preclinical and clinical trials. Many proteins have been proposed as LRRK2 kinase substrates, but low stoichiometry, lack of independent validation, or lack of *in vivo* confirmation using phospho-state-specific antibodies have hampered progress in the field.

In 2016, Steger et al. used an unbiased, dual-phosphoproteomic screening approach employing MEFs (murine embryonic fibroblasts) from LRRK2-G2019S KI mice as compared to inhibitor-insensitive point mutant LRRK2 versions, and highly potent and selective LRRK2 kinase inhibitors. Using this approach, they identified a subset of proteins from the Rab GTPase family as LRRK2 kinase substrates, which comprises a breakthrough in the field [75]. Three distinct Rab proteins (Rab8a, Rab10 and Rab12) were originally identified as physiological LRRK2 substrates. Interestingly, all pathogenic LRRK2 mutants increased Rab protein phosphorylation *in vivo*. Rab proteins were phosphorylated at a very conserved residue within the switch II domain responsible for regulator and effector binding, suggesting that LRRK2 phosphorylation may affect the function of these Rab proteins.

A further systematic analysis of Rab phosphorylation by LRRK2 identified 14 distinct Rab proteins as LRRK2 kinase substrates under co-overexpression

conditions (Rab3a/b/c/d, Rab5a/b/c, Rab7L1, Rab8a/b, Rab10, Rab12, Rab35 and Rab43), from which 10 were phosphorylated under mutant LRRK2 overexpression and endogenous Rab conditions (Rab3a/b/c/d, Rab8a/b, Rab10, Rab12, Rab35 and Rab43), and 4 under endogenous LRRK2 and Rab conditions (Rab8a, Rab10, Rab35 and Rab 43) [186].

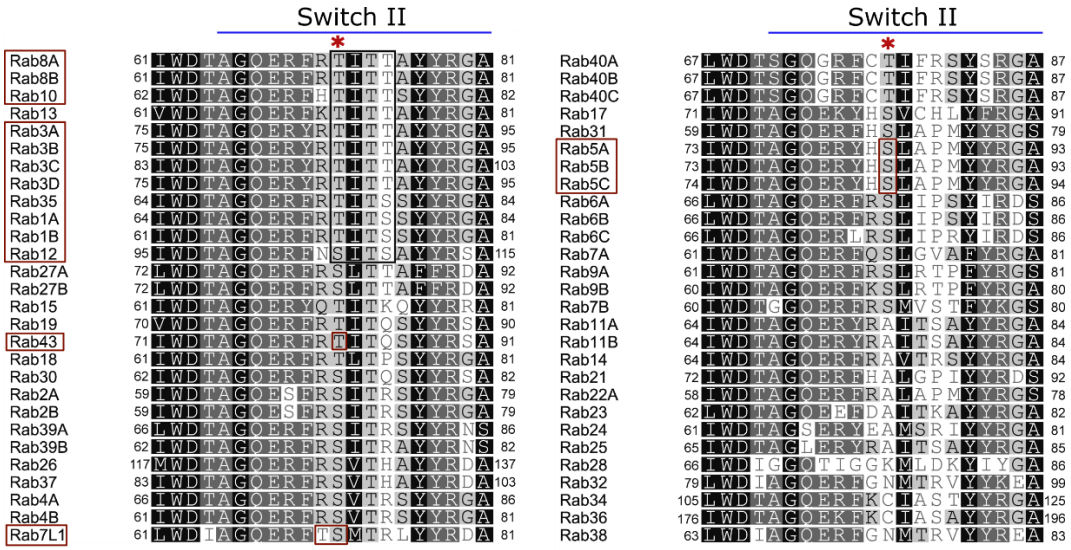

Fig. 7. Alignment of human Rab proteins. Sequences aligned with respect to the switch II region and with respect to the identified in vitro and in vivo substrates. Background color legend: Black, 100% similarity; dark gray, 80–100% similarity; light gray, 60–80% similarity; white, <60% similarity. In red blocks, the identified Rab proteins subject to LRRK2 phosphorylation. The red symbol "*" indicates the phosphorylated aminoacid within the switch II region. In black box, predicted substrates for LRRK2 phosphorylation based on the presence of TITT, TITS or SITS (T, threonine; I, isoleucine; S, serine) sequence**.**

In addition, other groups have independently validated the phosphorylation of some of these Rabs by LRRK2. For example, Rab1a/b, Rab3c, Rab8a/b and Rab35 have been recently identified as LRRK2 substrates using *in vitro* kinase assays, and when co-expressing Rabs and mutant LRRK2 in HEK293T cells, phosphorylation of these Rab proteins was confirmed, with the addition of Rab10 [187]. Rab10 and Rab12 were also confirmed as physiological LRRK2 substrates using proteomics and phosphoproteomics approaches in cultured and immune

stimulated human peripheral mononuclear blood cells treated with or without LRRK2 kinase inhibitors [188]. Similarly, using newly developed phospho-state specific antibodies [189], phosphorylated Rab10 was detected in human peripheral blood neutrophils and decreased upon LRRK2 kinase inhibitor treatment, suggesting that this readout can be used with peripheral samples from patients in clinical settings [190].

3. RAB GTPases

Rab proteins comprise the largest family of small GTPases formed by more than 60 members in humans [191, 192]. Localized to different and specific vesicular and organellar membranes, they play crucial roles in membrane trafficking events, including vesicle budding, tethering, transport and fusion [193, 194]. These proteins cycle between an active and an inactive state, which is tightly controlled by different regulators [195, 196]. In their active form, Rab proteins are bound to GTP and inserted into membranes, able to recruit their effectors with downstream effects on compartment-specific membrane trafficking events. Dependent on the specific Rab protein, effectors include sorting and tethering factors, kinases and phosphatases, and modulators of other small GTPases.

Once a Rab protein is synthesized, it is post-translationally modified at the C-terminus by prenyl groups that function as membrane anchors [197]. Most Rab proteins contain a variety of prenylation motifs such as CC, CXC, CCX, CCXX and CCXX, with C for cysteine and X for any amino acid, and generally both cysteine residues are modified by geranylgeranyl groups. The vast majority of Rab proteins are isoprenylated by geranylgeranyl transferase type II (GGTII). The prenylation motifs of the Rab proteins are insufficient for substrate recognition by GGTII, but require prior binding of unprenylated Rabs to the Rab escort proteins (REP1/2). GGTII then binds to this complex, lipid groups are transferred, GGTII dissociates and the REP/Rab protein complex is delivered to cellular membranes.

The initial membrane association of newly synthesized Rab proteins is regulated by REP proteins, but subsequent regulation of membrane association is subject to the action of Rab GDP dissociation inhibitor (GDI1/2), a protein capable of delivering and extracting prenylated Rab proteins from membranes [197].

Guanine nucleotide exchange factor proteins (GEFs) are considered the activators of Rab proteins [191]. These proteins promote the transition between a GDP-bound to GTP-bound status once Rab proteins are localized to their membranous compartment. On the contrary, conversion to their inactive forms is catalyzed by GTPase-activating proteins (GAPs), which stimulate the Rab protein GTPase activity, leading to a GDP-bound, inactive status.

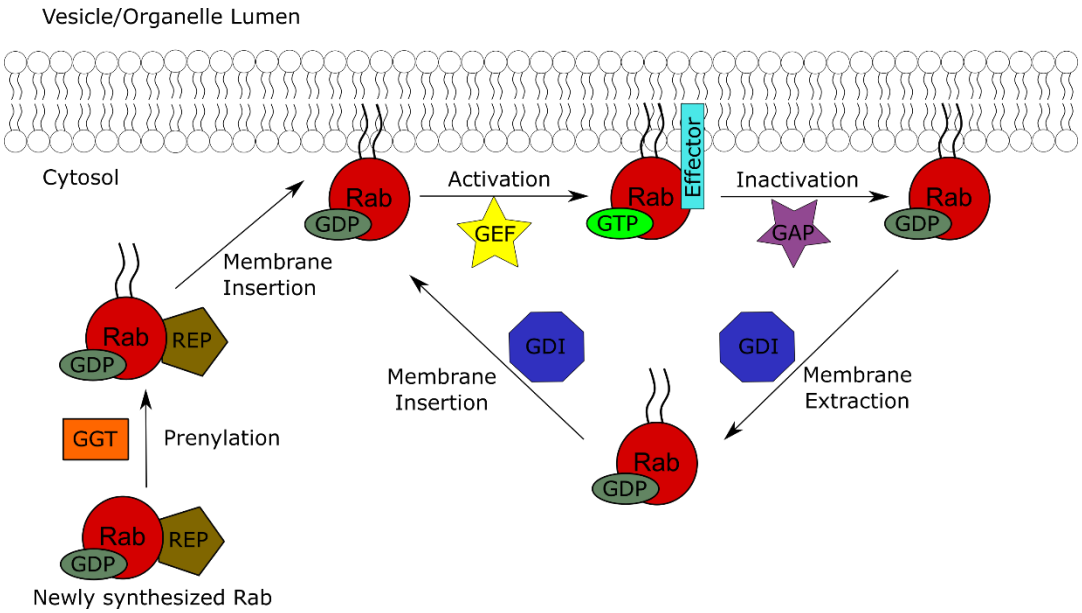

Fig. 8. Rab GTPases cycle. Upon synthesis, inactive Rab proteins are bound to REP. This complex is recognized by GGT that transfers usually two prenyl groups. GGT then dissociates, and the prenylated Rab–REP complex is delivered to membranes by REP. GEF can bind via interactions involving the switch II region and convert the Rab protein into its active, GTP-bound form capable of recruiting effector proteins. GAP promotes the conversion of GTP to GDP, and consequently promotes conversion to the GDP-Rab inactive form. Rab proteins bind to GDI1/2 via interactions involving the switch II regions and are reversibly extracted from membranes

Several GEFs have been described for different Rab proteins, in some cases cell-type specific, assuring a complex fine-control of Rab protein function [198]. However, for some Rab proteins, no GEFs have been identified to date, likely due to the existence of different GEF families and also unrelated proteins with low structure and sequence homology. On the contrary, most identified GAP proteins belong to the TBC protein family, which includes more than 40 members with a TBC domain [199]. In addition, many of these GAPs have been found to regulate many different Rabs, suggesting low specificity which would mean that most Rabs are constantly inactivated unless GEFs activate them.

3.1 Rab proteins and PD

Increasing evidence points towards a strong link between Rab protein dyshomeostasis and PD. Importantly, recent genetic studies found mutations and/or variations in distinct Rab genes that segregate with or increase risk for PD. Although large mutation screens suggest that these cases represent rare forms of PD, they provide valuable hints towards which intracellular pathways may be defective in PD.

Apart from genetic links of PD with Rab7L1 (see below), a loss of function mutation and truncated forms of Rab39B (encoding for a neuronally enriched Rab protein localized at the Golgi compartment) [200] were found to cause X-linked early-onset PD with α-synuclein pathology and intellectual disability in two distinct families [201]. Different genetic studies described additional mutations and truncations in Rab39b that also caused X-linked early-onset PD [202-204]. These mutations seem to work as loss-of-function mutations, and data further suggest that loss of Rab39B dysregulates α-synuclein homeostasis [201, 205].

Interestingly, recent studies reported increased levels of Rab35 in the serum of PD patients as compared to healthy controls. Serum levels of Rab35 correlated with the age of disease onset, with patients displaying a 5 year earlier onset when

having high levels of Rab35 [206]. Since Rab35 overexpression increased aggregation and secretion of A53T-α-synuclein, these data suggest a link between altered Rab protein functioning and protein aggregation [206]. Other links between α-synuclein and Rab proteins have emerged as well. Multiple Rab proteins (Rab1, Rab3a, Rab8a, Rab8b, Rab11a, Rab13) have been shown to interact and interfere with α-synuclein aggregation and toxicity [24, 205, 207]. In those studies, overexpression of these Rab proteins decreased α-synuclein aggregation, suggesting that their presence (and activity) exerts a protective effect, even though by a currently unknown mechanism. Altogether, current data indicate an important link between Rab proteins and PD, even though further work is needed to dissect the precise underlying molecular mechanism(s).

3.2 RAB8a, one of the major LRRK2 kinase substrates

As previously mentioned, Rab8a can interact with LRRK2, and is one of the physiological and independently validated LRRK2 kinase substrates [75, 186, 187]. All pathogenic LRRK2 mutations increase Rab8a phosphorylation *in vivo* at the T72 position, a residue that sits in the switch II motif, responsible for the interaction with various regulators and effectors. Indeed, a phosphomimetic Rab8a T72E mutant showed reduced interaction with the Rab8a GEF Rabin8. In addition, they found that phosphomimetic Rab8a T72E mutant also showed reduced interaction with GDI1/2, which is required for membrane extraction of GDP-bound Rabs [186]. At the same time, no differences in GTP binding affinities were observed between phosphomimetic and wildtype Rab8a, respectively. Together, these data suggested that GDP-bound inactive, phosphomimetic Rab8a accumulates on membranes but is not able to interact with its effectors. In contrast, another study indicated that phosphomimetic Rab mutants may display increased GTP-bound state [187]. Finally, another study using a phosphomimetic Rab10 mutant indicated that mimicking phosphorylation blocks the interaction with GAP,

suggesting that the Rab protein may remain inserted into the membrane in a GTP-bound state, but unable to interact with its effector proteins [76]. However, none of these studies determined the localization of endogenously phosphorylated Rab proteins, and the effect of LRRK2-mediated phosphorylation on Rab protein function and localization remains unclear.

i) Rab8a regulation

Several GEFs have been identified to interact with and modify the activity of Rab8a, including Rabin8 [208] GRAB [209], Mss4 [210] and C9Orf72 [211]. Rabin8 is the best described Rab8a GEF to date, and has been shown to act in a pathway that links Rab11 and Rab8 functioning in the control of polarized transport from the TGN and recycling endosomes to the plasma membrane [212]. Specifically, Rabin8 is recruited to membranes by Rab11, where it activates Rab8a, forming a Rab11-Rabin8-Rab8 cascade [212], that has been also described to act in ciliogenesis [213]. Additional regulation of this cascade implies the phosphorylation of Rabin8 by several upstream kinases, which alters its biochemical properties and interaction with Rab8a [214, 215]. Similar to Rabin8, GRAB acts as a GEF for Rab8a in the Rab11-GRAB-Rab8 cascade, playing an important role in axonal outgrowth [216]. Mss4 was suggested to be a GEF for Rab8, but the crystal structure analysis of the interaction and biochemical analysis [210, 217] suggest that Mss4 acts as a chaperone for cytosolic Rab8a rather than as a GEF. C9orf72, variations in which are the most common cause of Amyotrophic Lateral Sclerosis and Frontotemporal Dementia [218, 219], in complex with SMCR8 and WDR41 proteins, acts as GEF for Rab8a and Rab39b [211]. Interestingly, C9orf72 has recently been found to interact with Rab7L1 to regulate vesicle trafficking and Golgi integrity [220], suggesting a possible link between Rab8a, its GEF C9orf72, and Rab7L1.

Some members of the TBC protein family have been identified as GAP proteins for Rab8a, including TBC1D1, TBC1D4 and TBC1D30. However, these proteins show less specificity as compared to GEF proteins, as one protein can act as a GAP for several Rabs. For example, TBC1D1 is also a GAP for Rab2a, Rab8b, Rab10 and Rab14. Similarly, TBC1D4 also acts on Rab2a, Rab10 and Rab14. TBC1D30 is, until now, thought to be specific for Rab8a.

ii) Rab8a, recycling endosomes and polarized membrane trafficking

Receptors, ion channels and other proteins are continuously internalized via different endocytic processes. To maintain cell surface protein homeostasis, many of the internalized proteins are sorted and recycled back to the plasma membrane through recycling endosomes (RE) [221]. RE are dynamic, morphologically diverse organelles, including vesicular and pericentrosomal tubular-like membrane structures [221]. Several Rab proteins are implicated in such recycling pathways and are markers for those RE, including Rab4, Rab8a and Rab11 [222-224]. Rab8a is known to colocalize with the transferrin receptor (Tfn-R) in pericentrosomal RE [223, 225], and its activity is needed for the recycling of the Tfn-R to the plasma membrane [223].

Apart from recycling endosomes, Rab8a has also been shown to be localized to the TGN, and is involved in polarized transport of proteins to the plasma membrane. Specifically, Rab8a has been shown to be important for the polarized localization of apical proteins in intestinal epithelial cells, and together with Rab11 mediates epithelial polarization by controlling apical exocytosis [212, 226]. In this context, Rab8a at the RE can form an intermediate step between the Golgi and the polarized protein transport to the basolateral plasma membrane [227], acting as polarized sorting machinery for both the endocytic and secretory pathways. Rab6 and Rab8a double-positive vesicles have been defined to be

exocytotic vesicles that deliver secreted proteins [228], and this has been later demonstrated to be controlled by ARHGEF10 [229].

Rab8a has also been reported to regulate cell shape. For example, activation of Rab8a by its GEF Rabin8 can provoke actin remodeling and formation of polarized cell surface domains by controlling vesicle transport to these protrusions [208]. Indeed, expression of dominant-negative Rab8a mutants or depletion of Rab8a inhibit protrusion formation in HT1080 fibrosarcoma cells [223]. Finally, within neuronal cells, Rab8a has been reported to be involved in trafficking of neurotransmitter receptors in postsynaptic terminals [230]. In addition, several studies have shown a role of a Rab11-Rabin8-Rab8a cascade on axonal growth and cell migration [216, 231]. Downregulation of Rab8a led to a decrease in migration capacity of cultured Schwann cells [231]. Similarly, expression of dominant-negative Rab8a mutant led to neuronal axon shortening as compared to catalytically-active Rab8a mutants, and depletion of GRAB, a Rab8a GEF, led to migration deficits in neurons [216].

iii) Rab8a and the centrosome:

Several data indicate that Rab8a may play a role in functions related to the centrosome. The most studied phenomenon is the link between active Rab8a and ciliogenesis, a centrosome-related event (see below). Yoshimura et al. originally described that Rab8a is involved in ciliogenesis by specifically interacting with cenexin/ODF2 (cenexin3), a subdistal appendage protein localized to the basal body of cilia. Under serum starvation conditions that promote ciliogenesis, both Rab8a and cenexin 3 localized to microtubules and membrane of the cilia, and depletion of either of these two proteins abolished ciliogenesis [232]. The same year, another study independently identified Rab8a, in its GTP-bound active state, as a key regulator of the formation and extension of primary cilia. In this study, Nachury et al. showed that Rab8a locates to the basal body of cilia, and promotes

cilia elongation by vesicle delivery to the ciliary membrane. As another proof, Rab8 or Rabin8 depletion caused ciliogenesis defects [233]. Interestingly, Rab8a only accumulates on cilia at early stages of ciliogenesis, but disappears from mature cilia [232, 233]. A later study suggested that Rab8a functions in cilia formation, is upregulated by a Rab11-dependent recruitment and activation of the Rab8a-GEF Rabin8 [213, 234], and a more recent research also implicates Rab10 in ciliogenesis formation [235]. Interestingly, these Rab proteins can modify centrosomal behavior, but conversely, modification of centrosomal components can regulate and alter RE organization and function [236]. For example, Hehnly et al. showed that cenexin depletion decreases the rate of recycling, causing an accumulation of recycling endosomes (seen as Rab1-positive vesicles) around the centrosome [236]. Altogether, these studies indicate an important role for Rab8a in centrosome-related events related to ciliogenesis.

3.3 Rab7L1, one of the major LRRK2 protein interactors and PD risk factor

i) Genetics

Rab7L1 (also known as Rab29) is one of the five genes clustered within the PARK16 locus, variations in which either positively or negatively modify risk to develop PD [28, 29]. Overexpression of Rab7L1 was reported to rescue the neurite shortening induced by G2019S or R1441C-LRRK2 in primary rat neuronal cultures, and knockdown of Rab7L1 mimicked the reduction in neurite length caused by pathogenic G2019S-LRRK2 [150]. Similar results were found when testing the role of Rab7L1 overexpression or knockdown in a *Drosophila* model overexpressing G2019S-LRRK2, indicating that higher levels of Rab7L1 may be protective for PD [150]. A recent study has corroborated the positive effect of overexpressing Rab7L1 in rescuing the neurite shortening induced by pathogenic LRRK2 [237].

In contrast, another study using exome sequencing and RNA-Seq in postmortem samples found that a variant which caused lower expression of Rab7L1 was associated with a lower risk of PD, therefore suggesting that higher Rab7L1 expression correlate with higher risk for PD [45]. In agreement with these data, overexpression of Rab7L1 in primary mouse cortical neurons caused neurite shortening similar to the one caused by pathogenic LRRK2. Furthermore, the Golgi clustering and clearance observed upon LRRK2 mutations in HEK293T cells was enhanced by Rab7L1 overexpression [45]. Thus, whilst it remains unclear how Rab7L1 protein levels modulate PD risk, current genetic evidence indicates that Rab7L1 is one of the main risk loci for PD.

ii) LRRK2-mediated Rab7L1 Phosphorylation

Rab7L1 was not detected in the original phosphoproteomics screen which identified various Rab proteins as LRRK2 kinase substrates [75]. Subsequent studies have confirmed that Rab7L1 is barely phosphorylated under endogenous conditions as compared to Rab3, Rab8a, Rab10, Rab12, Rab35 and Rab43, although it is robustly phosphorylated under overexpression conditions [76, 186, 238]. In addition, it is not yet clear whether LRRK2 phosphorylates Rab7L1 on Thr71 [76], Ser72 [238], or on both residues [186]. The cellular implications of such LRRK2-mediated Rab7L1 phosphorylation remain unclear as well, even though a recent study suggests that it may alter Golgi morphology [238].

Similarly, the identity of GEFs or GAPs which regulate Rab7L1 function remains unknown. Rab7L1 has been reported to interact with C9orf72 [220], but it remains to be shown whether this interaction regulates the GTPase activity of Rab7L1. In fact, Rab7L1 may display very weak GTPase activity as compared to other Rab proteins [239], such that further studies are warranted to establish its capacity to act as a GTPase rather than a GTP-binding protein.

iii) The Rab7L1-LRRK2 interaction and effects on LRRK2 activity

What is currently most clearly established is that Rab7L1 is a main LRRK2 protein interactor, and when co-expressed in cells, causes recruitment of LRRK2 to the Golgi complex [45, 150]. Rab7L1 was found to form a complex together with LRRK2, GAK and BAG5 capable of promoting TGN removal by autophagy-dependent mechanisms, and/or structural alterations of the Golgi complex evident as "clustering" [45]. Further analysis of the regions involved in the specific interaction between LRRK2 and Rab7L1 showed that the LRRK2 ankyrin domain is responsible for the binding to Rab7L1, as point mutations (Cys727Asp, Leu728Asp, and Leu729Asp) within this domain abolish, or at least diminish, the interaction with Rab7L1 [93].

In agreement with the hypothesis that Rab7L1 acts upstream of LRRK2, two recent studies have further shown that the Rab7L1-LRRK2 interaction causes LRKK2 kinase activation, as measured by pS1292-LRRK2 autophosphorylation and by increased phosphorylation of the LRRK2 substrate Rab10. For this activation to happen, Rab7L1 needs to be anchored to the membrane, because when mutating the C-terminal cysteines to avoid prenylation and consequent integration into membranes, cytosolic Rab7L1 is not able to activate LRRK2 [76]. In addition, Rab7L1 needs to be bound to GTP to activate LRRK2 [76, 93].

iv) Cellular roles of Rab7L1

Multiple evidences indicate that LRRK2 and Rab7L1 form a functional network and act on the same cellular pathway(s). Most of these data come from KO studies in different animal models aimed at understanding the physiological role(s) of these two proteins. For example, Rab7L1-KO mice show lysosomal defects in the kidney nearly identical to those observed in the LRRK2-KO mice [83, 133, 240]. Similarly, knockdown of the LRRK2 and Rab7L1 orthologues in *C.elegans* (LRK-1 and GLO-1, respectively) were shown to produce similar defects on axonal

morphology and length [240]. Epistasis and rescue-type experiments further indicate that the Rab7L1 orthologue acts upstream of the LRRK2 orthologue in the same pathway that controls axonal morphology in specific *C. elegans* neurons [240]. Whilst further work is required to elucidate the precise cellular pathway(s) modulated by Rab7L1, there exists strong evidence for a Rab7L1-LRRK2 cascade *in vitro* and *in vivo*.

Rab7L1 has also been shown to modulate the effects on neurite shortening caused by pathogenic LRRK2. However, as discussed above, results have led to contradictory conclusions as to the positive or negative effects of Rab7L1 overexpression, with some studies showing a rescue of the neurite shortening caused by pathogenic LRRK2 [150, 237], and another study indicating that Rab7L1 overexpression on its own causes neurite shortening [45].

Rab7L1 has been observed at the Golgi apparatus, at both the cis-medial compartment [150, 241] and the TGN [45, 152]. Rab7L1 has been proposed to play a role in Golgi integrity, although different studies show contradictory results [45, 150, 152]. One study showed that knocking down Rab7L1 or expressing dominant-negative inactive Rab7L1-T21N mutant caused Golgi fragmentation [152]. On the contrary, two different studies failed to find significant changes in Golgi morphology after Rab7L1 depletion [150, 242]. As a third observation, Beilina et al. found that Rab7L1 overexpression caused clustering of the Golgi complex and/or autophagy-lysosome dependent TGN clearance, whilst depletion of Rab7L1 had no effect on Golgi morphology [45]. Rab7L1 and LRRK2 co-expression further increased the TGN clustering caused by single Rab7L1 or LRRK2 expression, again suggesting that both proteins act on the same pathway [45].

Finally, Rab7L1 has been shown to modulate retrograde transport of certain receptors from endolysosomes to the Golgi apparatus. Rab7L1 knockdown caused a significant reduction in lysosomal and Golgi accumulation of mannose 6-phosphate receptors (M6PR) [150, 152], phenocoping the MP6R missorting

phenotype caused by knockdown of the retromer complex unit VPS35 or by pathogenic LRRK2 expression [150]. Knockdown of Rab7L1 also provoked a reduction in the levels of VPS35 and VPS29 [150], suggesting that Rab7L1 is required for retromer complex formation.

4. CENTROSOME

The centrosome is a non-membranous organelle consisting of two centrioles surrounded by pericentriolar material (PCM). Each centriole is composed of nine MT triplets forming a cylinder-like structure, with defined intra- (cartwheel structure) and inter- (centrioles are perpendicular to each other) symmetry and length. One of the centrioles, the older one, is called the mother centriole, and presents sub-distal and distal protein appendages which are thought to play a role in MT anchoring. The PCM is a highly organized matrix of proteins, including cell cycle regulators and signaling molecules, and is especially enriched in pericentrin, involved in the initial establishment of MT [243], and γ-tubulin ring complexes (γTuRCs), large protein complexes which serve as MT nucleation sites [244].

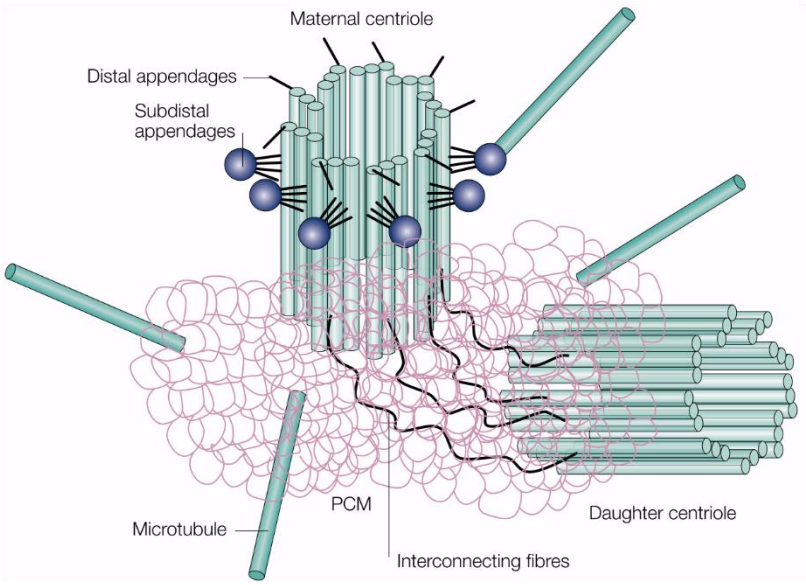

Fig. 9. Centrosome structure. From [245]

The centrosome acts as the major MTOC in most cells, playing an important role in cell polarity, shape and migration, and also forming the poles of the bipolar spindle during mitosis. Additionally, the centrosome acts as a signaling center. Since the mother centriole forms the basal body of the primary cilium, the centrosome is intimately related to ciliogenesis, further supporting its role in cell signaling events [246].

4.1 The centrosome along the cell cycle

During interphase, the centrosome displays the above-described organization, with a pair of centrioles engaged orthogonally to each other. During S-phase, the centrosome duplicates, forming two (immature) centrosomes which are tightly bound together by a proteinaceous linker [247]. Specifically, each centriole of the original centrosome serves as a template for the formation of the new centrioles. In this way, the new centrosome formed at the original mother centriole is called the mother centrosome, and the other new centrosome formed at the original daughter centriole is called the daughter centrosome. During G2, duplicated centrosomes undergo a process of maturation whereby they accumulate PCM, increase in size, and whereby the original daughter centriole acquires the sub-distal and distal appendages. During G2, duplicated centrosomes are microscopically discernible, and keep being held together by the same proteinaceous linker (also called “centrosome cohesion”) [247]. At the G2-to-M transition, the proteinaceous linker dissociates, and both centrosomes separate (a process called “centrosome splitting” or “centrosome separation”) to eventually form, in M phase, the poles of the mitotic bipolar spindle [244]. After cell division, each cell receives one of the two fully mature centrosomes.

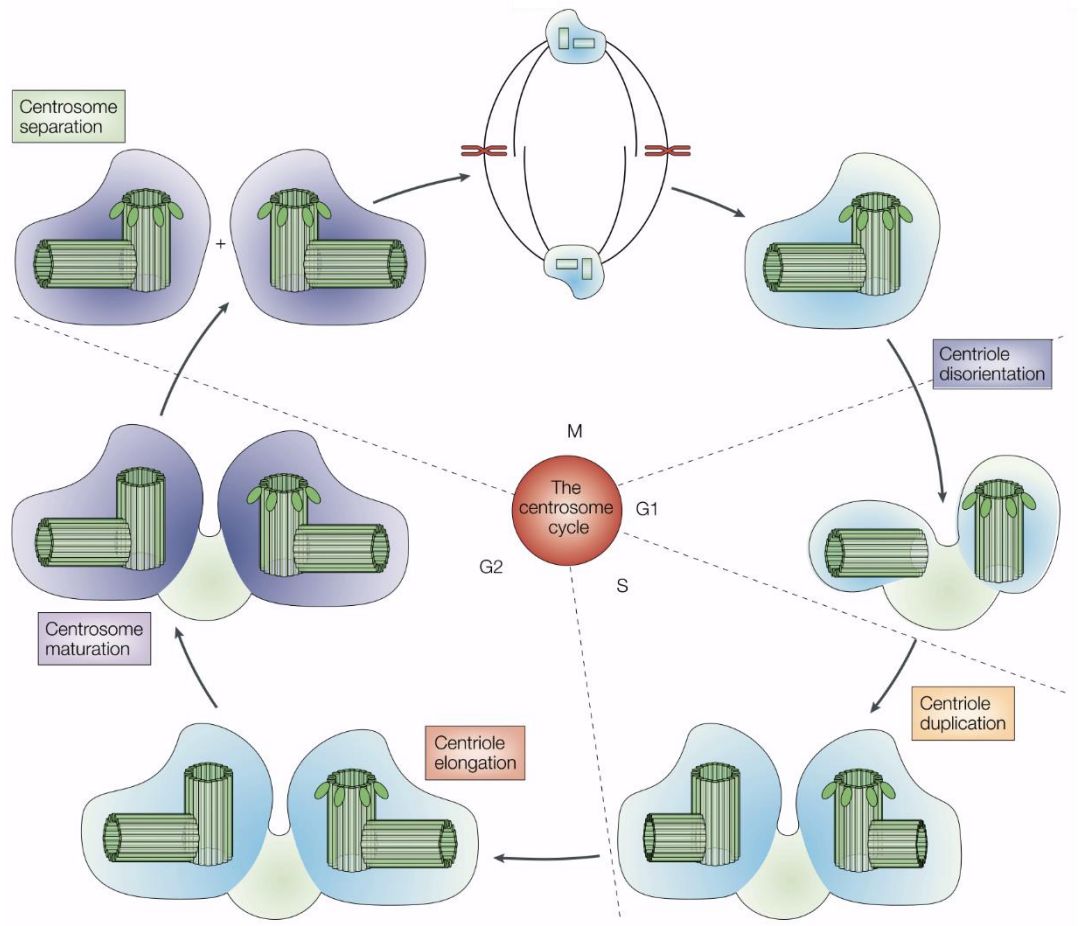

Fig. 10. Centrosome cycle. From [248]

All these processes are tightly regulated by complex regulatory pathways. In particular, centrosome cohesion is mediated by a proteinaceous linker composed of several proteins, including rootletin, C-Nap1, Cep68, Cep135, LRRC45 and Cdk5Rap2 [247, 249]. Under normal conditions, at the G2-M transition, Nek2A phosphorylates both C-Nap1 and rootletin, promoting their dissociation from the centrosome and leading to centrosome splitting [250, 251]. Depletion of C-Nap1 or rootletin [252, 253], or overexpression of Nek2 [254], leads to centrosome splitting in early G2 phase, a process called “premature centrosome splitting”, in which immature centrosomes are separated before the G2-M transition. The kinesin-5 motor protein Eg5 cooperates with Nek2 in the centrosomal separation process

initiating the motor-driven process [255]. Again, the spatio-temporal control of Eg5 on this process is tightly controlled by several kinases including Plk1 [256]. Similar to Eg5, dynein also acts as a motor protein involved in centrosome separation [257].

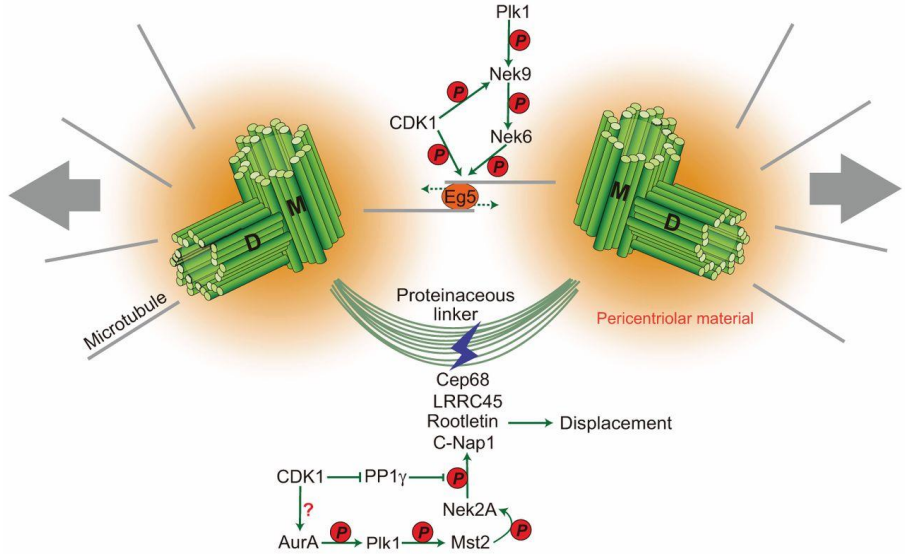

Fig. 11. Centrosome separation mechanisms. From [258]

4.2 Centrosomal functions

The centrosome is the major MTOC in most animal cells. Different components of the PCM, mainly γTuRCs are responsible for its MT nucleation capacity [259], whilst sub-distal and distal appendages of the mother centriole, including ninein, are responsible for MT anchoring [260]. MTs usually show a radial distribution from the centrosome towards the cell periphery.

The centrosome is also important for cell polarity, defined by the asymmetric accumulation of molecules, proteins or organelles within the cell and by the polarized distribution of cytoskeletal components. In many cell types, centrosome positioning contributes to the establishment of cell polarity [261, 262]. Generally, the centrosome occupies a central position within the cell, and the pericentrosomal positioning of the nucleus, Golgi apparatus and recycling

endosomes depends on MT organization mediated by the centrosome, including in differentiating neurons, where centrosome positioning precedes axon formation [263]. Such cell polarization is a pre-requisite for many cellular processes, including cell migration. In most migrating cells, the centrosome and Golgi apparatus re-orient towards the leading edge of the cells, which establishes the directionality of migration, including in neurons [264]. Interestingly, differentiating neurons expressing pathogenic LRRK2 have been reported to display reduced neurite number and arborization [126, 129], and pathogenic LRRK2-expressing cells such as mouse fibroblasts, microglia and rat myeloid cells have been reported to display alterations in migration capacity [265-267], suggesting a link between LRRK2 and altered cell polarity.

In dividing cells, centrosomes play an important role for mitotic spindle formation which ensures proper cell division and chromosome segregation [268]. As such, centrosomal abnormalities have been observed in several human diseases, most notably cancer [269, 270]. Centrosomal alterations, mainly events associated to centrosome over-amplification, are known to cause chromosome instability, which is observed in many human cancers [269]. Interestingly, LRRK2-PD patients have been reported to have a higher propensity to develop certain types of cancers [271-273]. Whilst the mechanism(s) underlying this association remains unknown, these findings suggest that pathogenic LRRK2 may also play a detrimental role in dividing cells, possibly at the level of centrosomal alterations.

Finally, the centrosome is also crucial for ciliogenesis. The mother centriole constitutes the basal body of the primary cilium [274], an antenna-like organelle with critical roles in cell signaling [275], and defects in cilia formation and/or function are the cause of a series of diseases called ciliopathies [276]. Nucleating from the centriole-derived basal body, the MT-based ciliary axoneme protrudes from the surface surrounded by the ciliary membrane, which is a continuum of the plasma membrane, but with a specific lipid and protein composition [277]. The

primary cilium is a non-motile, single-copy organelle present in many cell types with important functions in sensory perception and different signaling pathways [275]. Interestingly, neuronal cilia accumulate G protein-coupled receptors, including D1, D2 and D5-type dopamine receptors [278, 279], implicating cilia in neuronal dopamine signaling. In addition, a link between LRRK2 and cilia-related signaling pathways including Wnt signaling has been proposed [280-282], even though further studies are needed to correlate those events to possible pathomechanisms underlying PD.

Given the above-mentioned phenotypes observed in LRRK2 models and LRRK2-PD patients possibly related to centrosome dysfunction, and the link between LRRK2 and Rab8a, and between Rab8a and the centrosome, the present work attempts to discern a possible connection between pathogenic LRRK2, its substrate Rab8a and centrosomal alterations. In addition, due to the interaction between LRRK2 and Rab7L1, a risk variant for PD, the study aims to elucidate the contribution of Rab7L1 to LRRK2 pathogenicity.

II. OBJECTIVES

1. Evaluate the effects of pathogenic LRRK2 on centrosome positioning and its implications on neurite length, differentiation capacity and cell polarization in differentiated SH-SY5Y cells.
2. Determine the consequences of pathogenic LRRK2-mediated cell polarization alterations on directed migration in differentiated SH-SY5Y cells
3. Study the centrosome behavior upon pathogenic LRRK2 expression in dividing SH-SY5Y and HEK293T cells.
4. Asses the implication of LRRK2-kinase activity on centrosome behavior.
5. Analyze and compare the centrosome behavior in two distinct peripheral cell types from LRRK2 PD patients and healthy controls.
6. Investigate the role of the centrosome-related Rab8a protein on the pathogenic LRRK2-mediated centrosomal deficits.
7. Evaluate the phosphorylation of Rab8a by widltype and pathogenic LRRK2 upon different nucleotide binding state.
8. Asses the nucleotide binding/retention and effector-interaction capacity of phosphomimetic Rab8a mutants.
9. Evaluate the effects of phosphomimetic Rab8a on centrosome cohesion.
10. Analyze the centrosome behavior in the context of sporadic PD by increasing levels of the risk factor Rab7L1.
11. Determine Golgi integrity dependency for the centrosomal alterations caused by either pathogenic LRRK2 or wildtype LRRK2 and Rab7L1 co-expression.
12. Study the implication of LRRK2 kinase activity on the centrosomal behavior upon wildtype LRRK2 and Rab7L1 co-expression.
13. Investigate the role of Rab8a and its phosphorylated form on the centrosomal defects caused by wildtype LRRK2 and Rab7L1 co-expression.

III. MATERIALS AND METHODS

Cell culture and transfections

SH-SY5Y cells stably expressing GFP, flag-tagged wildtype LRRK2, or flag-tagged G2019S-mutant LRRK2 were cultured as described [283, 284]. Briefly, cells were grown in full medium (Dulbecco´s modified Eagle´s medium containing high glucose and 15 % fetal bovine serum, non-essential amino acids, 50 µg/ml gentamycin (Life Technologies) and 200 µg/ml hygromycin B (Invivogen), and subcultured at a ratio of 1:6 twice a week. Transfection of cells was carried out at 80% confluence with 0.4 µg DNA and 1.5 µl Lipofectamine 2000 (Invitrogen) per well of a 24-well plate in 200 µl OptiMEM. Five h later, cells were changed into full medium, and passaged the following day at a ratio of 1:5 onto coverslips, followed by fixation and staining 72 h after transfection. For differentiation, 10,000 cells were plated onto coverslips in 24-well plates and grown in full medium for 24 h to allow for proper attachment. Cells were then changed to medium containing 3 % fetal bovine serum and 10 µM retinoic acid (Sigma), and differentiated during 5 days, with medium changed every 48 h.

HEK293T cells were cultured as described [140, 145] and transfected at 80 % confluence with 2 µg of LRRK2 constructs (and 200 ng of Rab constructs where indicated) and 6 µl of LipoD293 (SignaGen Laboratories) per well of a 6 well plate for 5 h in full medium. Cells were split to 20 % confluence the following day, and processed for immunocytochemistry or Western blot analysis 24 h later.

HELA cells were cultured as previously described [145]. Cells were plated in 6-wells plates at 40 % confluence, and transfected the following day with 400 ng of GFP-tagged Rab8a constructs and 5 µl of Lipofectamine 2000 according to manufacturer´s instructions in full medium overnight. The following day, cells were split at a 1:4 ratio, plated onto coverslips, and processed 24 h later.

Primary human skin fibroblasts established from skin biopsies taken from five age- and sex-matched healthy control and five PD patients with the G2019S

mutation [145], with informed consent and ethical approval, were grown in IMDM and 10 % fetal bovine serum, with media changed every two days. Cells were subcultured at a ratio of 1:4, and seeded at equal densities on coverslips. All analyses were carried out on passages 3-8, and no passage-dependent differences were observed.

For lymphoblast generation, three healthy control and three PD patients due to the G2019S LRRK2 mutation were recruited at the Movement Disorders Unit of Lille University Medical Center (Lille, France, CPP Nord-Ouest 2008/09), with the two groups matched according to age and gender. Blood samples were collected in BD Vacutainer CPT Cell Preparation Tubes containing sodium heparin (Le Pont-de-Claix, France). The peripheral blood mononuclear cells (PBMCs) were collected and processed according to supplier´s recommendations. Lymphocytes were immortalized by infection with Epstein-Barr virus (EBV) as described [285]. Briefly, cell lines were established from freshly isolated lymphocytes or from cryopreserved lymphocytes using standard EBV transformation protocols that include cell separation by gradient centrifugation and lymphocyte growth enhancement by the mitogen phytohemagglutinin. Cell lines were maintained in RPMI 1640 medium supplemented with 20 % fetal bovine serum, L-glutamine, 20 units/ml penicillin and 20 μg/ml streptomycin in T75 flasks in 5 % CO_2 at 37°C. Cells were maintained at a density of 10^6 cells/ml, with cell density monitored every other day using trypan blue staining.

Where indicated, cells were treated with nocodazole (200 nM, 2 h, SigmaAldrich), brefeldin A (5 μg/ml, 2 h, SigmaAldrich), or the indicated concentrations of the LRRK2 kinase inhibitors for 1 hour, MLi-2 (MRC PPU, Dundee, UK), LRRK2-IN1 (obtained through the MJFF) or GSK2578215A (Tocris) before fixation.

DNA constructs and site-directed mutagenesis

GFP-tagged human LRRK2 constructs were obtained from Addgene. Where required, mutations were introduced by site-directed mutagenesis (QuikChange, Stratagene). The GFP-G2019S-K1906M kinase-dead LRRK2 construct was generated by site-directed mutagenesis introducing K1906M on top of the G2019S construct, and the identity of constructs verified by sequencing of the entire coding region. DNA was prepared from bacterial cultures grown at 28°C using a midiprep kit (Promega) according to manufacturer´s instructions.

Human GFP-tagged Rab8a, Rab8a-Q67L and Rab8a-T22N, as well as human GFP-tagged Rabin8 were obtained from Addgene. mRFP-tagged or triple-flag (3xFlag)-tagged Rab8a constructs were generated using Gibson Assembly Master Mix (New England Biolabs). Rab8a-T72A, Rab8a-T72D and Rab8a-T72E mutant constructs were generated by site-directed mutagenesis (QuikChange, Stratagene).

The siRNA-resistant forms of mRFP-Rab8a and mRFP-Rab8a-T72A were generated by introducing 3 silent mutations into the target sequence of the seed region of the Rab8a siRNA (Silencer Select Rab8a (Ambion, ThermoFisher, ID s8679, nr 4390824). Specifically, the original sequence of the mRFP-Rab8a plasmids (5´-GCAAGAGAATTAAACTGCA-3´) was mutated to 5´-GCAAGAGAATTAAGTTACA-3´). Identity of all constructs was verified by sequencing of the entire coding region. HttQ74-GFP was a generous gift from D. Rubinsztein (Cambridge University, UK).

mRFP-Rab7 and human dsRed-Rab9 were from Addgene, and human EGFP-Rab7L1 was kindly provided by Dr. J. Galán (Yale University School of Medicine, New Haven, USA). Human dsRed-Rab9 obtained from Addgene (containing two Rab9 sequences) was properly re-derived into pdsRed-Express-C1 (Clontech, #632430) by Gibson Assembly Master Mix (New England Biolabs). Human mRFP-Rab7L1 was generated by PCR amplification of the Rab7L1 coding

sequence using EGFP-Rab7L1 as template, followed by subcloning into an mRFP vector backbone using XhoI-HindIII restriction enzyme sites. All triple-flag (3xFlag)-tagged Rab constructs, as well as GFP-tagged Rab7 and Rab9 constructs were generated using Gibson Assembly Master Mix (New England Biolabs). The Rab7 Q67L and T22N mutants, Rab9 Q66L and S21N mutants and Rab7L1 Q67L and T21N mutants were generated by site-directed mutagenesis (QuickChange, Stratagene), and the identity of all constructs was verified by sequencing of the entire coding region.

Immunofluorescence and laser confocal imaging

HEK293T cells were fixed using 2 % paraformaldehyde (PFA) in PBS for 10 min at room temperature, followed by permeabilization in MeOH for 2 min at -20°C. Cells were subsequently incubated in PBS containing 50 mM NH_4Cl for 10 min [286], and then permeabilized with 0.2 % Triton-X100/PBS for 20 min. For determination of the size of pericentrin-positive structures and for phospho-Rab8a staining, the MeOH and NH_4Cl steps were omitted.

HELA cells expressing GFP-tagged Rab8a constructs were fixed using 4 % PFA in PBS for 15 min at room temperature, permeabilized with 0.5 % Triton-X100/PBS for 5 min, rinsed in PBS, and mounted with mounting medium containing DAPI.

SH-SY5Y cells were fixed using 2 % paraformaldehyde (PFA) in PBS containing 4 % sucrose for 20 min at room temperature, followed by permeabilization with 0.2 % Triton-X100/PBS for 20 min.

Primary fibroblasts were fixed with 2 % paraformaldehyde (PFA) in PBS for 10 min at room temperature, followed by permeabilization with 0.2 % Triton-X100/PBS for 20 min.

For lymphoblast immunocytochemistry, 13 mm diameter coverslips were placed into 24-well plates and coated with Cell-Tak Cell and Tissue Adhesive

solution (Corning) following manufacturer´s protocols. After 20 min at room temperature, the solution was removed, coverslips were rinsed twice with distilled water and air-dried. Lymphoblast cells (200.000 per well) were added to dry coated coverslips, and cells attached by slight centrifugation at 690 g for 10 min at room temperature (without brake). Lymphoblast cells were fixed using 2 % PFA in PBS for 20 min at room temperature, followed by permeabilization with 0.2 % Triton-X100/PBS for 20 min at room temperature.

After fixation and permeabilization, coverslips were blocked for 1 h with 0.5 % (w/v) BSA in 0.2 % Triton-X100/PBS (blocking solution), followed by incubation with primary antibodies in blocking solution overnight at 4°C. Primary antibodies included rabbit polyclonal anti-pericentrin (Abcam, ab4448, 1:1000), mouse monoclonal anti-pericentrin (Abcam, ab28144, 1:1000), mouse monoclonal anti-γ-tubulin (Abcam, ab11316, 1:1000), mouse monoclonal anti-c-Myc (Sigma, clone 9E10, M4439 1:500), mouse monoclonal anti-flag (Sigma, clone M2, 1:500), rabbit polyclonal anti-Rab8a (Millipore, ABC423, 1:1000), rabbit monoclonal anti-Rab8a (Abcam, ab188574, 1:1000), rabbit polyclonal anti-T72-phospho-Rab8a (1:500, generous gift of D. Alessi, University of Dundee, UK), mouse anti-Golgin97 (Molecular Probes, A-21270, 1:100), rabbit polyclonal anti-β-COP (Invitrogen, PA1-061, 1:750), and mouse monoclonal p230/Golgin-245 (Becton Dickinson, 611280, 1:400). The sheep polyclonal anti-Rab8a and anti-T72 phospho-Rab8a antibodies have been previously described (MRC PPU, S969D and S874D, respectively) [75]. For the sheep anti-Rab8a antibody, the NH_4Cl step was omitted, and for the sheep anti-T72-phospho-Rab8a antibody, both the MeOH and NH_4Cl steps were omitted. Sheep antibodies were used at a 1:50 dilution, and the anti-T72-phospho-Rab8a antibody was used in the presence of a 10-fold molar excess of dephospho-peptide, or of phospho-peptide where indicated. Importantly, all double- and triple-immunocytochemistry involving sheep antibodies were performed sequentially, with the sheep antibodies employed first.

Secondary antibodies included Alexa 405-conjugated goat anti-mouse or goat anti-rabbit, Alexa 488-conjugated goat anti-mouse or goat anti-rabbit, Alexa 594-conjugated goat anti-mouse or goat anti-rabbit, Alexa 633-conjugated goat anti-mouse or goat anti-rabbit (Invitrogen, 1:1000), Alexa 488-conjugated donkey anti-sheep (Invitrogen, 1:1000) or Alexa 594-conjugated donkey anti-sheep (Abcam, 1:1000). As indicated, cells were either mounted using mounting medium containing DAPI (Vector Laboratories), or incubated with TO-PRO-3 Iodide (642/661) (Invitrogen, 1:1000) for 3 min, followed by washes in PBS before mounting in ProLong Gold Antifade mounting medium (Invitrogen).

Images were acquired on a Leica TCS-SP5 confocal microscope using a 63X 1.4 NA oil UV objective (HCX PLAPO CS). Images were collected using single excitation for each wavelength separately and dependent on secondary antibodies (405 nm UV diode and a 415-455 nm emission band pass; 488 nm Argon Laser line and a 510-540 nm emission band pass; 543 HeNe Laser line and a 600-630 nm emission band pass; 633 HeNe Laser line and a 640-670 nm emission band pass). GFP-tagged proteins were excited with 488 nm Argon Laser line and a 500-530 nm emission band pass, and RFP-tagged proteins with 543 nm HeNe Laser line and a 560-590 nm emission band pass, respectively. DAPI was excited with the 405 nm UV diode and a 430-480 nm emission band pass, and TO-PRO with 633 nm HeNe Laser line and a 650-675 nm emission band pass, respectively.

10-15 image sections of selected areas were acquired with a step size of 0.5 μm, and z-stack images analyzed and processed using Leica Applied Systems (LAS AF6000) image acquisition software. The same laser intensity settings and exposure times were used for image acquisition of individual experiments to be quantified.

For quantification of centrosome size, a circle was drawn around individual centrosomes and area quantified using image acquisition software as described

above, where mature centrosomes were around 1 μm^2, and immature centrosomes around 0.5 μm^2.

Centrosomes were scored as being separated when the distance between their centers was > 1.5 μm (for HEK293T and SH-SY5Y cells) as analyzed by ImageJ software. For fibroblasts, the mean distance between separated centrosomes in control cells was 2.25 ± 0.2 μm (mean ± s.e.m., n=10 cells), and centrosomes scored as being separated when the distance was > 2.5 μm. Using equivalent criteria for lymphoblasts, centrosomes were scored as being separated when the distance was > 1.3 μm. In all cases, mitotic cells were excluded from this analysis.

Quantification of the phospho-Rab8a signal in SH-SY5Y cells was done over non-processed and non-saturated images acquired during the same day with the same laser intensities. Quantification was performed with Leica Applied Systems (LAS AF6000) image acquisition software. Circular ROIs of 2.2 μm width and 2.2 μm height were set on top of the centrosomal signal, and mean intensity from the phospho-Rab8a signal obtained from at least 50 cells per condition and experiment. Background signal was subtracted in all cases by placing the ROI in a different random place within the same cell. Similarly, to quantify phospho-Rab8a signals in lymphoblasts, a circle of 3 μm diameter was drawn around individual centrosomes as assessed by pericentrin staining, and the phospho-Rab8a fluorescence intensity from around 30-50 individual cells quantified from maximal intensity projections using Leica Applied Systems (LAS AF6000) image acquisition software.

Total and phospho-Rab8a signals in the presence of Rab7L1 were scored as present or absent over non-processed and non-saturated images acquired during the same day with the same laser intensities, and around 100 transfected cells quantified per condition per experiment. Most experiments were quantified by an additional observer blind to conditions, with similar results obtained in all cases.

Re-localization of LRRK2 to the Rab7L1 compartment in HEK293T and SH-SY5Y cells was quantified visually as being recruited/not recruited, as no intermediate phenotypes could be observed. At least 50 transfected cells per condition were analyzed in at least three independent experiments.

Most experiments were quantified by two independent observers, and some experiments were quantified by a third observer blind to condition, with similar results obtained in all cases.

Knockdown of Rab8a or Rab7L1 by RNA interference

HEK293T cells were seeded in 6-well plates at 30-40 % confluence one day prior to transfection such that they were at a confluence of 70-80 % the following day. They were transfected with 2 μg of GFP-LRRK2 DNA and 25 nM siRNA using 4 μl of jetPRIME Transfection Reagent (Polyplus-Transfection SA, nº 114-15) in 200 μl jetPRIME buffer. The mix was incubated for 15 min at room temperature and added to 2 ml of full medium per well of a 6-well plate overnight. For the experiments where two different RNAi reagents were used simultaneously, cells were transfected with 40 nM siRNA (20 nM siRNA 1 + 20 nM siRNA 2) using 4 μl of jetPRIME Transfection Reagent (Polyplus-Transfection SA, nº 114-15) in 200 μl jetPRIME buffer.

For knockdown experiments in the presence of both GFP-LRRK2 and mRFP-Rab8a or mRFP-Rab8a-T72A (sensitive or resistant to siRNA, respectively), cells were transfected with 50 nM of the indicated siRNA using 4 μl of jetPRIME Transfection Reagent as described above. Four hours later, media was replaced and cells transfected with 2 μg of the indicated LRRK2 constructs and 200 ng of the indicated Rab8a constructs and 6 μl of LipoD293 (SignaGen Laboratories) per well of a 6-well plate overnight in full medium. In all cases, cells were passaged 24 h later and processed for Western blot analyis or immunocytochemistry 48 h after transfection.

RNAi reagents included Silencer Select Negative Control no. 1 siRNA (Ambion, ThermoFisher, cat. nr 4390843; 50 nM) Silencer Select Rab8a (Ambion, ThermoFisher, ID S8679), Silencer Select Rab8a (Ambion, ThermoFisher, ID S8680), Silencer Select Rab7L1 (Ambion, ThermoFisher, ID S17082) and Silencer Select Rab7L1 (Ambion, ThermoFisher, ID S17083).

For determination of Rab8a or Rab7L1 levels, cells were washed in PBS and resuspended in cell lysis buffer (1 % SDS in PBS containing 1 mM PMSF, 1 mM Na_3VO_4, 5 mM NaF). Extracts were sonicated, boiled and centrifuged at 13,500 rpm for 10 min at 4 ºC. Protein concentration of supernatants was estimated using the BCA assay (Pierce), and 30 μg of extracts resolved by SDS-PAGE and analyzed by Western blotting.

Wound healing and cell migration assays

For wound-healing assays, 40,000 SH-SY5Y cells were seeded on each side of 35 mm insert-containing dishes (IBIDI) and grown to confluence in full medium. The wound (500 μm diameter) was generated by removing the insert, cells were gently washed three times in full medium, and phase contrast images acquired every 10 min for 15 h on a Leica TCS-SP5 confocal microscope using a 10X objective (C-PLAN 10.0x0.22 POL) and 1.3X zoom. Overall wound healing migration speed was calculated as average speed of the cell front using ImageJ software analysis. For single cell tracking, individual cells in the first row facing the wound were tracked (ImageJ manual tracking plugin) until reaching the middle of the wound [287], and individual cell migration speed, directionality (D) and forward migration index in Y (FMI Y) calculated from at least 30 cells per condition and experiment using the Chemotaxis and Migration Tool (IBIDI).

For determination of cell polarity, cells were processed for immunocytochemistry 4 h after generating the wound using anti-pericentrin and anti-golgin97 antibodies as described above. The first row of cells facing the

wound was analyzed, and cells were scored as polarized when located in a 90° sector emerging from the center of the nucleus and facing the wound edge [288]. Basal levels of expected random orientation of 25 % were confirmed by analyzing centrosome orientation immediately after generating the wound.

Cell extracts and Western blotting

HEK293T and SH-SY5Y cells were collected 48 h after transfection, washed in PBS and resuspended in cell lysis buffer (1 % SDS in PBS containing 1 mM PMSF, 1 mM Na_3VO_4, 5 mM NaF). Extracts were sonicated, boiled and centrifuged at 13,500 rpm for 10 min at 4°C. Protein concentration of supernatants was estimated using the BCA assay (Pierce), and 40 μg of extracts resolved by SDS-PAGE and analyzed by Western blot.

The following primary antibodies were used to develop the Western blot: rabbit polyclonal anti-GFP antibody (ab6556, 1:3000, Abcam), phospho-S935 LRRK2 antibody (ab133450, Abcam, 1:500), mouse monoclonal anti-myc antibody (clone 9E10, 1:1000, Sigma), sheep polyclonal anti-Rab8a (MRC PPU, S969D, 1:200), sheep polyclonal anti-phospho-Rab8a (MRC PPU, S874D, 1:200), rabbit monoclonal anti-Rab8a antibody (ab188574, Abcam, 1:1000), rabbit polyclonal phospho-Rab8a antibody (1:500, generously provided by D. Alessi, University of Dundee, UK), sheep polyclonal anti-Rab7L1 (MRC PPU, S984D, 1:250), mouse monoclonal anti-flag antibody (clone M2, 1:2000, Sigma), mouse monoclonal anti-GAPDH (ab9484, 1:2000, Abcam) and mouse monoclonal anti-tubulin antibody (clone DM1A, 1:10,000, Sigma) as loading controls.

For lymphoblast cell extracts, 10^6 cells were centrifuged at 300 g for 10 min at 4 °C. The pellet was resuspended in 100 μl of lysis buffer (20 mM Tris-HCl pH 7.4, 150 mM NaCl, 1 mM EDTA, 10 % glycerol, 1 % Triton-X100) containing protease and phosphatase inhibitor cocktails (SigmaAldrich), and incubated for 30 min on a rotary wheel at 4 °C. Cell extracts were centrifuged at 13,500 rpm for

5 min at 4 ºC, and supernatants quick-frozen in liquid N_2 and stored at -80 °C. Protein concentration of supernatants was estimated using the BCA assay (Pierce), and 20 µg of extracts resolved by SDS-PAGE and analyzed by Western blot, using a rabbit polyclonal phospho-S935-LRRK2 antibody (ab133450, Abcam, 1:500), a mouse monoclonal anti-LRRK2 antibody (UC Davies/NIH NeuroMab clone 75-253, 1:1000), a sheep polyclonal anti-Rab8a (MRC PPU, S969D, 1:200) and a mouse monoclonal anti-tubulin antibody (clone DM1A, 1:10,000, Sigma) as loading control.

Some Westerns were developed with ECL reagents (Roche), and a series of timed exposures to ensure that densitometric analyses were performed at exposures within the linear range. Quantification was performed using QuantityOne software (BioRad). Western blotting of phospho-S935 and total LRRK2 in extracts from lymphoblasts was performed with ECL Prime Western Blotting Detection Reagent (GEHealthcare), and analysis in Amersham Imager 600 (GEHealthcare).

The majority of Western blotting was performed according to the protocol described by LI-COR for Near-Infrared Western Blot Detection. In all cases, incubation with primary antibodies was performed overnight at 4 ºC, and secondary antibodies were incubated for 1 h at RT. Blots were imaged using an Odyssey CLx system, and quantification was done using the instrument´s Image Studio software.

Co-Immunoprecipitation

For co-immunoprecipitation of Rab proteins with LRRK2, HEK293T cells were cultured as described and co-transfected at 80 % confluence with 2 µg of LRRK2 constructs and 200 ng of Rab constructs as indicated, and 6 µl of LipoD293 (SignaGen Laboratories) per well of a 6-well plate for 5 h in full medium.

For co-immunoprecipitation of Rabin8 with Rab8a, HEK293T cells were cultured as described and co-transfected at 80 % confluence with 600 ng of

GFP-Rabin8 and 200 ng of flag-tagged Rab8a constructs using 6 µl of LipoD293 (SignaGen Laboratories) per well of a 6-well plate overnight in full medium.

In both cases, the following day, cells were split into 100 mm tissue culture plates, and were collected 48 hours after transfection. Cells were washed in PBS, followed by resuspension in 1 ml of lysis buffer (50 mM Tris-HCl, pH 7.6, 150 mM NaCl, 2 mM $MgCl_2$, 1 % Triton-X100, 1 mM DTT, protease inhibitor cocktail (Roche) and phosphatase inhibitor cocktail 3 (Sigma)), and incubated on a rotary wheel for 1 h at 4ºC. Lysates were subsequently spun at 13.000 rpm for 10 min at 4 ºC, and protein concentration of supernatants estimated by BCA assay (Sigma), with 1 mg of total protein subjected to immunoprecipitation with a rabbit polyclonal anti-GFP antibody (Abcam, ab6556, 1 µg per sample). Lysates were incubated with antibody for 2 h at 4ºC, followed by addition of protein G Sepharose Fast Flow (Amersham) and incubation overnight at 4 ºC. The next day, beads were washed three times with lysis buffer, and bound proteins eluted with Laemmli sample buffer and heating at 95ºC for 4 min prior to separation by SDS-PAGE and Western blotting as indicated above, using a mouse monoclonal anti-GFP antibody (Roche, 1:1000) or a mouse monoclonal anti-flag antibody (clone M2, 1:1000, Sigma), respectively.

For co-immunoprecipitation of GDI1/2 with Rab8a, HEK293FT cells transfected with 3xflag-Rab8a plasmids were lysed 24 hours after transfection in IP buffer (20 mM Tris-HCl pH 7.5, 150 mM NaCl, 1 mM EDTA, 0.3 % Triton X-100, 10 % Glycerol, and protease inhibitor cocktail (Roche)) for 30 min on ice. Lysates were centrifuged at 4 °C for 10 min at 20.000 g and supernatants were further cleared by incubation with Easy view Protein G agarose beads (Sigma) for 30 min at 4°C. After agarose bead removal by centrifugation, lysates were incubated with anti-flag M2 agarose beads (Sigma) for 1 h at 4°C with mild agitation. Beads were washed three times with IP wash buffer (20 mM Tris-HCl pH 7.5, 150 mM NaCl, 1 mM EDTA, 0.1 % Triton X-100, 10 % Glycerol) and eluted in buffer containing

20 mM Tris-HCl, 100 mM NaCl, 5 mM $MgCl_2$ and 150 ng/µl of 3xflag peptide by shaking for 15 minutes at 4°C. Each co-immunoprecipitation was repeated in 3 independent experiments, and samples analyzed by Western blotting using an anti-GDI1/2 antibody (Life Technologies, 710300, 1:2000) or an anti-flag antibody (Sigma, F3165, 1:500).

Cell transfection and protein purification for *in vitro* kinase assays

HEK293T cells were cultured in Dulbecco's modified Eagle's medium (DMEM) supplemented with 10 % (v/v) fetal bovine serum, penicillin (100 units/ml) and streptomycin (100 µg/ml) (Life Technologies) at 37 °C and 5 % CO_2. 3xFlag-LRRK2 (wildtype and G2019S mutant) and 3xFlag-Rab8a (wildtype and T72A mutant) were transiently transfected using linear polyethylenimine (PEI, Polyscience) with a 1:2 DNA:PEI ratio. The transfection mixes were prepared by dissolving 40 µg of DNA in 1 ml of OPTI-MEM with 80 µl of PEI (40 µM final). Mixes were incubated at room temperature for 20 min and subsequently added to HEK293T cells previously plated on a 15 cm^2 Petri dish.

Seventy-two hours after transfection, cells were resuspended in 1 ml of lysis buffer (10 mM Tris-HCl pH 7.5, 150 mM NaCl, 5 mM EDTA, 2.5 mM $Na_4P_2O_7$, 1 mM beta-glycerophosphate, 1 mM Na_3VO_4, supplemented with protease inhibitor mixture (Sigma-Aldrich) and 1% (v/v) Tween-20). Samples were left on ice for 30 min, and cell lysates collected after centrifugation at 18000xg for 35 min at 4°C. Supernatants were collected and incubated overnight with 40 µl of Anti-Flag M2 Affinity Gel beads (Sigma-Aldrich) at 4°C with mild agitation. Beads were pelleted and washed with 1 ml of five different wash buffers (WB): WB1 (20 mM Tris-HCl pH 7.5, 500 mM NaCl, 1% (v/v) Tween-20) twice, WB2 (20 mM Tris-HCl pH 7.5, 350 mM NaCl, 1% (v/v) Tween-20) twice, WB3 (20 mM Tris-HCl pH 7.5, 150 mM NaCl, 1% (v/v) Tween-20) twice, WB4 (20 mM Tris-HCl pH 7.5, 150 mM NaCl, 0.1% (v/v) Tween-20) twice and WB5 (20 mM Tris-HCl pH 7.5,

150 mM NaCl, 0.02% (v/v) Tween-20) once. All 3xFlag-tagged proteins were eluted in elution buffer (25 mM Tris-HCl pH 7.5, 5 mM beta-glycerophosphate, 2 mM DTT, 0.1 mM Na_3VO_4, 10 mM $MgCl_2$ supplemented with 0.007 % Tween-20, 150 ng/µl 3xFlag peptide (Sigma-Aldrich) for subsequent *in vitro* kinase assays.

For experiments in which Rab8a was loaded with specific guanine nucleotides, affinity resin bound-protein was washed as above, rinsed in loading buffer (20 mM Tris pH 7.5, 150 mM NaCl, 5 mM EDTA, 0.02 % (v/v) Tween-20) and incubated with an excess (200 µM) GDP or GTPγS for 30 min at 30°C with slight agitation. Nucleotide exchange was stopped and excess nucleotides removed by rinsing beads three times in kinase buffer (25 mM Tris-HCl pH 7.5, 10 mM $MgCl_2$, 2 mM dithiothreitol (DTT), 0.02 % (v/v) Tween-20, 5 mM beta-glycerophosphate, 0.1 mM Na_3VO_4) [289] followed by elution with kinase buffer supplemented with 150 ng/µl 3xFlag peptide.

For *in vitro* kinase assays, purified wildtype or T72A-mutant 3xFlag-Rab8a proteins eluted in kinase buffer, with and without nucleotide loading, were incubated with wildtype or G2019S mutant 3xFlag-LRRK2 at a ratio of 50:1 (Rab8a:LRRK2). Reactions were kept at 30°C for 1 h in the presence of ATP-γ^{33}P (1 µCi/reaction) and 2.5 µM cold ATP and then stopped by adding Laemmli buffer (100 mM Tris-HCl pH 6.8, 4 % (w/v) SDS, 200 mM DTT, 20 % (v/v) glycerol and Bromophenol Blue). Incorporated ^{33}P was detected by autoradiography with a Phospho-Imager system (Cyclone, Perkin-Elmer). The same membranes were stained with Coomassie Blue or probed with an anti-Flag antibody for total protein loading, and quantification performed using ImageJ software.

Rab8a GTP binding and GTP retention assays

HEK293T cells were transfected with 3xFlag-Rab8a wildtype or mutant plasmids as indicated and 24 h later cells were lysed in buffer containing 20 mM

Tris-HCl pH 7.5, 150 mM NaCl, 1 mM EDTA, 1 % Triton X-100, 10 % glycerol and protease inhibitor cocktail (Roche) for 30 min on ice. Lysates were centrifuged (10 min, 20.000*g*), supernatants were precleared with Easy view Protein G agarose (Sigma-Aldrich) for 30 min at 4°C, followed by incubation with anti-Flag M2 agarose beads (Sigma-Aldrich) for 1h at 4°C with mild agitation. Proteins bound to beads were washed 4 times with 25 mM Tris-HCl pH 7.5, 400 mM NaCl, and 1 % Triton X-100.

For GTP or GDP binding assays, equal amounts of wildtype or mutant 3xFlag-Rab8a fusion proteins bound to anti-Flag M2 agarose beads (Sigma-Aldrich) were washed twice with Buffer A (20 mM Tris–HCl pH 7.5, 100 mM NaCl, 5 mM $MgCl_2$, 1 mM NaH_2PO_4, 2 mM DTT) and incubated overnight on ice in Buffer A containing 0.1 µM ^{3}H-GTP or ^{3}H-GDP. Beads were then washed twice in Buffer A to remove unbound nucleotides, added to Bio-safe II (RPI) scintillation cocktail, and binding quantified using scintillation counting for H^3 (Tri-Carb 2810TR scintillation counter, Perkin Elmer).

To assay GTP or GDP retention, agarose-bound Rab8a proteins were incubated in Buffer A containing 0.1 µM ^{3}H-GTP or ^{3}H-GDP overnight on ice and washed twice with Buffer A to remove unbound nucleotide. Subsequently, proteins were incubated in Buffer A containing a 100-fold excess of unlabeled GTP or GDP for 0, 15, 30 or 60 min, and shaking at 37°C. After each time point, Rab8a proteins were washed twice with Buffer A, and retained ^{3}H-GTP or ^{3}H-GDP bound to proteins was quantified using scintillation counting. The amount of ^{3}H-GTP or ^{3}H-GDP bound at 15, 30 and 60 min for each sample was calculated as a fraction of initial binding.

Mass spectrometry

Purified wildtype and mutant Rab8a proteins were separated on 4-20 % SDS-PAGE, stained with Coomassie brilliant blue staining (Thermo Scientific) and

a band corresponding to a ~50 kDa protein was excised. Protein identification was performed using MASCOT.

Statistical analysis

All data are expressed as means ± s.e.m. Unless otherwise noted, data were analyzed by one-way ANOVA with Tukey´s *post-hoc* test, and $p < 0.05$ was considered significant. Statistical details to all experiments can be found in the figure legends. **** $p < 0.001$; ***$p < 0.005$; **$p < 0.01$; *$p < 0.05$.

IV. RESULTS

1. Parkinson disease-associated mutations in LRRK2 cause centrosomal defects via Rab8a phosphorylation

Pathogenic LRRK2 causes deficits in centrosomal positioning critical for cell polarization and directed migration

To evaluate effects of pathogenic LRRK2 on cell polarity, we employed human neuroblastoma SH-SY5Y cells stably expressing flag-tagged wildtype or G2019S mutant LRRK2 [283, 284]. Cells were differentiated with retinoic acid, and average neurite length quantified. Pathogenic G2019S LRRK2-expressing cells showed a significant decrease in the percentage of differentiated cells as compared to control or wildtype LRRK2-expressing cells (Fig. 12 a-c). Since proper positioning of the centrosome is important for cell polarization and directed migration [262, 290], we analyzed centrosome positioning from non-contiguous differentiated cells by staining for pericentrin, a component of the pericentriolar matrix [291]. The centrosome was facing the longest neurite in the majority of control and wildtype LRRK2-expressing cells, whilst a significant amount of G2019S-expressing cells had their centrosome positioned on the side, or opposite the longest neurite (Fig. 12 d and e).

As cell polarization is a prerequisite for cell migration [262], we wondered whether pathogenic LRRK2-expressing cells display deficits in cell migration associated with altered centrosome positioning. Scratch wounding was performed on control GFP, wildtype or G2019S mutant LRRK2-expressing SH-SY5Y cells, and cells counted as oriented when the centrosome was located within a 90° angle facing the wound [287, 288, 292] (Fig. 13a). After 4 h of wounding, around 40 % of control GFP and wildtype LRRK2-expressing cells had already reoriented the centrosome, whilst the percentage of reoriented centrosomes was significantly less in G2019S LRRK2-expressing cells (Fig. 13b). To test for potential migration defects, cells were recorded by live cell microscopy after performing a scratch wound (Fig. 13c and d). G2019S-LRRK2-expressing cells displayed a decrease in cell migration in the wound healing assay as compared to wildtype LRRK2-expressing cells. Whereas wildtype LRRK2-expressing cells exhibited persistent

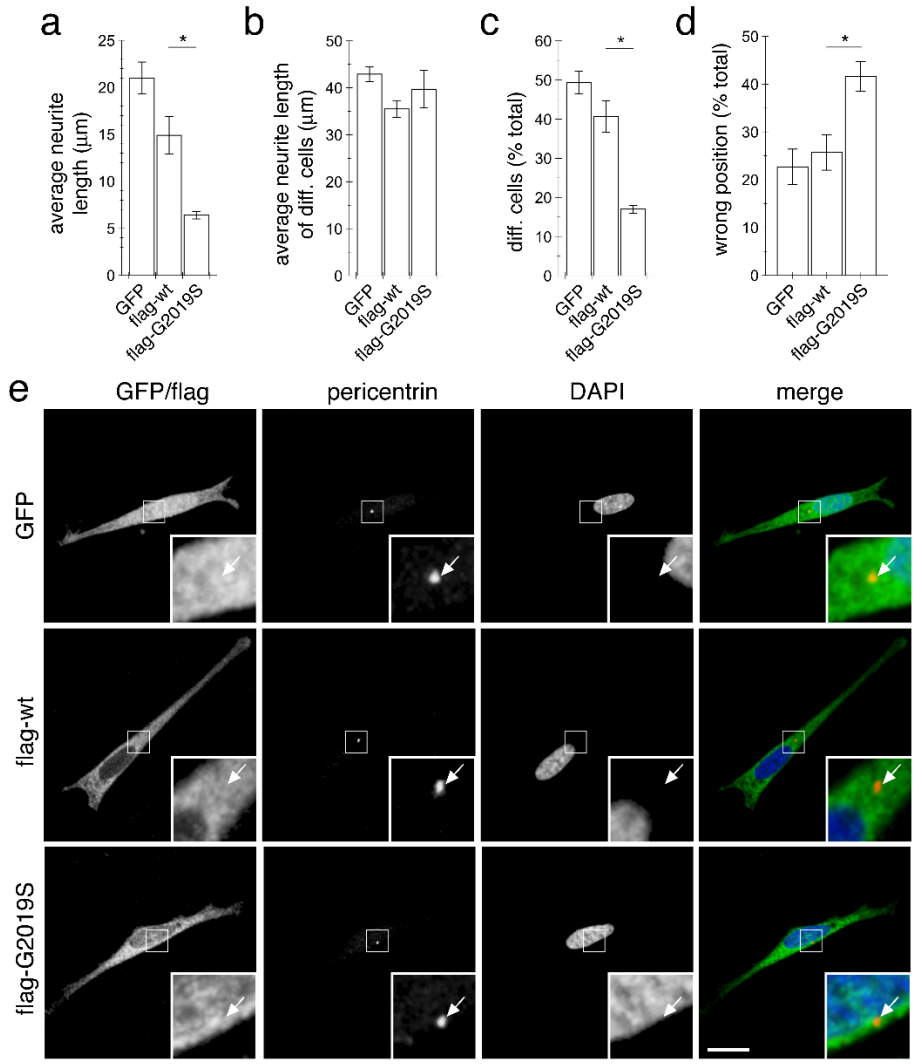

Fig. 12. Pathogenic LRRK2 causes deficits in differentiation and altered centrosome positioning in differentiated SH-SY5Y cells. a) Quantification of neurite length in SH-SY5Y cells differentiated with retinoic acid for 5 days. Around 150 cells were analyzed per condition and experiment. Bars represent mean ± s.e.m., (n=3 independent experiments); *, $p < 0.05$. **b)** Quantification of neurite length only including differentiated cells. Around 150 differentiated cells were analyzed per condition and experiment. Bars represent mean ± s.e.m., (n=3 independent experiments). **c)** Quantification of percentage of differentiated cells. Bars represent mean ± s.e.m., (n=3 independent experiments); *, $p < 0.05$. **d)** Quantification of differentiated cells where centrosome is positioned on the side or opposite the longest neurite in the distinct cells as indicated. Around 30 non-contiguous differentiated cells were analyzed per condition and experiment. Bars represent mean ± s.e.m., (n=3 independent experiments); *, $p < 0.05$. **e)** Example of non-contiguous SH-SY5Y cells stably expressing GFP, or flag-tagged wildtype or G2019S-mutant LRRK2 as indicated, and stained for pericentrin and DAPI. Scale bar, 10 µm.

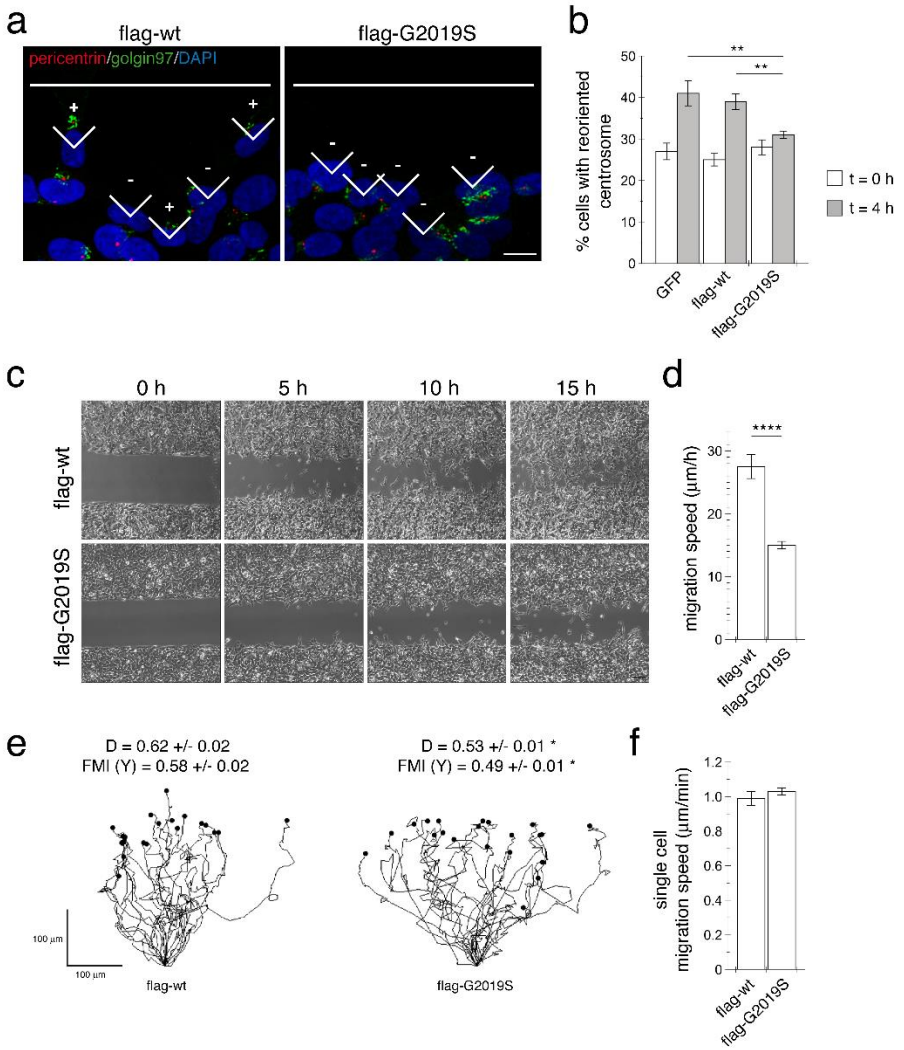

Fig. 13. Pathogenic LRRK2 causes deficits in centrosomal positioning critical for cell polarization and directed migration. a) Example of reorientation of the centrosome 4 h after wounding in SH-SY5Y cells stably expressing flag-tagged wildtype or G2019S mutant LRRK2. The white lines indicate scratch orientation, and cells were stained with anti-pericentrin, anti-Golgin97, and DAPI. Angles are labeled as having oriented (+) or not oriented (-) centrosomes for the first row of cells facing the scratch wound. Scale bar, 10 µm. **b)** Quantification of centrosome reorientation in cells stably expressing GFP, flag-tagged wildtype or G2019S-mutant LRRK2 immediately after (t = 0 h), or 4 h after generating the wound (t = 4 h). Random orientation is expected to be 25%. N > 100 cells were quantified for each condition in each experiment. Bars represent mean ± s.e.m. (n=3 independent experiments); **, $p < 0.01$. **c)** Wound-healing assays in either flag-tagged wildtype or G2019S-mutant LRRK2-expressing SH-SY5Y cells. Phase-contrast images at the indicated times are shown. Scale bar, 150 µm. **d)** Quantitative analysis of wound-healing assays as described in Methods. Bars represent mean ± s.e.m. (n=6 independent experiments); ****, $p < 0.001$. **e)** Example of tracking of individual cells expressing flag-tagged wildtype or G2019S mutant LRRK2. Individual cells in the first row facing the wound were tracked until reaching the middle of the wound. Directionality index (D) and forward migration index in Y axis (FMI Y) were calculated for at least 30 cells per condition in three independent experiments, and are expressed as mean ± s.e.m. on top of each graph. *, $p < 0.05$. **f)** Single cell wound healing migration speed was calculated for at least 30 cells per condition in 3 independent experiments.

directional migration until the closure of the gap, G2019S-LRRK2-expressing cells displayed less directional migration, without a reduction in cell motility (Fig. 13e and f). Together, these data indicate that mutant LRRK2 causes deficits in proper centrosome positioning with effects on polarity required for cells to properly respond to directional migration signals.

Distinct pathogenic LRRK2 mutants cause centrosomal cohesion deficits in a kinase activity-dependent manner

In dividing cells, centrosomes duplicate in S phase, but are held together by a flexible linker which gradually elongates during S and G2, allowing the duplicated centrosomes to mature by accumulating pericentriolar material. At the G2/M transition, the flexible linker holding the centrosomes together is lost, and mature centrosomes can subsequently constitute the poles of the mitotic spindle [293]. To determine for possible centrosomal alterations in dividing cells, we examined cells with duplicated centrosomes from non-differentiated SH-SY5Y cells. When quantifying cells where duplicated centrosomes could be clearly visualized as separate from each other, the mean distance between duplicated split centrosomes in GFP expressing cells was 1.49 ± 0.07 μm (mean ± s.e.m, n=13 cells), and centrosomes were therefore scored as split when > 1.5 μm apart. As compared to GFP or wildtype LRRK2, pathogenic G2019S LRRK2 was found to significantly increase the percentage of cells with split centrosomes, indicative of a centrosomal cohesion deficit (Fig. 14a and b). To assess whether such centrosomal alterations induced by mutant LRRK2 were dependent on LRRK2 kinase activity, we evaluated the effects of two structurally distinct and specific LRRK2 kinase inhibitors, and quantified dephosphorylation of S935 on LRRK2 as an established readout for kinase inhibition [294, 295]. Short-term addition of these inhibitors significantly reverted the observed cohesion deficits in G2019S-LRRK2 expressing

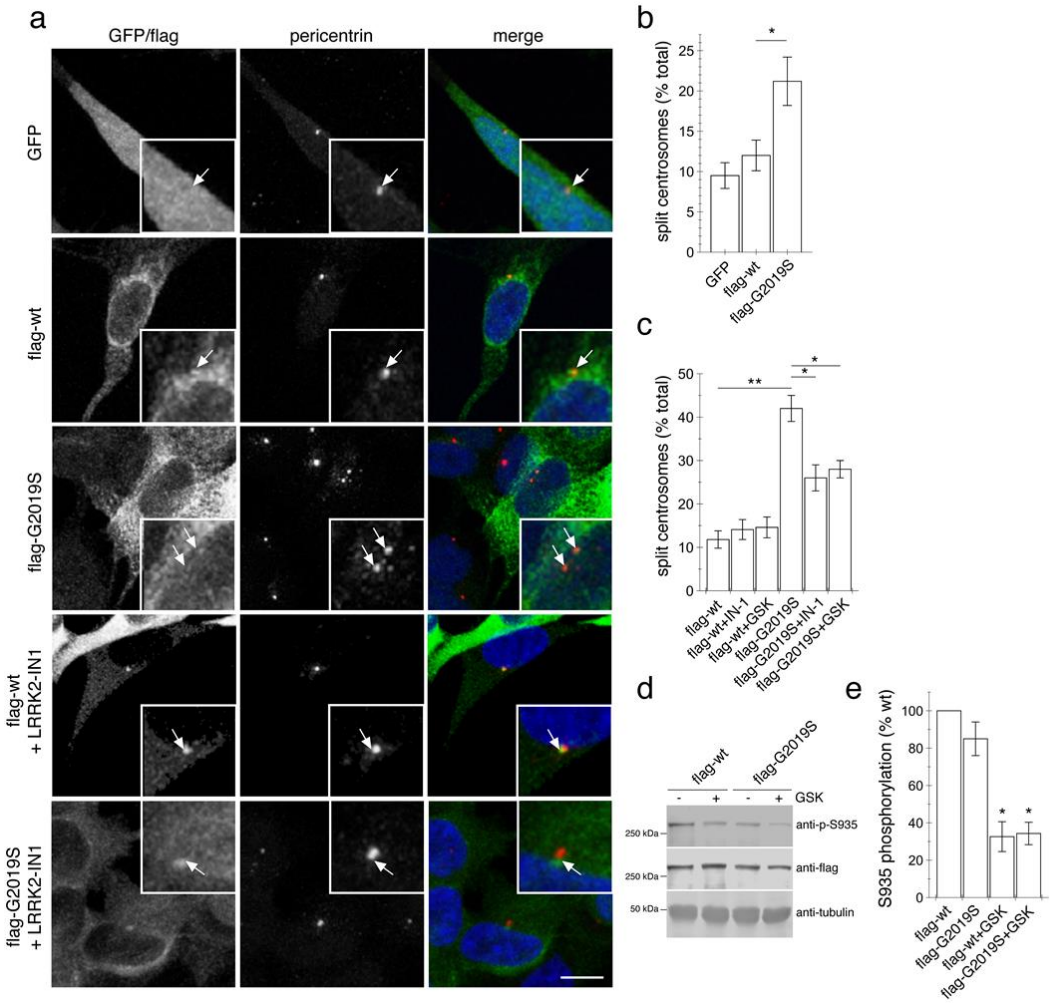

Fig. 14. Pathogenic LRRK2 causes deficits in centrosome cohesion in SH-SY5Y cells. **a)** Example of non-differentiated SH-SY5Y cells stably expressing GFP, or flag-tagged wildtype or G2019S-mutant LRRK2 as indicated, and stained for pericentrin and DAPI. Scale bar, 10 μm. **b)** Quantification of the split centrosome phenotype in cells expressing GFP, or flag-tagged wildtype or G2019S-mutant LRRK2 as indicated. Around 20 cells with duplicated centrosomes were analyzed per condition. Bars represent mean ± s.e.m. (n=4 independent experiments); *, $p < 0.05$. **c)** Quantification of the split centrosome phenotype in cells expressing flag-tagged wildtype or G2019S-mutant LRRK2 as indicated, in either the absence or presence of kinase inhibitors (500 nM LRRK2-IN-1 or GSK2578215A for 1 h) as indicated. Around 20 cells with duplicated centrosomes were analyzed per condition. Bars represent mean ± s.e.m. (n=3 independent experiments); **, $p < 0.01$; *, $p < 0.05$. **d)** Cells were either left untreated or incubated with 500 nM GSK2578215A for 1 h, and extracts analyzed for phosphorylated (p-S935) or total (flag) LRRK2. **e)** Quantification of S935 dephosphorylation in cells expressing flag-tagged wildtype or G2019S-mutant LRRK2 as indicated, in either the absence or presence of 500 nM GSK2578215A for 1 h. Bars represent mean ± s.e.m. (n=3); *, $p < 0.05$.

cells (Fig. 14 c) and inhibited kinase activity as assessed by S935 dephosphorylation (Fig. 14d and e), suggesting that these cohesion deficits are kinase activity-mediated.

We next wondered whether the centrosomal cohesion deficits comprised a phenotype shared amongst distinct pathogenic LRRK2 mutants. For this purpose, HEK293T cells were transiently transfected with various mutant LRRK2 constructs. Similar to SH-SY5Y cells, the mean distance between duplicated split centrosomes in non-transfected HEK293T cells was 1.38 ± 0.05 μm (mean ± s.e.m, n=12 cells), and centrosomes were scored as split when > 1.5 μm apart. As compared to non-transfected cells or to cells expressing wildtype LRRK2, a larger percentage of duplicated centrosomes displayed a split phenotype in cells expressing either G2019S-, R1441C- or Y1699C-mutant LRRK2, respectively, which was not observed with a kinase-dead G2019S-K1906M mutant (Fig. 15a and b), even though all LRRK2 variants were expressed to similar degrees (Fig. 15c). As previously described [296], under the overexpression conditions in HEK293T cells employed here, pathogenic mutant LRRK2 also displayed more visible accumulation at and/or around centrosomes as compared to wildtype or kinase-inactive G2019S-K1906M mutant LRRK2, which were cytosolic in the majority of cells (Fig. 15a and d), and additional localization of R1441C and Y1699C mutant LRRK2 to filamentous structures could be observed in some cells as well (Fig. 15e) [176]. Alterations in centrosomal cohesion were not due to aggregation-related events of LRRK2 protein overexpression, as triggering the formation of pericentrosomal protein aggregates (aggresomes) either by proteasomal inhibition in LRRK2-expressing cells, or by overexpression of a mutant version of huntingtin protein, did not cause centrosome splitting (Fig. 15f). Consistent with premature centrosome splitting in pathogenic LRRK2-expressing cells, the duplicated centrosomes were smaller than normal, mature centrosomes as determined in control or wildtype LRRK2-transfected cells (Fig. 15g and h). Thus, the observed

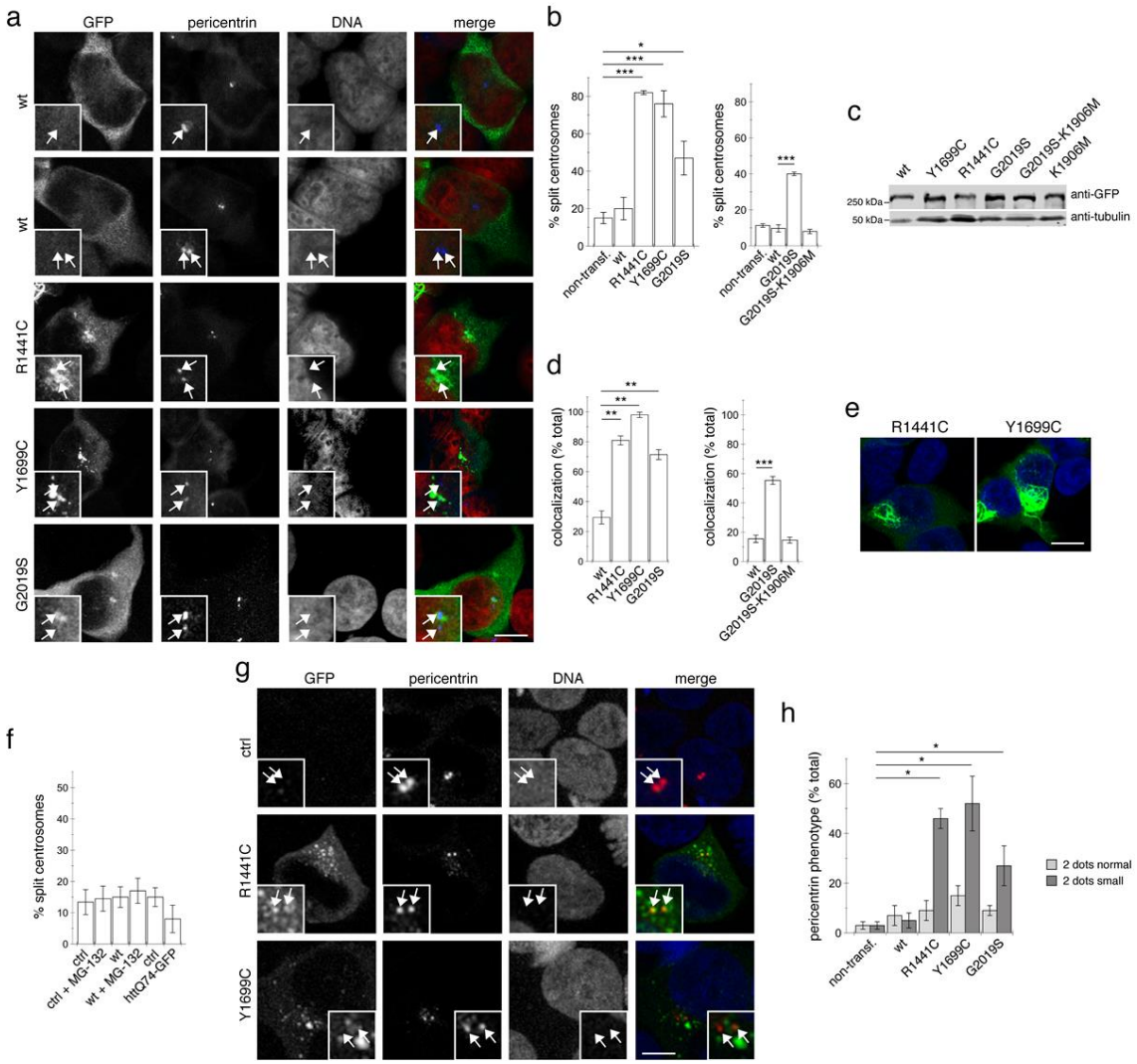

Fig. 15. Distinct pathogenic LRRK2 mutants cause deficits in centrosome cohesion in transfected HEK293T cells. a) Examples of transfected cells displaying either one centrosome (interphase), or upon duplication and concomitant maturation (G2), two attached centrosomes (first two panels in wildtype LRRK2-expressing cells). Mutant LRRK2-expressing cells display a split centrosome phenotype. Scale bar, 5 μm. **b)** The split centrosome phenotype was quantified by determining the percentage of cells displaying two pericentrin-positive structures with a distance between their centers > 1.5 μm, as compared to two attached (≤ 1.5 μm) structures. Around 30 cells with duplicated centrosomes were analyzed per condition per experiment. Bars represent mean ± s.e.m. (n=3 independent experiments); ***, $p < 0.005$; *, $p < 0.05$. **c)** Cells were transfected with constructs as indicated, and 40 μg of cellular lysates subjected to Western blotting with an anti-GFP antibody. Tubulin was used as loading control. **d)** Quantification of percentage of cells displaying colocalization of GFP-tagged LRRK2 with centrosomes. Around 30 cells were quantified per experimental condition. Bars represent mean ± s.e.m. (n=3 independent experiments);

***, $p < 0.005$; **, $p < 0.01$. **e)** Examples of filament-like localization of GFP-tagged R1441C and Y1699C mutant LRRK2. Scale bar, 10 μm. **f)** Centrosome splitting was quantified from cells transfected with pCMV (ctrl) or wildtype LRRK2 and treated 42 h after transfection with 5 μM MG-132 for 6 h, or from cells transfected with pCMV (ctrl) or HttQ74-GFP 24 h after transfection. N=3 independent experiments. **g)** For determination of centrosomal size, cells were fixed and processed as described in Methods. Note that colocalization of mutant LRRK2 with split centrosomes can be more or less extensive (arrows). Scale bar, 5 μm. **h)** Quantification of centrosome size from experiments of the type depicted in A. An average of 30 cells with two centrosomes were analyzed for each condition. Bars represent mean ± s.e.m. (n=3 independent experiments); *, $p < 0.05$.

---

centrosomal cohesion deficits seem to be a cellular feature shared amongst all three pathogenic LRRK2 mutants.

To assess whether premature centrosome splitting induced by mutant LRRK2 was dependent on LRRK2 kinase activity, we evaluated the effects of two distinct and selective LRRK2 kinase inhibitors [294, 295]. Addition of either inhibitor to wildtype LRRK2-expressing cells caused rapid recruitment of LRRK2 to the centrosome, but such centrosomal localization of kinase-inhibited LRRK2 did not cause centrosome splitting (Fig. 16a-c). However, whilst not causing a change in the centrosomal localization of pathogenic LRRK2 (Fig. 16d), treatment with either inhibitor reversed centrosome splitting in mutant LRRK2-expressing cells (Fig. 16e). Inhibitor-mediated reversal of centrosomal cohesion deficits were observed with all three pathogenic LRRK2 mutants (Fig. 16e,f), indicating that premature centrosome splitting is a shared feature of distinct pathogenic LRRK2 mutants and mediated by the kinase activity in both HEK293T and SH-SY5Y cells.

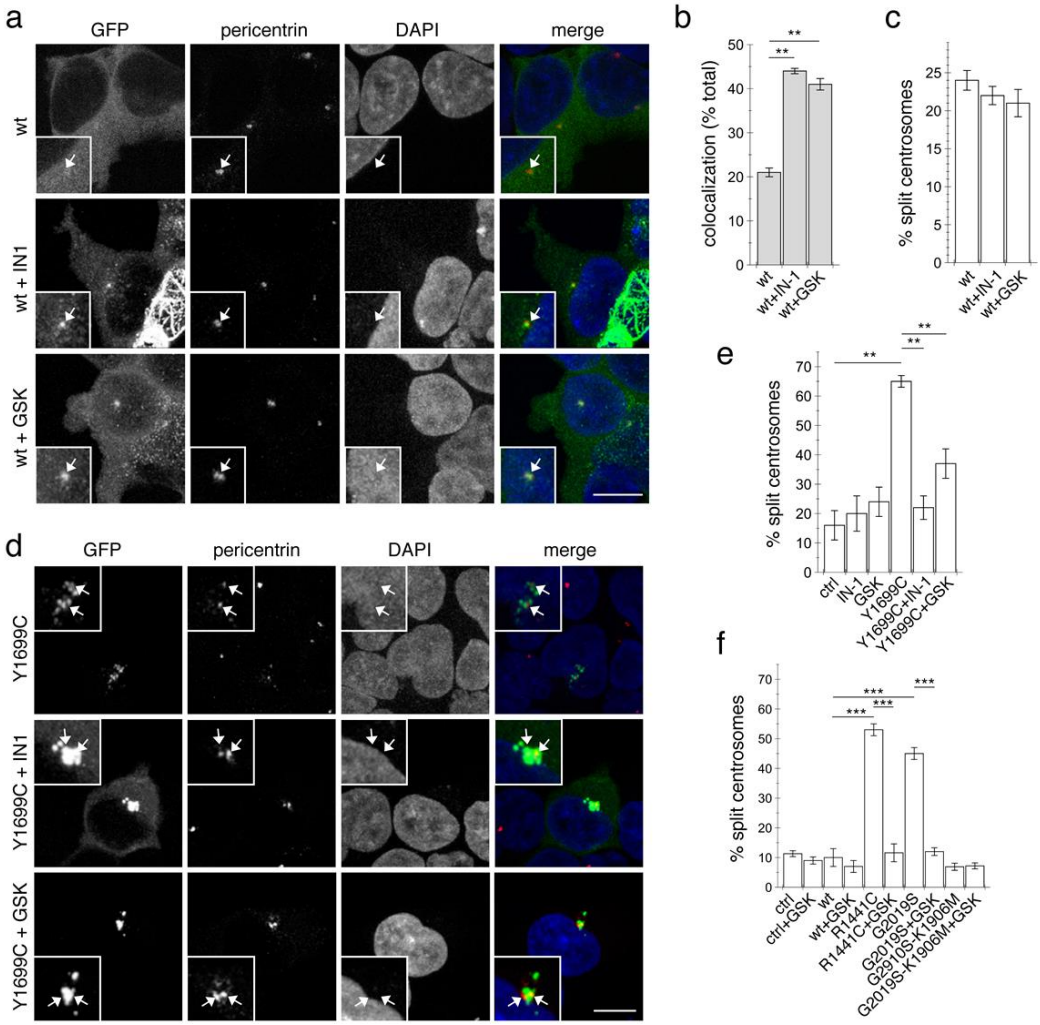

Fig. 16. Pathogenic LRRK2 disturbs centrosome cohesion in a kinase-dependent manner. a) GFP-tagged wildtype LRRK2-transfected HEK293T cells were either untreated (ctrl), or treated with LRRK2-IN-1 (500 nM) or GSK2578215A (500 nM) for 60 min, followed by staining with pericentrin antibody. Scale bar, 10 µm. **b**) Quantification of the percentage of LRRK2-expressing cells displaying visible colocalization with pericentrin in the absence or presence of kinase inhibitors as indicated. Around 100 cells were analyzed per condition. Bars represent mean ± s.e.m. (n=3 independent experiments); **, $p < 0.01$. **c)** Quantification of the percentage of wildtype LRRK2-expressing cells displaying a split centrosome phenotype in the absence or presence of kinase inhibitors as indicated. Around 30 cells with duplicated centrosomes were analyzed per condition. Bars represent mean ± s.e.m. (n=3 independent experiments). **d)** Examples of GFP-tagged Y1699C mutant LRRK2 in the absence (ctrl) or presence of LRRK2-IN-1 or GSK2578215A treatment as indicated above, followed by staining with pericentrin antibody. Scale bar, 10 µm. **e)** The split centrosome phenotype was quantified as indicated above. An average of 30 cells with two centrosomes were analyzed for each condition. Bars represent mean ± s.e.m. (n=3 independent experiments); **, $p < 0.01$. **f)** The split centrosome phenotype was quantified as indicated above and an average of 30 cells with two centrosomes analyzed for each condition. Bars represent mean ± s.e.m. (n=3 independent experiments); ***, $p < 0.005$.

Centrosomal cohesion deficits are detectable in two distinct peripheral cell types from LRRK2 PD patients as compared to healthy controls

LRRK2 is known to be expressed in non-neuronal cells such as fibroblasts or lymphoblasts [297], and these patient-derived cells may comprise promising cellular models for future pharmacodynamic assays in clinical studies employing LRRK2 kinase inhibitors. Therefore, we next used either skin fibroblasts or lymphoblasts from age- and sex-matched G2019S mutant LRRK2 PD patients and controls, respectively. Primary fibroblasts from five G2019S mutant LRRK2 PD patients displayed increased centrosome splitting as compared to five control patients, which was reverted by application of either GSK2578215A or LRRK2-IN-1 kinase inhibitors, respectively (Fig.17a and b). Similarly, lymphoblasts from three G2019S mutant LRRK2 PD patients displayed deficits in centrosomal cohesion as compared to three healthy control cells. Such deficits were reverted by application of 500 nM GSK2578215A kinase inhibitor (Fig.17c and d). In addition, application of either 10 nM or 100 nM of MLi-2, a recently developed novel and highly selective LRRK2 kinase inhibitor [298] also reverted the centrosomal cohesion deficits (Fig. 17c and d), and inhibited LRRK2 kinase activity as assessed by S935 dephosphorylation (Fig. 17e and f). Together, these data indicate that endogenous mutant LRRK2 protein causes centrosomal alterations in a kinase activity-dependent manner also in two distinct patient-derived cell types.

Pathogenic LRRK2-induced centrosomal cohesion deficits correlate with aberrant centrosomal accumulation of phosphorylated Rab8a

We next aimed to determine the mechanism(s) by which pathogenic LRRK2 may cause the observed centrosomal alterations. Recent studies have identified a subset of Rab GTPases as LRRK2 kinase substrates, with Rab8a being one of the most prominent substrates [75], and known to be involved in centrosome-related events. Indeed, we confirmed that Rab8a was subject to

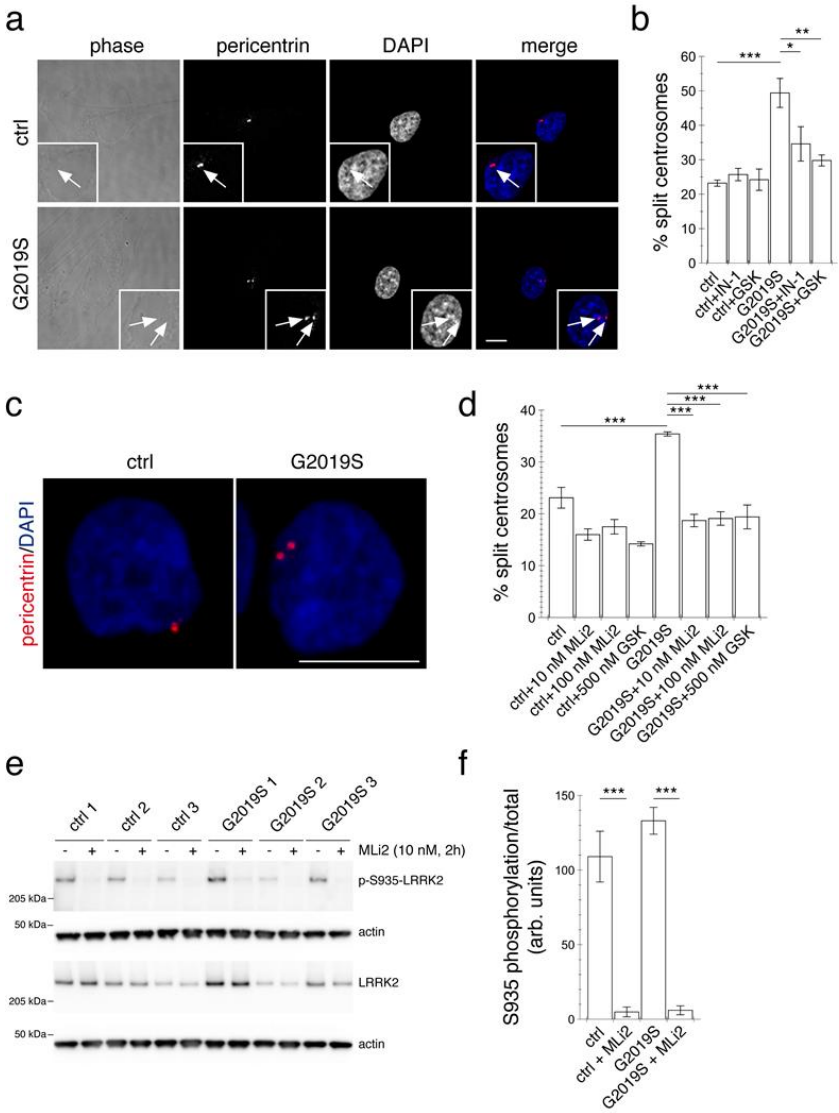

Fig. 17. Centrosome splitting in human dermal fibroblasts and lymphoblasts from G2019S mutant LRRK2 PD patients compared to healthy controls. a) Example of control (ctrl) and G2019S mutant LRRK2 PD patient fibroblast stained with pericentrin antibody and DAPI. Scale bar, 10 µm. **b)** Centrosome phenotype was quantified from 300 cells per line, and from 5 control and 5 G2019S mutant LRRK2 fibroblast lines. Control or G2019S mutant LRRK2 fibroblasts were treated with LRRK2-IN-1 (500 nM) or GSK2578215A (500 nM) for 60 min. Bars represent mean ± s.e.m. (between five independent lines). ***, $p < 0.005$; **, $p < 0.01$; *, $p < 0.05$. **c)** Example of control (ctrl) and G2019S mutant LRRK2 PD patient lymphoblast stained with pericentrin antibody and DAPI. Scale bar, 10 µm. **d)** Centrosome phenotype was quantified from 200-300 cells per line, and from three control and three G2019S mutant LRRK2 lymphoblast lines. Control or G2019S mutant LRRK2 lymphoblasts were treated with MLi2 (10 nM or 100 nM) or GSK2578215A (500 nM) for 2 h. Bars represent mean ± s.e.m. (between three independent lines). ***, $p < 0.005$. **e)** Cells were either left untreated or incubated with 10 nM MLi2 as indicated, and extracts analyzed for phosphorylated (p-S935) or total LRRK2. **f)** Quantification of S935 dephosphorylation in either control or G2019S-mutant LRRK2 lymphoblasts as indicated, in either the absence or presence of 10 nM MLi2. Bars represent mean ± s.e.m. (n=3 lines each); ***, $p < 0.005$.

phosphorylation by LRRK2 *in vitro*, that phosphorylation was increased with pathogenic as compared to wildtype LRRK2, and that phosphorylation was largely abolished when mutating the previously identified phosphorylation site (T72) in the switch II domain (Fig. 18a and b). Moreover, we found that phosphorylation was not altered by either GDP or GTP binding to Rab8a (Fig. 18a-d), indicating that it was not dependent on the nucleotide-bound status of Rab8a.

Rab proteins interact with a variety of regulatory proteins. For example, the localization of Rab proteins is regulated by binding to GDP dissociation inhibitor (GDI1/2), which is able to deliver as well as extract Rab proteins from membranes [299], and their activity is modulated by binding to GDP/GTP exchange factors (GEFs) [195]. To test for differential interactions with regulatory proteins, we next generated phospho-deficient (Rab8a-T72A) and phospho-mimetic (Rab8a-T72D/Rab8a-T72E), as well as GTP-preferring (Rab8a-Q67L) and GDP-preferring (Rab8a-T22N) Rab8a variants, which were all expressed to similar degrees (Fig. 18e). All mutants with the exception of Rab8a-T22N were competent to bind GTP and GDP, and the rates of GTP/GDP dissociation were not affected by the mutations, indicating that mimicking phosphorylation does not change the nucleotide state of Rab8a (Fig. 18f-i). As previously described [75], whilst GDI1/2 coimmunoprecipitated with wildtype Rab8a as determined by mass spectroscopy, this interaction was lost with the phospho-mimetic Rab8a mutants (Fig. 19a-c), which also displayed a decreased interaction with the GEF Rabin8 (Rab3IP) (Fig. 19d and e), suggesting that mimicking Rab8a phosphorylation interferes with its interaction with multiple regulatory proteins. When expressed on their own phospho-mimetic Rab8a mutants did not cause centrosomal cohesion deficits and were found to be largely cytosolic (Fig. 19f,g). Thus, these mutants cannot properly mimick a phosphorylated version of Rab8a in a cellular context. Rab8a has been shown to be localized to a pericentrosomal recycling compartment which is in

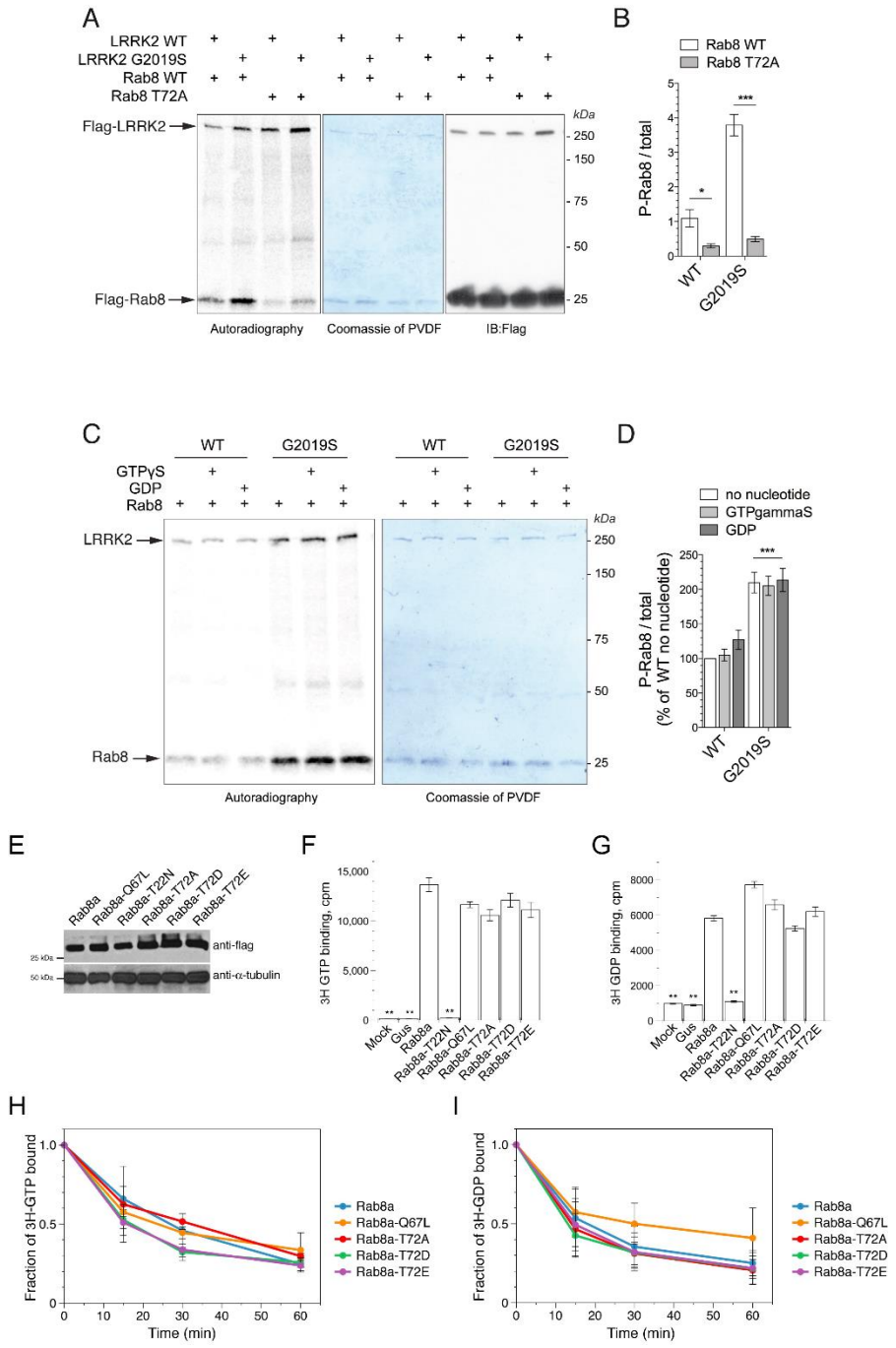

Fig. 18. LRRK2 phosphorylates Rab8a at T72, and phosphomimetic mutants do not display altered nucleotide binding or retention. a) *In vitro* kinase assays using purified wildtype or G2019S mutant flag-tagged LRRK2 and purified wildtype or T72A mutant flag-tagged Rab8a (1:50 ratio). ^{33}P incorporation was revealed by autoradiography (left panel), and total protein loading by

Coomassie Brilliant Blue staining (middle panel) or anti-flag immunoblotting (right panel) of the same PVDF membrane. **b)** Quantification of ^{33}P incorporated into Rab8a as compared to total Rab8a as determined by Coomassie Brilliant Blue staining. Bars represent mean ± s.e.m. (n=3 independent experiments); *, $p < 0.05$; ***, $p < 0.001$ (two-way ANOVA with Bonferroni *post-hoc* test). **c)** *In vitro* kinase assays using purified wildtype or G2019S mutant flag-tagged LRRK2 and purified wildtype flag-tagged Rab8a in the absence of nucleotide, or loaded with GTPγS or GDP, respectively. ^{33}P incorporation was revealed by autoradiography (left panel), and total protein loading by Coomassie Brilliant Blue staining (right panel) of the same PVDF membrane. **d)** Quantification of ^{33}P incorporated into Rab8a as compared to total Rab8a from 10 independent experiments. Bars represent mean ± s.e.m; ***, $p < 0.001$ (two-way ANOVA with Bonferroni *post-hoc* test). **e)** Cells were transfected with the indicated flag-tagged Rab8a constructs, and extracts (20 µg) analyzed by Western blotting with an anti-flag antibody, and tubulin as loading control. **f)** GTP binding for Rab8a proteins or β-glucoronidase (Gus) was measured by loading with radiolabelled ^{3}H-GTP, and normalized to total protein levels. Bars represent mean ± s.e.m. (n=3 experiments); **, $p < 0.01$. **g)** GDP binding for Rab8a proteins or β-glucoronidase (Gus) was measured by loading with radiolabelled ^{3}H-GDP, and normalized to total protein levels. Bars represent mean ± s.e.m. (n=3 experiments); **, $p < 0.01$. **h)** GTP retention assay from different Rab8a variants as indicated. Purified proteins were incubated with ^{3}H-GTP, a one hundred-fold molar excess of cold GTP was added, and dissociation of nucleotide was measured as a fraction of initial binding at time 0. Data points represent mean ± s.d. (n=3 experiments). Statistical significance was estimated by two-way ANOVA for time versus mutation with Tukey´s *post-hoc* test for comparison to wildtype protein at each time point. **i)** GDP retention assay from different Rab8a variants as indicated. Purified proteins were incubated with ^{3}H-GDP, a one hundred-fold molar excess of cold GDP was added, and dissociation of nucleotide was measured as a fraction of initial binding at time 0. Data points represent mean ± s.d. (n=3 experiments). Statistical significance was estimated by two-way ANOVA for time versus mutation with Tukey´s *post-hoc* test for comparison to wildtype protein at each time point.

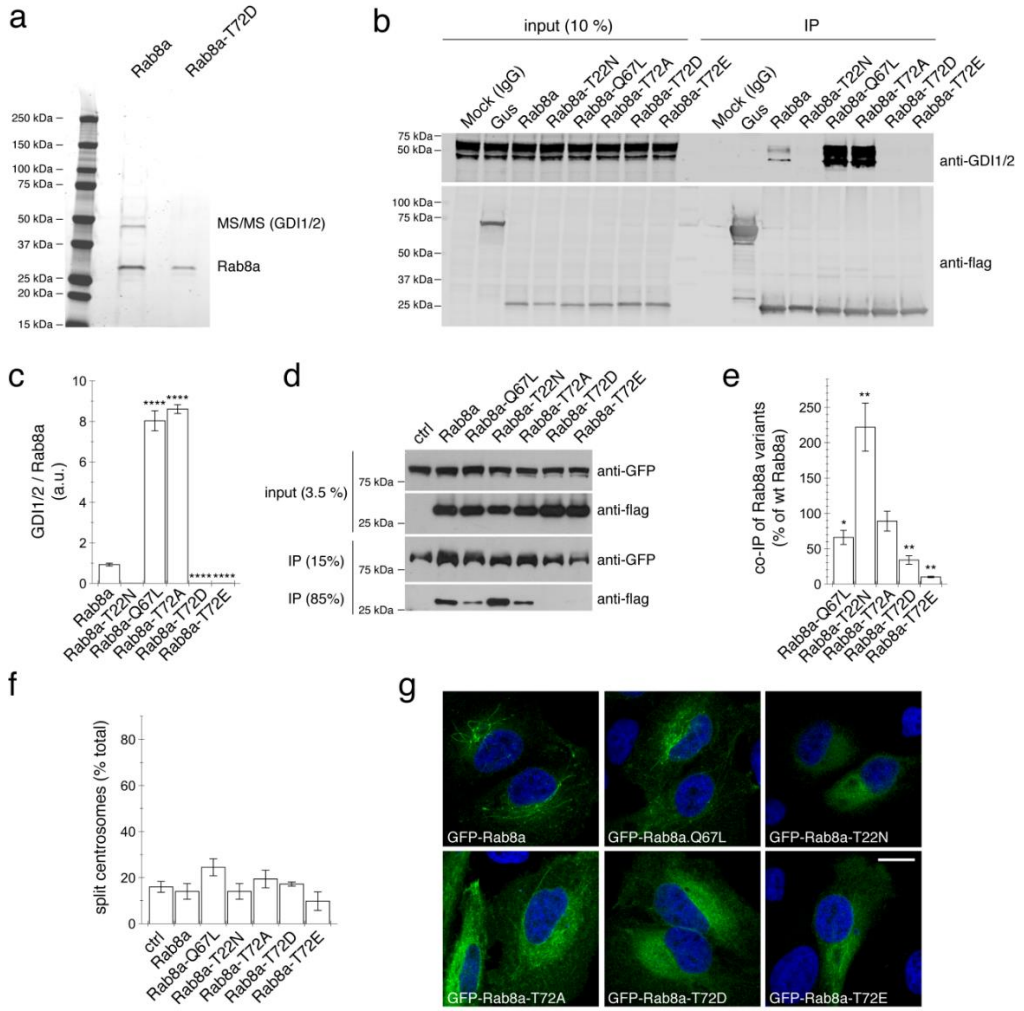

Fig. 19. Differential interactions of wildtype and phospho-mimetic Rab8a mutants with GDI1/2 and Rabin8, effects on centrosome splitting and subcellular localization. **a)** Flag-tagged wildtype and mutant Rab8a were immunoprecipitated from HEK293T cells, followed by SDS-PAGE and Commassie Brilliant Blue staining. The band around 50 kDa co-purifying with wildtype Rab8a was excised from the gel and identified by LC-MS/MS as Rab GDP dissociation inhibitor alpha (GDI1) and beta (GDI2). **b)** HEK293T cells were either non-transfected (mock), or transfected with flag-tagged β-glucoronidase (Gus) or Rab8a constructs as indicated, proteins immunoprecipitated with an anti-flag antibody, and immunoprecipitates blotted for endogenous GDI1/2 (upper panel) or flag-tagged proteins (lower panel). **c)** Quantification of the amount of GDI1/2 relative to Rab8a in immunoprecipitated complexes from the type of experiments as depicted in B. Bars represent mean ± s.e.m. (n=3 experiments); ****, $p < 0.0001$ (versus wildtype Rab8a). **d)** Cells were transfected with GFP-Rabin8 and either empty vector (ctrl) or different Rab8a variants as indicated. Whole-cell lysates (1 mg) were subjected to immunoprecipitation with a polyclonal anti-GFP antibody followed by immunoblotting with a monoclonal anti-GFP antibody or an anti-flag antibody as indicated, and input was probed for expression levels of GFP-Rabin8 and the different flag-tagged Rab8a constructs. **e)** Quantification of the type of experiments depicted in d, normalized to the amount of input, and the amount of coimmunoprecipitation (co-IP) of wildtype Rab8a. Bars represent mean ± s.e.m. (n=3 experiments); **, $p < 0.01$; * $p < 0.05$. **f)** Quantification of the split centrosome phenotype in either non-transfected HEK293T cells (ctrl) or cells expressing the indicated Rab8a variants. Bars represent mean ± s.e.m. (n=3 experiments). **g)** Example of HELA cells expressing the indicated GFP-tagged Rab8a constructs, and stained with DAPI.

direct contact with the centrosome to regulate a variety of centrosome-related events [234, 236, 300]. We thus wondered whether pathogenic LRRK2 may alter the subcellular localization of endogenous Rab8a. Whilst endogenous Rab8a was rarely localized to a pericentrosomal/centrosomal compartment in control cells, all pathogenic LRRK2 mutants caused a prominent increase in the amount of cells displaying pericentrosomal/centrosomal Rab8a accumulation (Fig. 20a and b) without changes in the total levels of endogenous Rab8a protein (Fig. 20c).

Rab8a can also localize to the Golgi complex which is in tight contact with the centrosome [290, 301], and such centrosome-Golgi nexus is known to be important for cell polarity [156]. To determine whether the pericentrosomal/ centrosomal accumulation of Rab8a is reflective of enhanced Golgi association, non-transfected or LRRK2-transfected cells were either treated with nocodazole, which causes Golgi fragmentation and dispersal, or with brefeldin A, which causes redistribution of the Golgi complex into the ER [302]. Golgi dispersal or complete Golgi redistribution did not alter the accumulation of Rab8a in pathogenic LRRK2-expressing cells (Fig. 21), indicating that Rab8a genuinely associates with a centrosomal/pericentrosomal compartment.

The centrosomal/pericentrosomal Rab8a accumulation was reverted upon application of the LRRK2 kinase inhibitor GSK2578215A (Fig. 20a and b). Whilst S935 phosphorylation is a reliable readout to determine whether pharmacological kinase inhibitors block the LRRK2 kinase activity, it is not predictive of kinase activity of pathogenic mutants *per se* [88, 96, 183, 184, 303-305]. Indeed, whilst varying S935 phosphorylation levels were detected in wildtype and mutant LRRK2, application of GSK2578215A effectively inhibited the activity of both wildtype and mutant LRRK2 variants as measured by S935 dephosphorylation

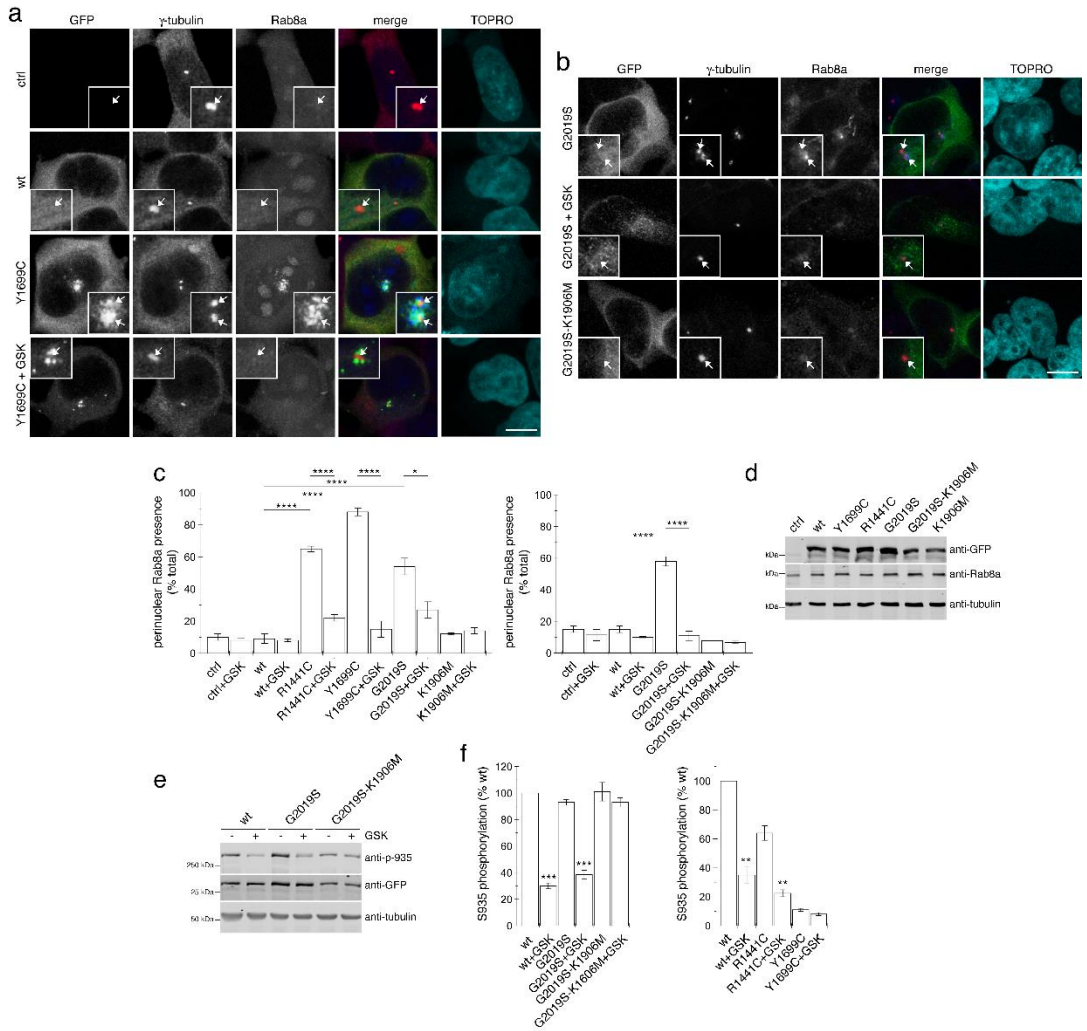

Fig. 20. Pathogenic LRRK2 causes kinase-dependent pericentrosomal/centrosomal accumulation of endogenous Rab8a. a) and **b)** Examples of non-transfected HEK293T cells (ctrl) or cells transfected with either wildtype or pathogenic LRRK2, or with kinase-dead pathogenic LRRK2 as indicated, and stained with γ-tubulin antibody, Rab8a antibody (rabbit polyclonal Rab8a antibody for panel a, sheep polyclonal antibody for panel b), and TOPRO. Scale bar, 5 µm. **c)** Quantification of the percentage of cells displaying pericentrosomal Rab8a staining in either non-transfected cells (ctrl), or pathogenic LRRK2-transfected cells as indicated, either in the absence or presence of GSK2578215A (GSK) (500 nM, 1 h). Bars represent mean ± s.e.m., (n = 3 independent experiments); ****, $p < 0.001$; *, $p < 0.05$. **d)** Cells were transfected with the indicated constructs, and extracts blotted for GFP-tagged LRRK2, endogenous Rab8a, and tubulin as loading control. **e)** Cells were either left untreated or incubated with 500 nM GSK2578215A for 1 h as indicated, and extracts analyzed for phosphorylated (p-S935) or total (GFP) LRRK2. **f)** Quantification of S935 dephosphorylation in cells expressing wildtype or mutant LRRK2 as indicated, in either the absence or presence of 500 nM GSK2578215A for 1 h. Bars represent mean ± s.e.m. (n = 3); ***, $p < 0.005$; **, $p < 0.01$

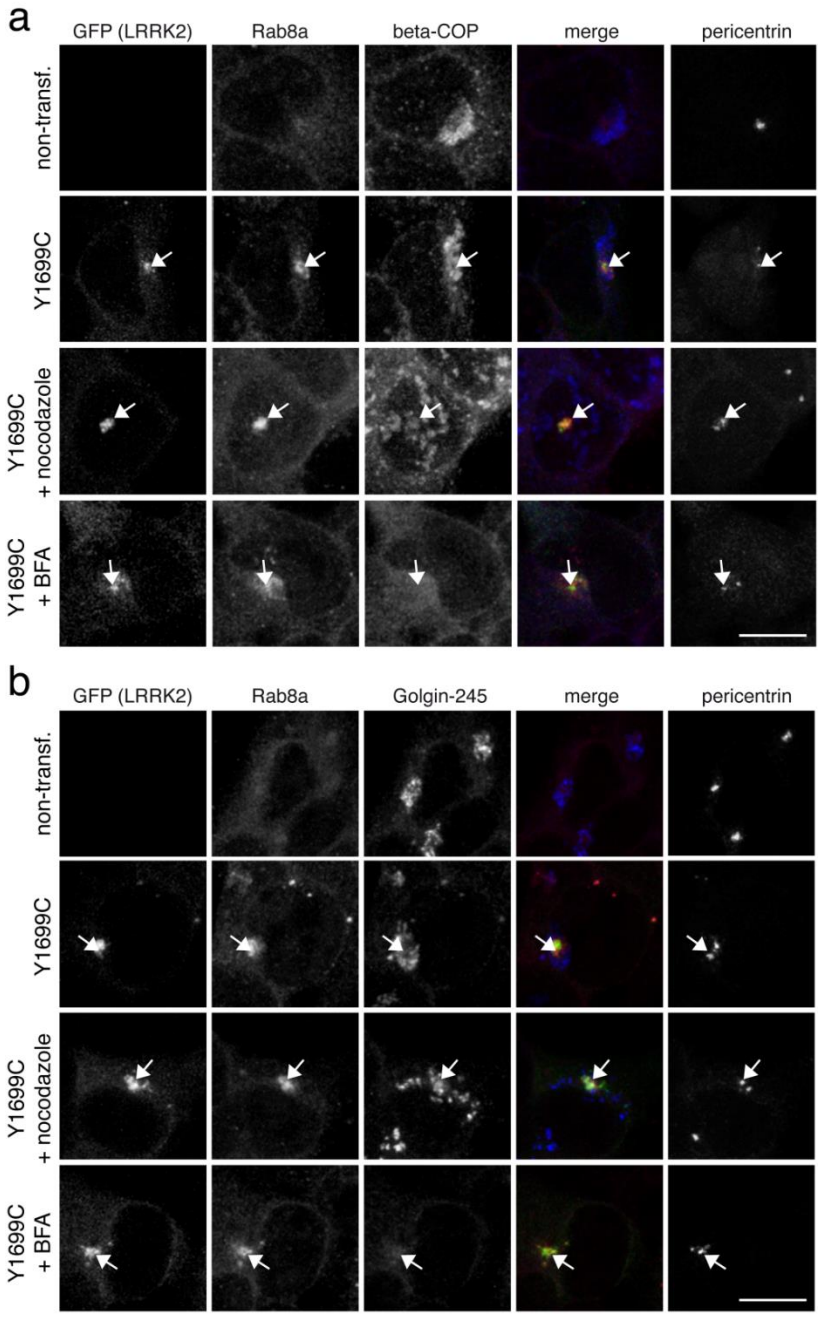

Fig. 21. Golgi dispersal/disruption has no effect on LRRK2-mediated pericentrosomal/centrosomal accumulation of Rab8a. **a)** Example of control cells (non-transf.) or pathogenic LRRK2-transfected cells, either left untreated or treated with nocodazole (200 nM, 2 h) or brefeldin A (BFA, 5 μg/ml, 2h) as indicated, and stained with antibodies against Rab8a, the Golgi marker β-COP, and pericentrin as indicated. Scale bar, 10 μm. **b)** Same as in a, but stained with Golgi marker Golgin-245. Scale bar, 10 μm.

(Fig. 20d, e). Furthermore, Rab8a accumulation was not observed when expressing the kinase-dead pathogenic LRRK2 mutant G2019S-K1906M (Fig. 20b). We thus wondered whether the accumulating Rab8a species may be a phosphorylated version of the protein. For this purpose, non-transfected or pathogenic LRRK2-transfected cells were stained with an antibody raised for the specific detection of phospho-T72-Rab8a [75]. Mutant LRRK2 expression caused a centrosomal/pericentrosomal accumulation of phosphorylated Rab8a, which was not observed when preincubating the phospho-antibody with phospho-peptide, and was reversed upon pretreatment of cells expressing either pathogenic G2019S, R1441C or Y1699C LRRK2 with MLi-2 (Fig. 22a-c). Therefore, the accumulating Rab8a species in LRRK2-expressing HEK293T cells seems to represent a phosphorylated version of the protein.

Amongst all cell types analyzed here, lymphoblasts seem to contain the highest levels of endogenous Rab8a (Fig. 23a). We therefore attempted to determine whether alterations in endogenous phospho-Rab8a accumulation could be detected in lymphoblasts derived from G2019S LRRK2-PD patients as compared to healthy controls. No significant differences in the total levels of Rab8a were detected between lymphoblasts from control versus G2019S LRRK2-PD patients (Fig. 23b and c). Staining with the phospho-Rab8a antibody revealed a pericentrosomal/centrosomal accumulation of phospho-Rab8a in control and G2019S LRRK2-PD samples, which was absent when preincubating the antibody with phosphopeptide (Fig. 23d). Quantification of the intensity of the fluorescence signal revealed a slight, but not significant increase in phospho-Rab8a staining in G2019S LRRK2-PD samples as compared to controls (Fig. 23e), suggesting that higher affinity phospho-antibodies will be required to detect possible changes in the localization of endogenous phosphorylated Rab8a.

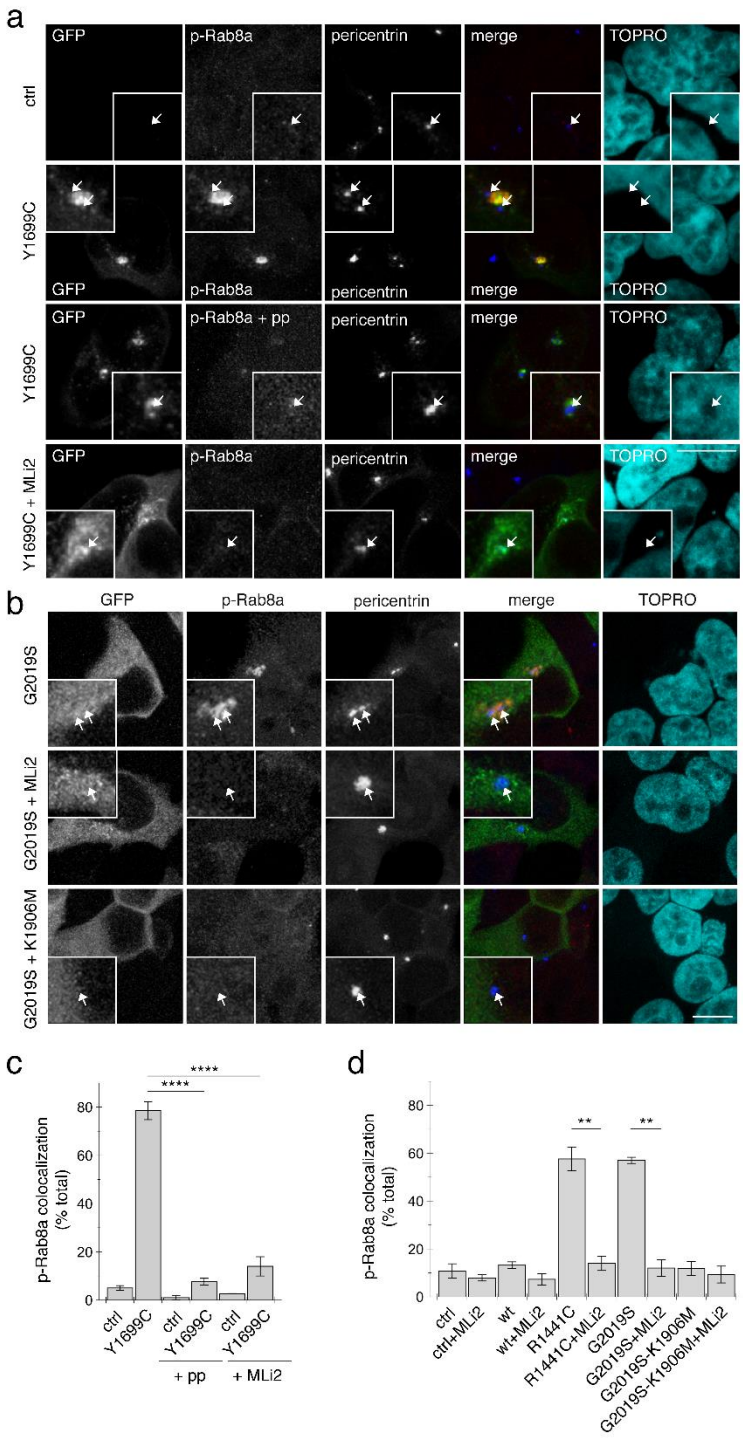

Fig. 22. Pathogenic LRRK2 causes kinase-dependent pericentrosomal/centrosomal accumulation of endogenous phospho-Rab8a. **a,b)** Cells were transfected with pathogenic LRRK2 or with kinase-dead pathogenic LRRK2 as indicated, and stained using an anti-phospho

T72-Rab8a antibody preabsorbed either with dephospho-peptide (p-Rab8a) or with phospho-peptide (p-Rab8a + pp), or with an anti-phospho-T72-Rab8a antibody preabsorbed with dephospho-peptide upon incubation of cells with 100 nM MLi-2 for 60 min prior to immunocytochemistry as indicated. Scale bar, 5 μm. **c)** Quantification of the percentage of non-transfected or transfected cells displaying phospho-Rab8a staining colocalizing with centrosomes within a 3 μm diameter circle in either the absence or presence of antibody preabsorption with peptides or pretreatment of cells with MLi2 as described above. Around 50 cells were quantified per condition per experiment. Bars represent mean ± s.e.m., (n=3 independent experiments); ****, $p < 0.001$. **d)** Quantification of the percentage of non-transfected or transfected cells displaying phospho-Rab8a staining colocalizing with centrosomes as described above. Around 50 cells were quantified per condition per experiment. Bars represent mean ± s.e.m., (n=3 independent experiments); **, $p < 0.01$.

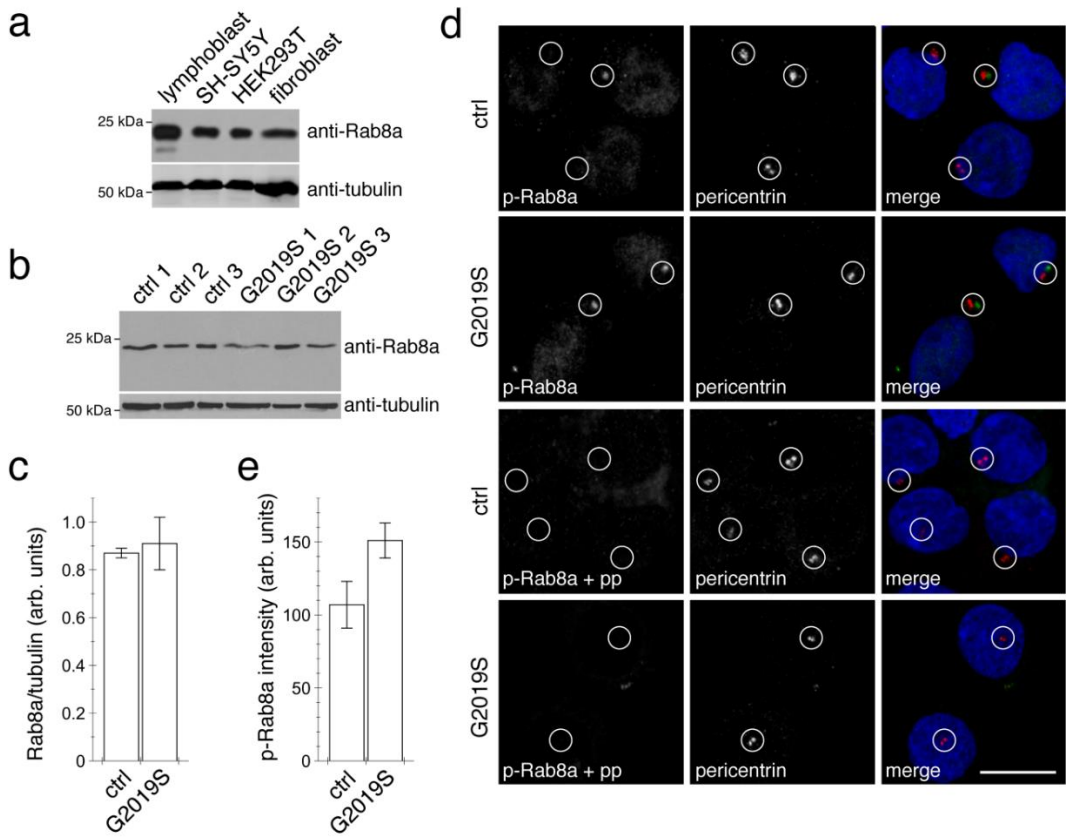

Fig. 23. Rab8a protein levels and pericentrosomal/centrosomal accumulation of phosphorylated Rab8a in lymphoblasts from control and G2019S mutant LRRK2 PD patients. a) Extracts (20 μg protein each) from the indicated cells were resolved by SDS-PAGE and blotted with antibodies against Rab8a or tubulin as loading control. **b)** Extracts (20 μg protein each) from control and G2019S mutant LRRK2-PD patient lymphoblasts were resolved by SDS-PAGE and blotted with antibodies against Rab8a or tubulin as loading control. **c)** Quantification of experiment depicted in b, normalizing Rab8a protein levels to tubulin. **d)** Examples of control or G2019S mutant LRRK2-PD patient lymphoblasts stained with phospho-Rab8a antibody preabsorbed with dephosphopeptide (p-Rab8a), or preabsorbed with phosphopeptide (p-Rab8a + pp) as indicated, and stained with centrosomal marker (pericentrin) and DAPI. Scale bar, 10 μm. **e)** Quantification of fluorescence intensity of phospho-Rab8a staining in healthy control or LRRK2 mutant PD lymphoblasts. Fluorescence intensity was measured in a circle of 3 μm diameter around individual centrosomes as defined by pericentrin staining, and fluorescence intensity from 30-50 individual cells quantified per cell line (three control, three LRRK2 G2019S mutant cell lines).

The phospho-Rab8a antibody was also not able to detect differences in the centrosomal accumulation of endogenous phospho-Rab8a in wildtype versus G2019S LRRK2-mutant SH-SY5Y cells (Fig. 24a and b). Therefore, as a means to increase phosphorylated Rab8a species, we expressed wildtype Rab8a in either wildtype or G2019S LRRK2-mutant SH-SY5Y cells. Under these conditions, a drastic increase in Rab8a phospho-signal was observed (Fig. 24c and d), which was abolished when pretreating cells with a LRRK2 kinase inhibitor, and which was not observed when expressing the non-phosphorylatable Rab8a-T72A mutant (Fig. 24b-d), indicating that it was specifically detecting a LRRK2-phosphorylated version of Rab8a. Even though the expressed RFP-tagged Rab8a protein was widely distributed, the phospho-Rab8a signal was confined to a localization overlapping with that of a centrosomal marker, indicating that the phosphorylated Rab8a species preferentially accumulates in a centrosomal compartment (Fig. 24c and d). Moreover, phosphorylated Rab8a accumulated in a centrosomal compartment irrespective of whether the cells had duplicated centrosomes or not (Fig. 24c and d), suggesting that such localization reflects a general feature not limited to a specific phase of the cell cycle.

We next analyzed whether an increase in centrosomal phospho-Rab8a may cause the observed alterations in centrosomal cohesion. Expression of wildtype Rab8a in wildtype or G2019S mutant LRRK2-expressing SH-SY5Y cells caused a prominent deficit in centrosomal cohesion (Fig. 24e and f). Such cohesion deficits were not observed when expressing the non-phosphorylatable Rab8a-T72A mutant (Fig. 24e and f), even though both Rab8a variants were expressed to similar degrees (Fig. 24g). Premature centrosome splitting induced by G2019S-mutant LRRK2 was not further modulated by the non-phosphorylatable mutant (Fig. 24f), indicating that this mutant does not act as a dominant-negative in this context.

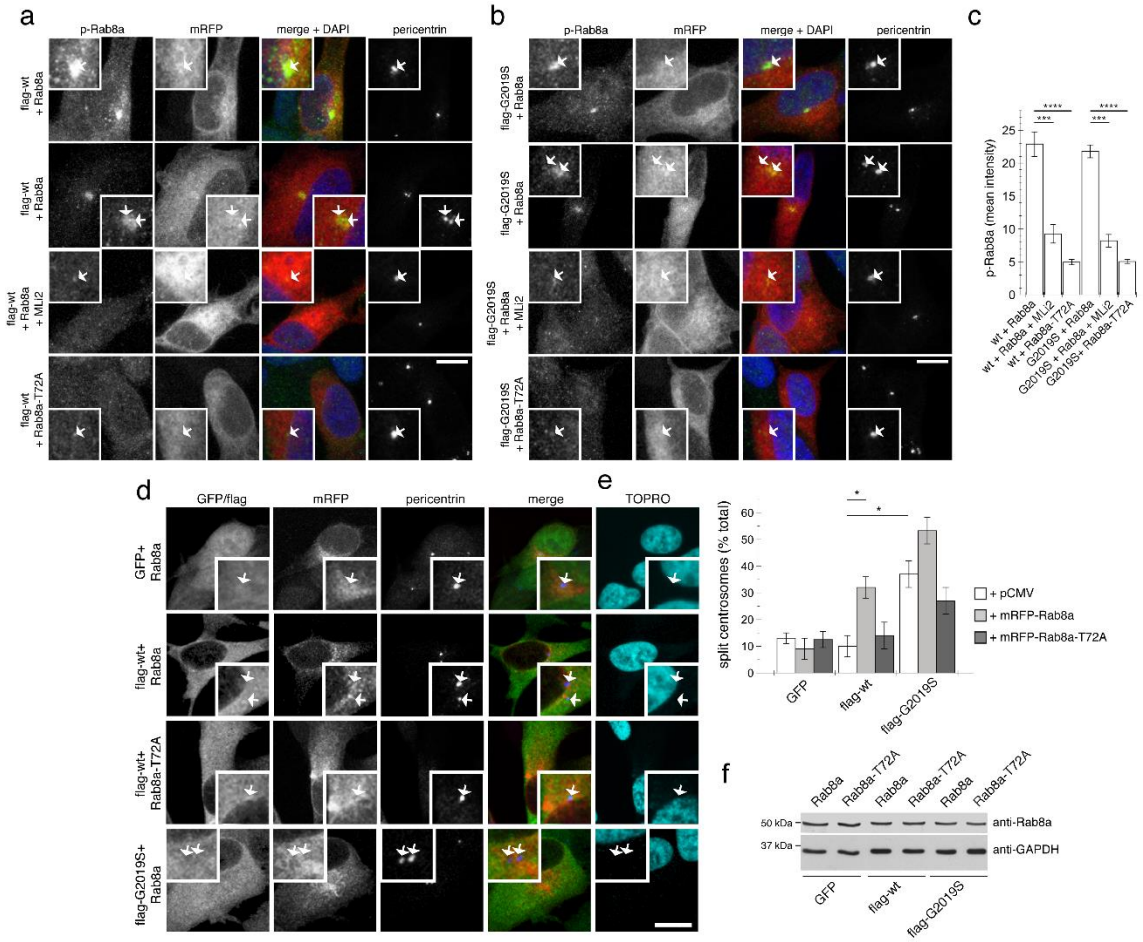

Fig. 24. Expression of wildtype but not phosphorylation-deficient Rab8a causes centrosomal accumulation of phospho-Rab8a and centrosome cohesion deficits in wildtype LRRK2-expressing SH-SY5Y cells. **a**) Example of SH-SY5Y cells stably expressing flag-tagged wildtype LRRK2, and transfected with mRFP-tagged wildtype or T72A-mutant Rab8a as indicated, stained with an anti-phospho-T72-Rab8a antibody preabsorbed with dephosphopeptide, for pericentrin and DAPI. Where indicated, cells were treated with 100 nM MLi2 for 2 h before immunocytochemistry. Note that phospho-Rab8 can be detected both in cells with one centrosome (first panel) as well as in cells with duplicated centrosomes (second panel). Scale bar, 10 μm. **b)** Same as in a, but SH-SY5Y cells stably expressing flag-tagged G2019S mutant LRRK2. Scale bar, 10 μm. **c)** Quantification of mean fluorescence intensity of phospho-Rab8a signal as described in Methods in cells either stably expressing wildtype (wt) or G2019S mutant LRRK2, transfected with RFP-tagged Rab8a or T72-mutant Rab8a, and treated with 100 nM MLi2 for 2 h before immunocytochemistry as indicated. Bars represent mean ± s.e.m., (n=3 independent experiments); ****, $p < 0.001$; ***, $p < 0.005$. **d)** Example of non-differentiated SH-SY5Y cells stably expressing GFP, flag-tagged wildtype or G2019S-mutant LRRK2 as indicated, and transfected with Rab8a or phosphorylation-deficient Rab8a (Rab8a-T72A) as indicated, and stained for pericentrin and TOPRO. Scare bar, 10 μm. **e)** Quantification of the split centrosome phenotype in SH-SY5Y cells from the type of experiments depicted in a. Bars represent mean ± s.e.m. (n=3 experiments); *, $p < 0.05$. **f)** SH-SY5Y cells stably expressing GFP, flag-tagged wildtype or G2019S-mutant LRRK2 as indicated were transfected with mRFP-tagged wildtype or phosphorylation-deficient Rab8a (Rab8a-T72A) as indicated, and extracts blotted for Rab8a levels and GAPDH as loading control.

Similar results were obtained in HEK293T cells (Fig. 25). Co-expression of wildtype LRRK2 with wildtype Rab8a resulted in LRRK2-mediated Rab8a phosphorylation, which was further enhanced when co-expressing the distinct pathogenic, but not kinase-dead K1906M or G2019S-K1906M LRRK2 mutants (Fig. 25a). Co-expression of wildtype LRRK2 with wildtype Rab8a caused a centrosomal cohesion deficit which was not observed when expressing the non-phosphorylatable Rab8a-T72A mutant (Fig. 25b and c) or when treating cells with kinase inhibitor (Fig. 25d). Altogether, these data indicate that increasing the centrosomal amount of LRRK2-phosphorylated Rab8a correlates with the observed centrosomal cohesion deficits.

Pathogenic LRRK2-induced centrosomal cohesion and polarity deficits are mediated by Rab8a

To determine whether the centrosomal deficits caused by pathogenic LRRK2 kinase were Rab8a-mediated, HEK293T cells were transiently transfected with small interfering RNAs (siRNA) directed against a control sequence or against Rab8a. Cells transfected with the Rab8a-specific siRNA showed a significant decrease in Rab8a protein content when compared to control siRNA (Fig. 26a and b). Whilst knocking down Rab8a protein levels did not cause alterations in centrosomal cohesion in non-transfected cells or in cells transfected with wildtype LRRK2, it caused a significant reversal in the centrosomal cohesion deficits induced by pathogenic G2019S, R1441C or Y1699C LRRK2 expression (Fig. 26c and d).

As an additional means to assure that the observed reversal of the LRRK2-mediated centrosomal cohesion deficits were due to knockdown of Rab8a, we generated siRNA-resistant versions of Rab8a as well as Rab8a-T72A (Fig. 26e).

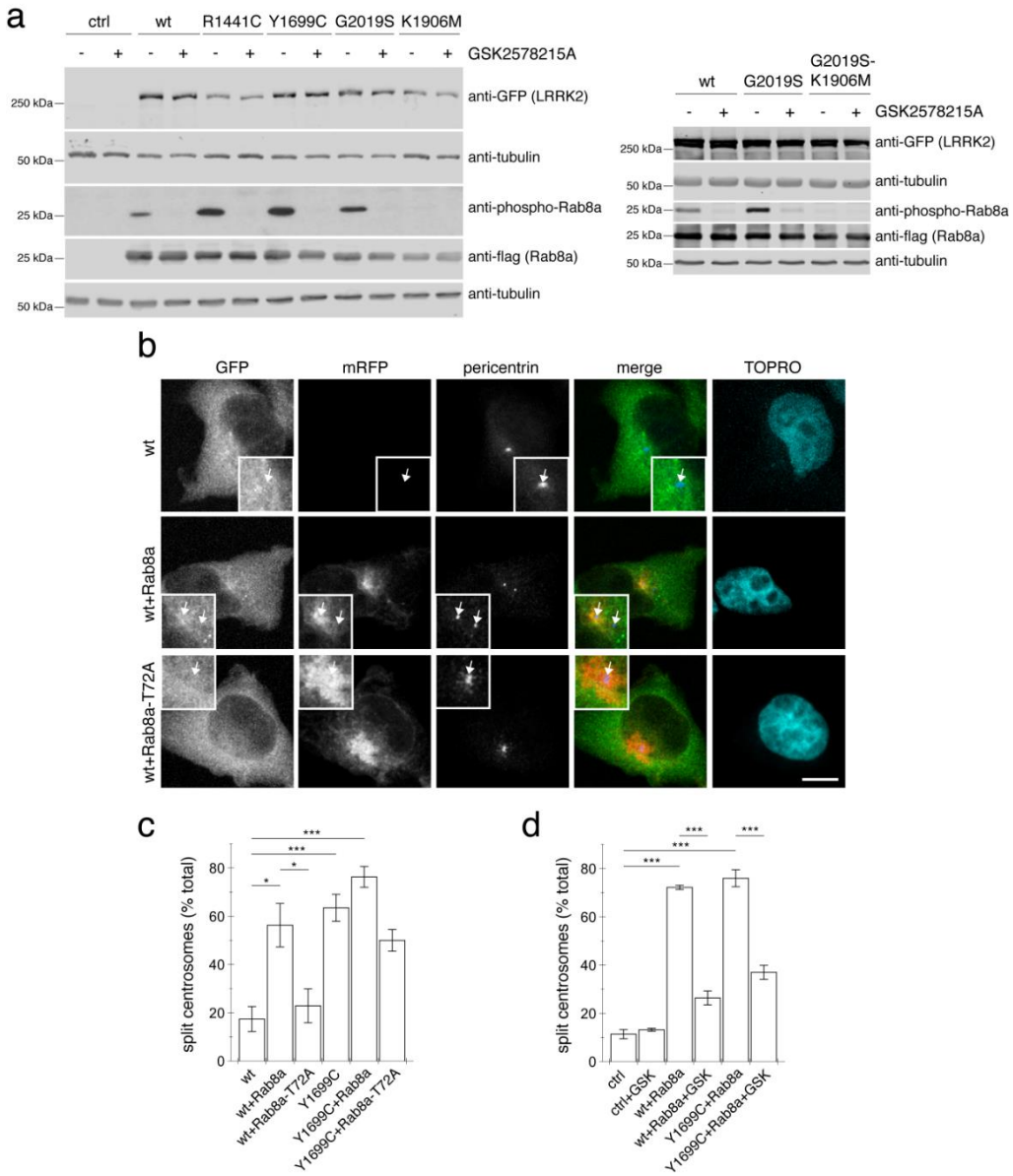

Fig. 25. Detection of phospho-Rab8a in pathogenic LRRK2-expressing cells as well as in cells co-transfected with wildtype LRRK2 and wildtype Rab8a, but not phospho-deficient Rab8a. **a)** Cells were transfected with constructs as indicated, and cellular lysates subjected to Western blotting with an anti-phospho-Rab8a antibody. Anti-GFP and anti-flag antibodies were used to measure total LRRK2 and Rab8a levels. **b)** Example of HEK293T cells co-transfected with GFP-tagged wildtype LRRK2 and either mRFP-Rab8a or mRFP-Rab8a-T72A as indicated, and stained with pericentrin antibody and TO-PRO. Scale bar, 5 μm. **c)** Quantification of the split centrosome phenotype in HEK293T cells co-expressing wildtype or pathogenic mutant LRRK2 and wildtype or phospho-deficient Rab8a mutant as indicated. Bars represent mean ± s.e.m. (n=3 independent experiments); *** $p < 0.005$; * $p < 0.05$. **d)** Quantification of the split centrosome phenotype in non-transfected HEK293T cells (ctrl), or in cells co-expressing wildtype or pathogenic mutant LRRK2 along with Rab8a, in either the presence or absence of 500 nM GSK2578215A for 1h as indicated. Bars represent mean ± s.e.m. (n=3 independent experiments); *** $p < 0.005$.

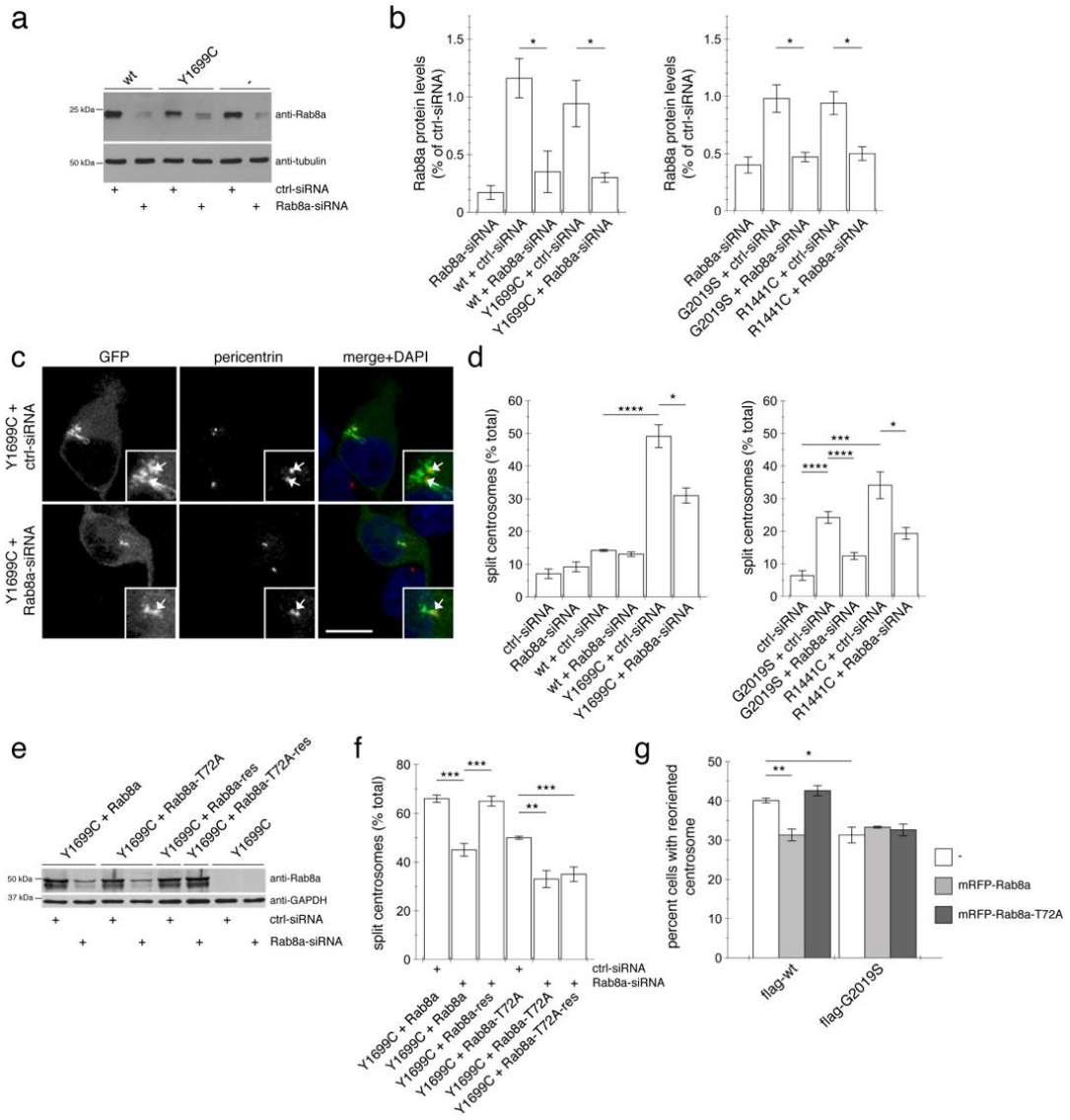

Fig. 26. Knockdown of Rab8a significantly reverses the centrosomal deficits mediated by pathogenic LRRK2. a) Representative Western blot of extracts from control cells (ctrl), or cells transfected with wildtype (wt) or Y1699C-mutant LRRK2, along with either ctrl-siRNA or Rab8a-siRNA as indicated, and blotted against Rab8a or tubulin as loading control. **b)** Quantification of the type of experiments depicted in **a**, with levels of Rab8a normalized to tubulin and to Rab8a levels in the presence of ctrl-siRNA. Bars represent mean ± s.e.m. (n=3-5 independent experiments); * $p < 0.05$. **c)** Example of cells co-transfected with GFP-tagged pathogenic LRRK2 and either ctrl-siRNA or Rab8a-siRNA as indicated, and stained with pericentrin antibody and DAPI. Scale bar, 10 µm. **d)** Quantification of the split centrosome phenotype in control cells transfected with either ctrl-siRNA or Rab8a-siRNA, or in cells co-transfected with wildtype or mutant LRRK2 as indicated. Bars represent mean ± s.e.m. (n=3-5 independent experiments); **** $p < 0.001$; * $p < 0.05$. **e)** Western

blot of cell extracts transfected with either ctrl-siRNA or Rab8a-siRNA as indicated, and four hours later cotransfected with mutant LRRK2 and mRFP-tagged Rab8a, Rab8a-T72A, or siRNA-resistant versions thereof (res), and blotted against Rab8a and GAPDH as loading control. **f)** Quantification of the split centrosome phenotype in the presence of ctrl-siRNA or Rab8a-siRNA, and in the presence of pathogenic mutant LRRK2 and mRFP-tagged Rab8a, Rab8a-T72A or siRNA-resistant versions thereof (res) as indicated. Bars represent mean ± s.e.m. (n=3 independent experiments); *** $p < 0.005$; ** $p < 0.01$. **g)** Quantification of centrosome reorientation in cells stably expressing flag-tagged wildtype or G2019S-mutant LRRK2 together with RFP-tagged wildtype or phospho-deficient T72A Rab8a 4 h after generating the wound (t = 4 h). Random orientation is expected to be 25%. n > 50 cells were quantified for each condition in each experiment. Bars represent mean ± s.e.m. (n=3 independent experiments); **, $p < 0.01$; *, $p < 0.05$.

Whilst siRNA of Rab8a reduced the mutant LRRK2-mediated centrosomal cohesion deficits in transiently transfected HEK293T cells, those deficits were restored in the presence of siRNA-resistant Rab8a, but not of siRNA-resistant Rab8a-T72A mutant (Fig. 26f). Therefore, Rab8a, and specifically a phosphorylatable form of Rab8a, is important for pathogenic LRRK2 to cause the observed centrosomal deficits.

Finally, when analyzing cell polarization upon scratch wounding, expression of wildtype Rab8a, but not phosphorylation-deficient Rab8a, caused a pronounced decrease in the percentage of cells with reoriented centrosomes in wildtype LRRK2-expressing cells after 4 h of wounding, whilst not further altering the deficits observed in G2019S LRRK2-expressing cells (Fig. 26g). Thus, the effects of pathogenic LRRK2 on centrosome positioning in the context of cell polarity also seem to involve a Rab8a-mediated phosphorylation event.

2. Rab7L1-mediated relocalization of LRRK2 to the Golgi complex causes centrosomal deficits via Rab8a

Rab7L1 recruits LRRK2 to the Golgi in a manner independent on the LRRK2 kinase activity

We first determined the localization of mRFP-tagged Rab7L1 constructs in HEK293T cells. Rab7L1 was localized to a perinuclear area largely overlapping with a trans-Golgi marker, whilst a mutant shown to lack GTP binding (Rab7L1-T21N) was more cytosolic (Fig. 27a). Similarly, a mutant designed to impair GTP hydrolysis (Rab7L1-Q67L) but shown to display higher GTP/GDP dissociation rates was more cytosolic (Fig. 27a), even though expressed to similar degrees (Fig. 27b). Thus, and as previously described [45], both Rab7L1-Q67L and Rab7L1-S21N mutants seem to act as loss-of-function variants.

When expressed on its own, wildtype GFP-tagged LRRK2 displayed a largely cytosolic localization (Fig. 28a). In contrast, co-expression of wildtype LRRK2 with wildtype but not loss-of-function mutant Rab7L1 caused recruitment of LRRK2 to the Rab7L1 compartment in all co-transfected cells (Fig. 28a). Three distinct pathogenic LRRK2 mutants (G2019S, R1441C, Y1699C) were preferentially localized to the cytosol, but also to a pericentrosomal/centrosomal area, or in addition to filamentous structures reported to colocalize with microtubules (Fig. 28b) [88, 176, 306]. Coexpression with Rab7L1 caused the relocalization of all pathogenic LRRK2 mutants in all cells analyzed (Fig. 28b). Similarly, cytosolic kinase-inactive K1906M mutant LRRK2, as well as pharmacologically kinase-inhibited LRRK2, which tends to colocalize with microtubules [88, 184, 294], were recruited upon co-expression with Rab7L1 in all cells examined (Fig. 28c). When assessed by co-immunoprecipitation assays from detergent-solubilized extracts, 3xFlag-tagged Rab7L1 was found to similarly interact with wildtype, pathogenic mutant or kinase-inhibited LRRK2 (Fig. 28d,e) [45]. In contrast, 3xFlag-tagged Rab7 or Rab9 did not interact with wildtype LRRK2 (Fig. 29e,f). Thus, in a cellular context, Rab7L1 causes the relocalization of wildtype, pathogenic, kinase-dead as well as kinase-inhibited LRRK2, indicating

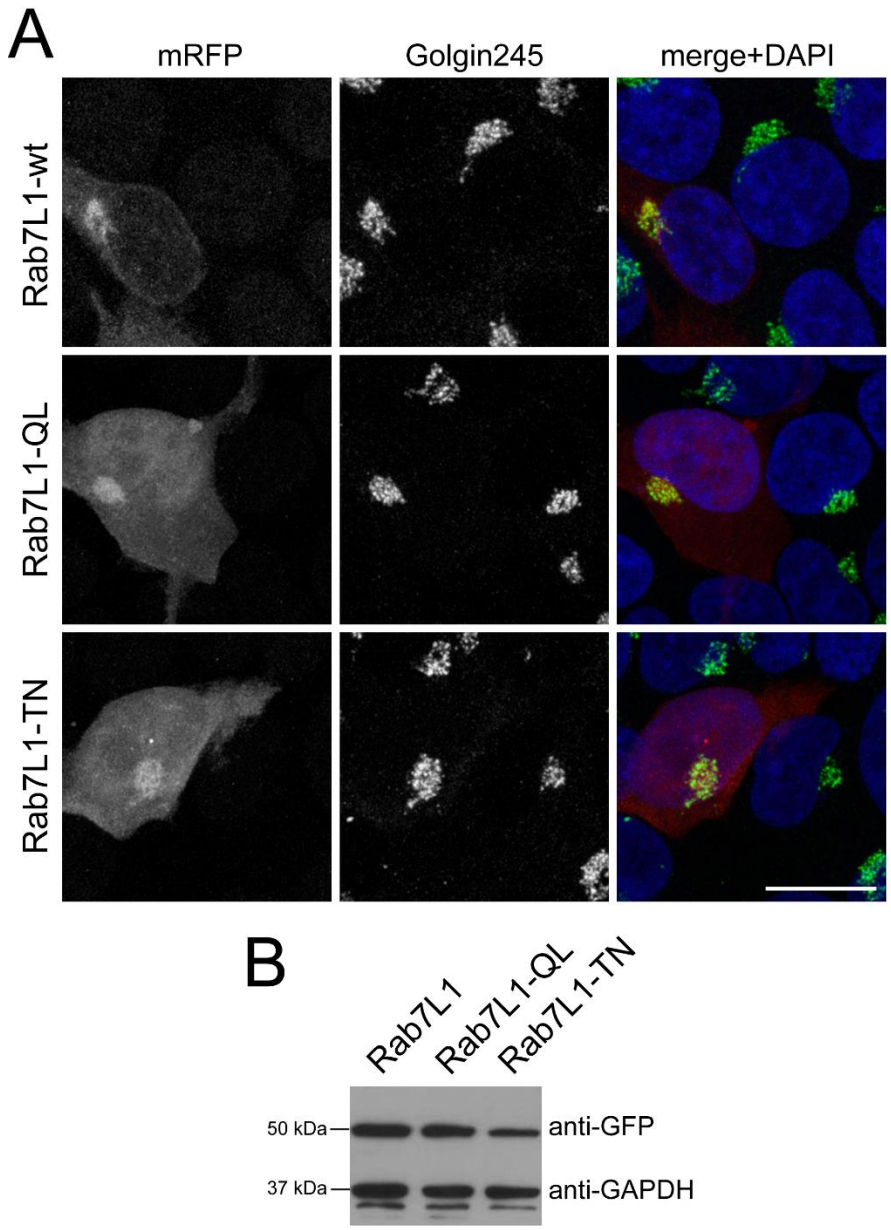

Fig. 27. mRFP-tagged wildtype Rab7L1, but not inactive Rab7L1 variants, are localized to the Golgi apparatus. a) Example of HEK293T cells transfected with mRFP-tagged wildtype or mutant Rab7L1 constructs (red) as indicated, and stained with a trans-Golgi marker antibody (Golgin245, Alexa 488-conjugated secondary antibody, green) and DAPI (blue). Scale bar, 10 µm. **b)** Cells were transfected with the indicated GFP-tagged Rab7L1 constructs, and extracts blotted with an anti-GFP antibody or anti-GAPDH as loading control to confirm similar expression levels of the distinct Rab7L1 variants. Values were normalized to GAPDH, and then normalized to wildtype Rab7L1.

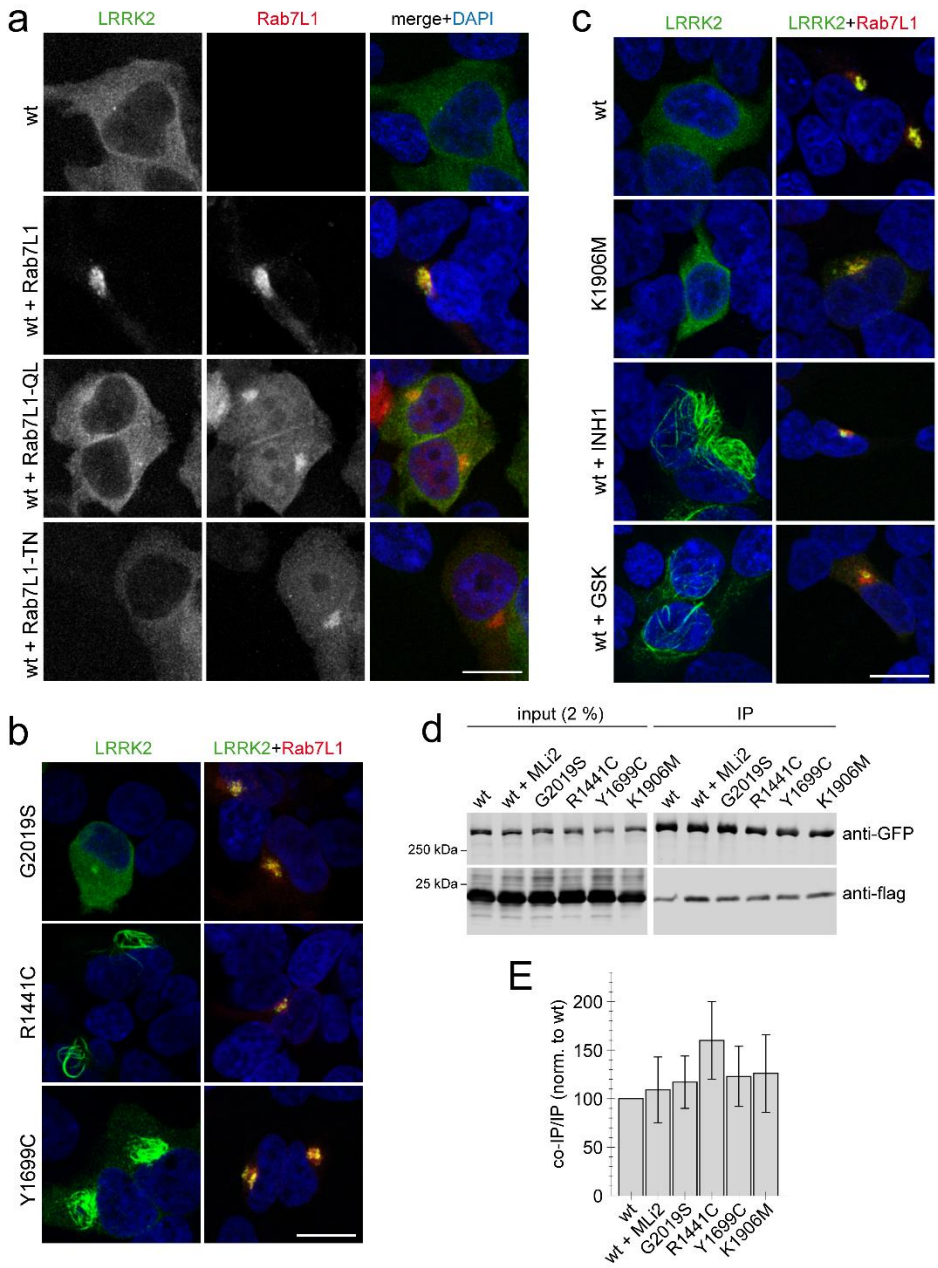

Fig. 28. Rab7L1 causes recruitment of LRRK2 in a manner independent on kinase activity. a) Example of HEK293T cells transfected with either GFP-tagged wildtype LRRK2 (green), or cotransfected with wildtype LRRK2 and wildtype or mutant mRFP-tagged Rab7L1 (red) as indicated, and stained with DAPI (blue). Scale bar, 10 µm. **b)** Example of cells cotransfected with the indicated pathogenic GFP-LRRK2 mutants (green) and mRFP-Rab7L1 (red) as indicated, and stained with DAPI (blue). Scale bar, 10 µm. **c)** Example of cells cotransfected with mRFP-Rab7L1 (red) and either wildtype or K1906M kinase-dead mutant GFP-LRRK2 (green), or cotransfected

with wildtype GFP-LRRK2 (green) and treated with 500 nM LRRK2-IN-1 (INH1) or 500 nM GSK2578215A (GSK) for 60 min before fixation, and stained with DAPI (blue). Scale bar, 10 µm. **d)** Cells were cotransfected with the indicated GFP-tagged LRRK2 constructs and flag-tagged Rab7L1, and treated with 100 nM MLi2 for 60 min where indicated. Binding between LRRK2 and Rab7L1 was assessed by co-immunoprecipitation of GFP-tagged LRRK2 variants with flag-tagged Rab7L1 using a polyclonal GFP antibody. Left panel shows inputs, and right panel shows samples after immunoprecipitation, probed for GFP (using a monoclonal GFP antibody) as well as for flag. **e)** Quantification of experiments as depicted in (d) were performed by comparing the amount of coimmunoprecipitated Rab7L1 to the amount of LRRK2 in the immunoprecipitation (IP). Data are mean ± s.e.m. (n=5 independent experiments).

---

that the kinase activity is not required for such Rab7L1-mediated recruitment of LRRK2.

The Rab7L1-mediated recruitment of wildtype LRRK2 causes centrosomal cohesion deficits

Our previous studies have revealed a centrosomal cohesion deficit in pathogenic LRRK2-expressing cells [306]. Since the centrosome is in close apposition to the Golgi apparatus [156, 290], we next wondered whether the Rab7L1-mediated recruitment of wildtype LRRK2 to the Golgi complex may also cause centrosomal alterations. In HEK293T cells, no centrosomal cohesion deficits were observed when active or inactive Rab7L1 mutants were expressed on their own (Fig. 30a,b). However, when co-expressed with wildtype LRRK2, active but not inactive Rab7L1 mutants caused relocalization of LRRK2, concomitant with an increase in the percentage of split centrosomes (Fig. 30a,b). No further cohesion deficits were observed when expressing active Rab7L1 with pathogenic LRRK2 (Fig. 30b,c), possibly because the overexpression of this pathogenic LRRK2 mutant already caused a maximal centrosomal cohesion deficit in this cell type.

To determine whether the effects were specific to Rab7L1, we co-expressed LRRK2 with either Rab7 or Rab9, two Rab proteins involved in endolysosomal and/or retromer-mediated trafficking pathways [307-309] and reported to be

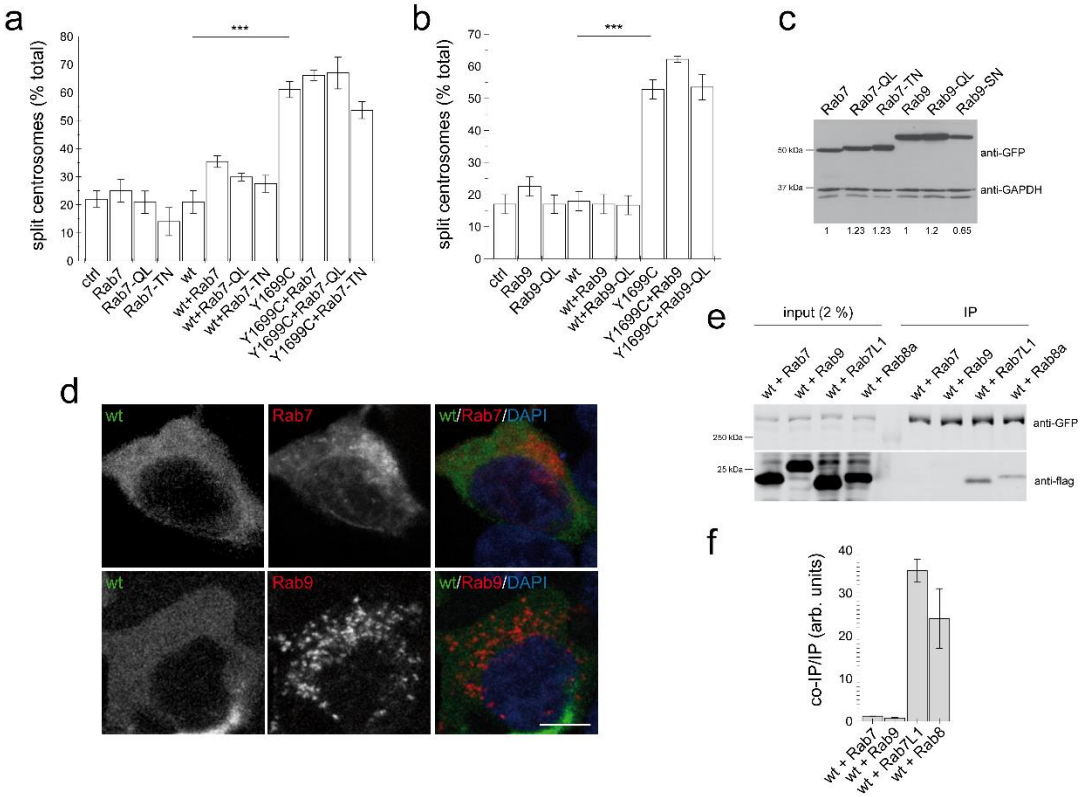

Fig. 29. No effect of Rab7 or Rab9 on LRRK2 localization or on LRRK2-mediated centrosomal cohesion deficits. a) Quantification of the split centrosome phenotype in cells expressing mRFP-tagged Rab7 or mutants thereof, in the absence or presence of wildtype or pathogenic Y1699C-mutant GFP-tagged LRRK2 as indicated. At least 50 transfected cells were analyzed per condition per experiment. Bars represent mean ± s.e.m. (n=3 experiments); ***, $p < 0.005$. **b)** Quantification of the split centrosome phenotype in cells expressing ds-Red-tagged Rab9 or mutants thereof, in the absence or presence of wildtype or pathogenic Y1699C-mutant LRRK2 as indicated. Bars represent mean ± s.e.m. (n=3 experiments); ***, $p < 0.005$. At least 50 transfected cells were analyzed per condition per experiment. **c)** Cells were transfected with the indicated GFP-tagged Rab7 or Rab9 constructs, and extracts blotted with an anti-GFP antibody or anti-GAPDH as loading control to confirm similar expression levels of the distinct Rab variants. Values were normalized to GAPDH, and then normalized to wildtype Rab7 or Rab9, respectively. **d)** Example of HEK293T cells expressing GFP-tagged wildtype LRRK2 (green) and either mRFP-Rab7 (red) or dsRed-Rab9 (red), and stained with DAPI (blue). Images are maximal intensity projections of 4 consecutive z-stack images. Scale bar, 5 µm. **e)** Cells were cotransfected with wildtype GFP-tagged LRRK2 (wt) and the indicated flag-tagged Rab constructs, and binding between LRRK2 and Rabs assessed by co-immunoprecipitation of GFP-tagged LRRK2 with flag-tagged Rab proteins using a polyclonal GFP antibody. Left panel shows inputs, and right panel shows samples after immunoprecipitation, probed for GFP (using a monoclonal GFP antibody) as well as for flag. **f)** Quantification of experiments as depicted in (e) were performed by comparing the amount of coimmunoprecipitated Rab proteins to the amount of wildtype LRRK2 in the immunoprecipitation (IP). Data are mean ± s.e.m. (n=3 independent experiments).

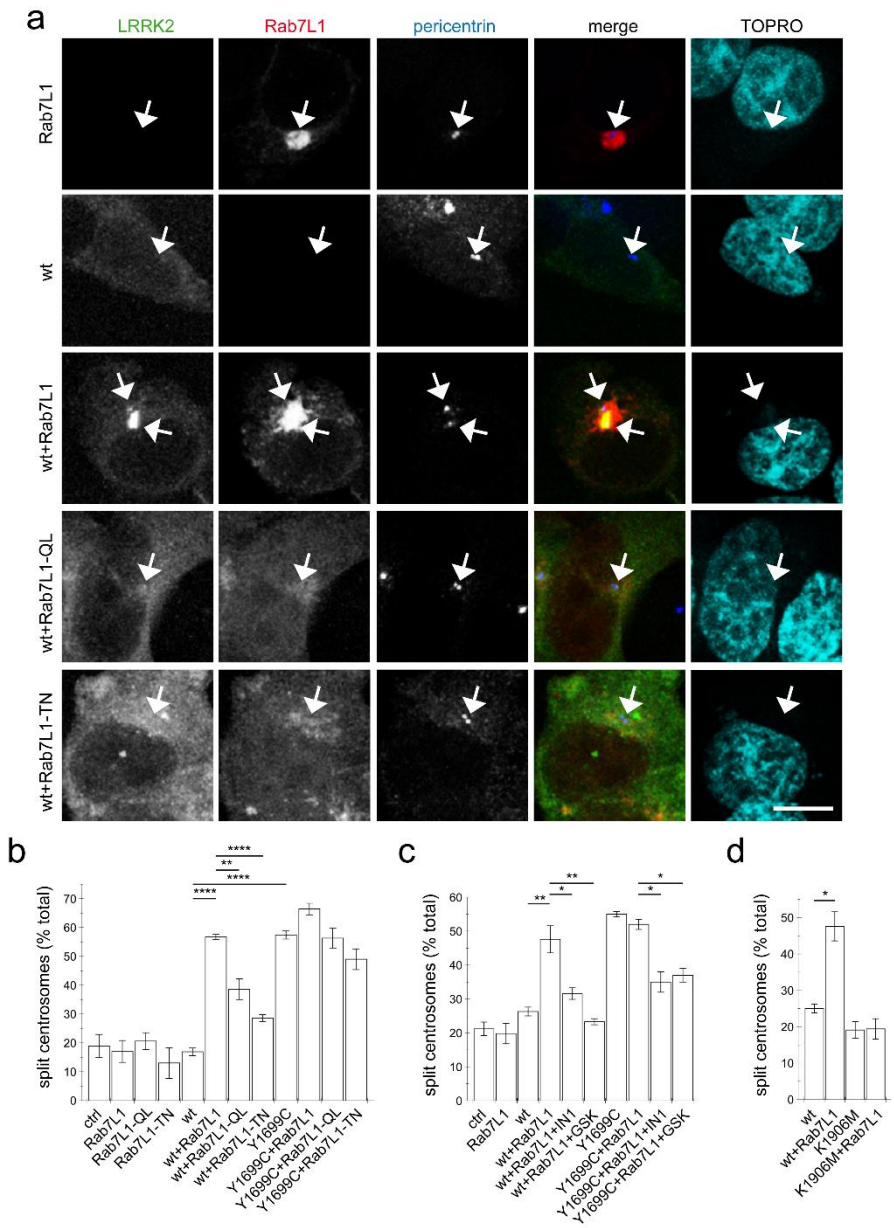

Fig. 30. The Rab7L1-mediated recruitment of wildtype LRRK2 causes centrosomal cohesion deficits in a manner dependent on LRRK2 kinase activity and similar to those of pathogenic LRRK2. a) Example of HEK293T cells transfected with either GFP-tagged wildtype LRRK2 (green), mRFP-tagged Rab7L1 (red), or a combination of wildtype LRRK2 and Rab7L1 or mutants thereof as indicated, and stained with pericentrin antibody (Alexa 405-conjugated secondary antibody, blue) and TO-PRO-3 (far red fluorescence similar to Alexa 647, pseudo-colored in cyan). Scale bar, 5 µm. **b)** Quantification of the split centrosome phenotype in cells expressing Rab7L1 or mutants thereof, or co-expressing wildtype or Y1699C-mutant LRRK2 and Rab7L1 or mutants

thereof, as indicated. At least 50 transfected cells were analyzed per condition per experiment. Bars represent mean ± s.e.m. (n=3 experiments); ****, $p < 0.001$; **, $p < 0.01$. **c)** Quantification of the split centrosome phenotype in cells expressing Rab7L1 or mutants thereof, or co-expressing wildtype or Y1699C-mutant LRRK2 and Rab7L1 or mutants thereof, and treated with LRRK2-IN-1 (500 nM) or GSK2578215A (500 nM) for 60 min as indicated. At least 50 transfected cells were analyzed per condition per experiment. Bars represent mean ± s.e.m. (n=3 experiments); **, $p < 0.01$; *, $p < 0.05$. **d)** Quantification of the split centrosome phenotype in cells expressing wildtype or K1906M kinase-dead mutant LRRK2 and Rab7L1 as indicated. At least 50 transfected cells were analyzed per condition per experiment. Bars represent mean ± s.e.m. (n=3 experiments); *, $p < 0.05$.

---

modulated and/or interact with LRRK2 [144, 151]. Neither active nor inactive Rab7 nor Rab9 variants caused centrosomal cohesion deficits on their own, albeit expressed to comparable degrees (Fig. 29a-c). Rab7 or Rab9 also did not cause centrosomal deficits when co-expressed with wildtype LRRK2, and did not alter the centrosomal deficits induced by pathogenic LRRK2 (Fig. 29a,b). Expression of either Rab7 or Rab9 failed to cause recruitment of wildtype LRRK2 to the respective Rab7/Rab9 compartments (Fig. 29d). This was paralleled by a lack of detectable interaction between LRRK2 and Rab7 or Rab9, in contrast to the interaction observed with Rab7L1 (Fig. 29e,f). Thus, and at least amongst the Rab proteins analyzed here, the subcellular relocalization of wildtype LRRK2 seems rather specific to Rab7L1 and is associated with centrosomal cohesion deficits identical to those previously described for all pathogenic LRRK2 mutants [306].

The Rab7L1-induced centrosomal cohesion deficits of wildtype LRRK2 are kinase activity-mediated

We next determined whether the Rab7L1-induced centrosomal deficits in the presence of wildtype LRRK2 are due to the kinase activity of LRRK2. Short-term application of two specific and structurally distinct LRRK2 kinase inhibitors [294, 295] significantly reverted the centrosomal cohesion deficits induced in the presence of Rab7L1 and wildtype LRRK2, and a similar reversal was observed when co-expressing Rab7L1 with pathogenic LRRK2 (Fig. 30c). Conversely, even

though both are recruited to the Rab7L1 compartment (Fig. 28), centrosomal cohesion deficits were induced when coexpressing Rab7L1 with wildtype LRRK2, but not with kinase-inactive K1906M mutant LRRK2, respectively (Fig. 30d).

To probe for possible cell type-specific differences, we examined the effects of Rab7L1 expression in human SH-SY5Y neuroblastoma cells stably transduced with GFP, or with flag-tagged wildtype or G2019S mutant LRRK2, respectively [283, 284]. As previously described [306], there was no difference in centrosome cohesion between control GFP and flag-tagged wildtype LRRK2-expressing cells, whilst the flag-tagged G2019S LRRK2-expressing cells displayed a bigger percentage of cells with split centrosomes (Fig. 31a,b). In this cell system, expression of Rab7L1 on its own, in control cells and thus in the context of endogenous LRRK2 levels, caused a centrosomal cohesion phenotype (Fig. 31b). Such Rab7L1-mediated enhancement of the centrosomal deficits was more pronounced in wildtype LRRK2-expressing cells as compared to control cells, and further enhanced in cells stably expressing G2019S mutant as compared to wildtype LRRK2, respectively (Fig. 31b). In both wildtype and G2019S mutant LRRK2-expressing cells, Rab7L1 expression caused recruitment of the majority of LRRK2 to the Rab7L1 compartment (91 ± 4.5 % recruitment in wildtype, 80 ± 4.7 % recruitment in G2019S; n=3 independent experiments), suggesting that the observed differences in centrosomal cohesion in the presence of Rab7L1 are due to the enhanced kinase activity of G2019S mutant versus wildtype LRRK2. Indeed, and in all cases examined, the centrosomal alterations were reverted upon short-term application of MLi2, a recently developed novel and highly selective LRRK2 kinase inhibitor [298], revealing that they were mediated by the LRRK2 kinase activity (Fig. 31b). Therefore, expression of Rab7L1 in both HEK293T and SH-SY5Y cells causes the relocalization of wildtype and pathogenic LRRK2 to a Rab7L1 compartment largely overlapping with the trans-Golgi, and triggers centrosomal cohesion deficits which are dependent on the LRRK2 kinase activity.

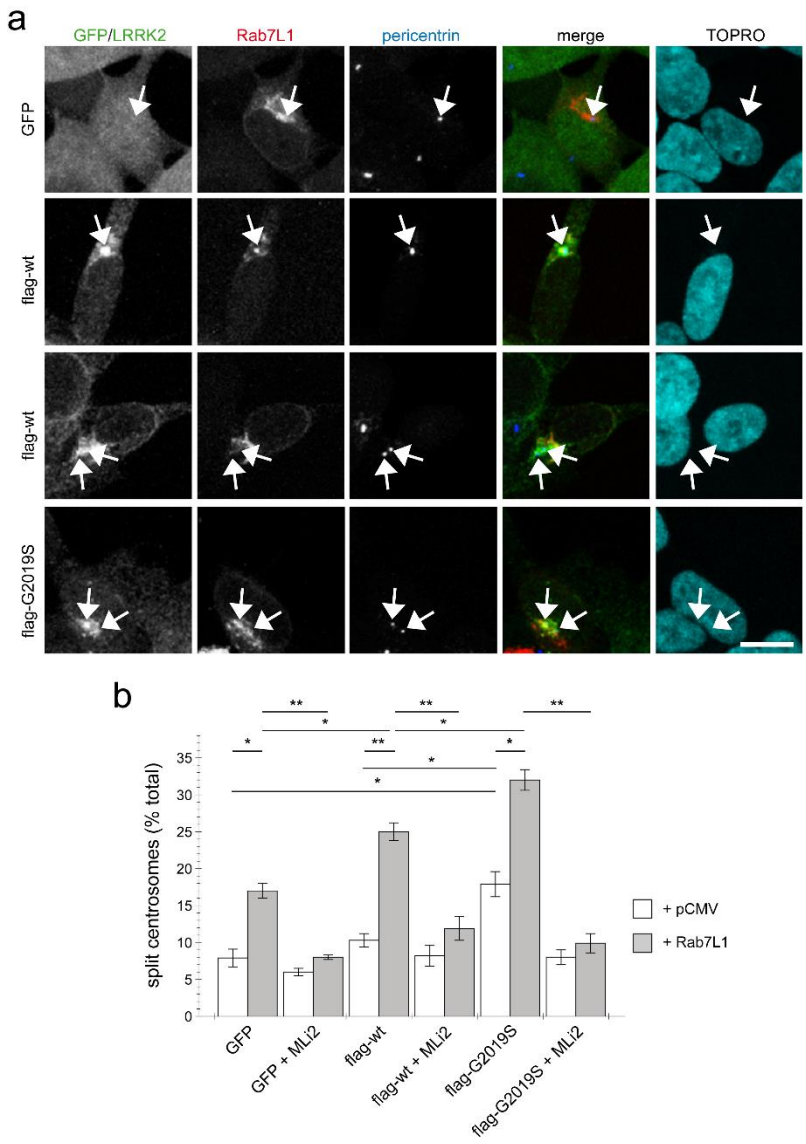

Fig. 31. Rab7L1 potentiates the LRRK2-mediated centrosomal cohesion deficits in SH-SY5Y cells. a) Example of SH-SY5Y cells stably expressing GFP (green), or flag-tagged wildtype or G2019S-mutant LRRK2 (Alexa 488-conjugated secondary antibody, green), and transiently transfected with mRFP-Rab7L1 (red), followed by staining for pericentrin (Alexa 405-conjugated secondary antibody, blue) and TO-PRO-3 (far red fluorescence similar to Alexa 647, pseudo-colored in cyan). Depicted are the most prominent centrosomal phenotypes, namely one centrosome in GFP-expressing cells, one centrosome or two split centrosomes in wildtype LRRK2-expressing cells, and two split centrosomes in G2019S mutant LRRK2-expressing cells, respectively. Scale bar, 10 µm. **b)** Quantification of the split centrosome phenotype in SH-SY5Y cells expressing GFP, flag-tagged wildtype or G2019S-mutant LRRK2, and transfected with either empty vector (pCMV) or Rab7L1, and treated with MLi-2 (100 nM) for 60 min as indicated. At least 100 transfected cells were analyzed per condition per experiment. Bars represent mean ± s.e.m. (n=3 experiments); **, $p < 0.01$; *, $p < 0.05$.

The cohesion deficits induced by Rab7L1-mediated LRRK2 recruitment correlate with aberrant centrosomal accumulation of phosphorylated Rab8a

We previously showed that the centrosomal cohesion deficits induced by pathogenic LRRK2 are mediated by the aberrant pericentrosomal/centrosomal accumulation of phosphorylated Rab8a [306]. We therefore next wondered whether the Rab7L1-mediated centrosomal alterations in the presence of wildtype LRRK2 may also be caused by the same mechanism. Co-expression of Rab7L1 with wildtype LRRK2 in HEK293T cells caused a prominent increase in the amount of cells displaying accumulation of pericentrosomal/centrosomal Rab8a (Fig. 32a,b). Such accumulation was reverted upon application of the LRRK2 kinase inhibitor MLi2 (Fig. 32a,b), indicating that it may correspond to the phosphorylated form of Rab8a. When staining transfected cells with an antibody raised for the specific detection of phospho-T72-Rab8a [75], cells co-expressing Rab7L1 and wildtype LRRK2 displayed prominent centrosomal/pericentrosomal accumulation of phospho-Rab8a which was reversed when treating cells with MLi-2, and which was not observed when preincubating the phospho-antibody with phospho-peptide (Fig. 33a,b). Similarly, co-expression of Rab7L1 and wildtype LRRK2 caused detectable phosphorylation of endogenous Rab8a as measured by Western blotting, without changes in total Rab8a protein levels (Fig. 33c). Such phospho-Rab8a signal was abolished when treating cells with kinase inhibitor, and was not observed when expressing wildtype LRRK2 alone (Fig. 33c). Whilst accumulation of phospho-Rab8a by immunocytochemistry in SH-SY5Y cells stably expressing pathogenic LRRK2 could only be detected when overexpressing Rab8a [306], expression of Rab7L1 caused a detectable accumulation of endogenous phospho-Rab8a in SH-SY5Y cells expressing wildtype LRRK2, and a further accumulation in cells expressing G2019S-mutant LRRK2 (20.7 ± 5 % of wildtype versus 50 ± 3.7 % of G2019S-mutant LRRK2 cells; n=3 experiments, $p < 0.05$; Fig. 34). Thus, increasing the levels of Rab7L1 causes accumulation of endogenous phospho-Rab8

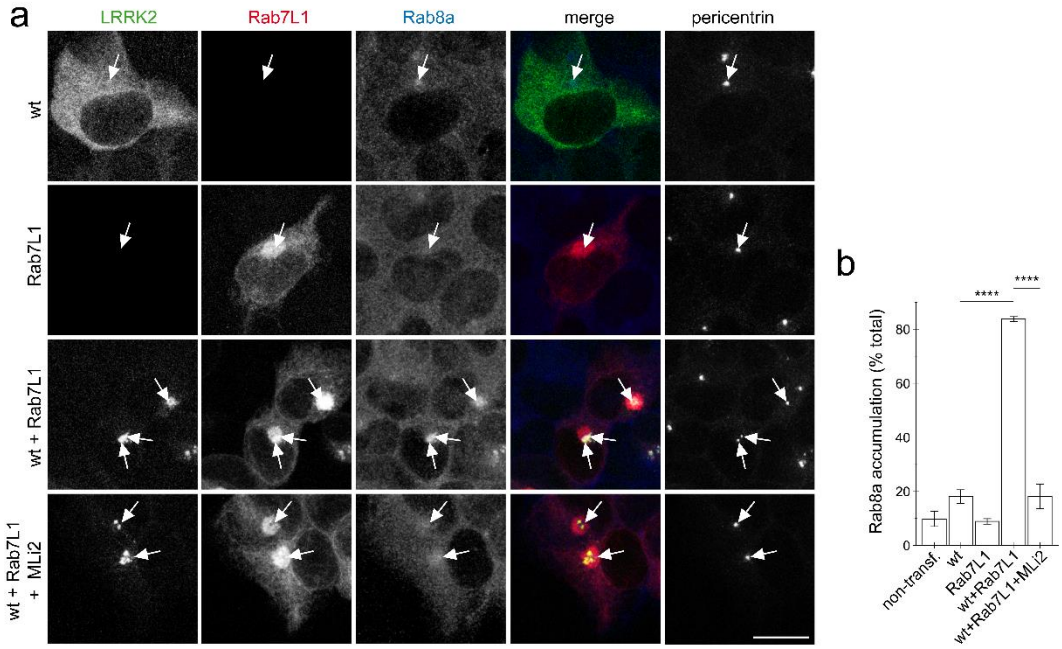

Fig. 32. Rab7L1 causes kinase-dependent pericentrosomal/centrosomal accumulation of endogenous Rab8a in the presence of wildtype LRRK2. a) Example of HEK293T cells transfected with either GFP-tagged wildtype LRRK2 (wt) (green), mRFP-tagged Rab7L1 (red), or a combination thereof, treated with 100 nM MLi2 for 60 min where indicated, and stained with Rab8a (Alexa 647-conjugated secondary antibody, pseudo-colored in blue) and with pericentrin antibody (Alexa 405-conjugated secondary antibody, pseudo-colored in grey). Scale bar, 10 µm. **b)** Quantification of the percentage of transfected cells displaying pericentrosomal Rab8a staining of the type of experiments depicted in (A). At least 50 transfected cells were analyzed per condition per experiment. Bars represent mean ± s.e.m. (n=3 experiments); ****, $p < 0.0001$.

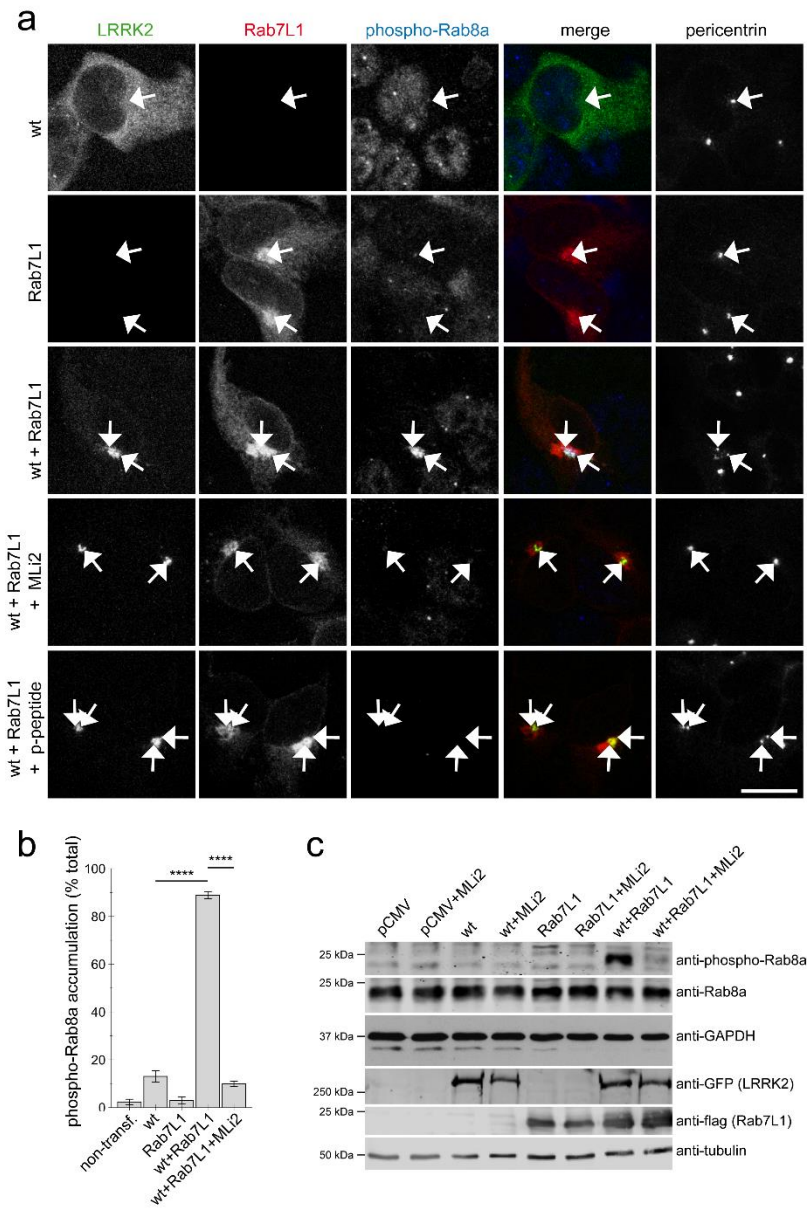

Fig. 33. Coexpression of Rab7L1 and wildtype LRRK2 cause kinase-dependent pericentrosomal/centrosomal accumulation of endogenous phospho-Rab8a. a) Example of HEK293T cells transfected with GFP-tagged wildtype LRRK2 (wt) (green), mRFP-tagged Rab7L1 (red), or a combination thereof, and stained with pericentrin (Alexa 405-conjugated secondary antibody, pseudo-colored in grey), and an anti-phospho-T72-Rab8a antibody (Alexa 647-conjugated secondary antibody, pseudo-colored in blue), the antibody preabsorbed with phospho-peptide (p-peptide), or cells treated with 100 nM MLi-2 for 60 min prior to immunocytochemistry, as indicated. Scale bar, 10 µm. **b)** Quantification of the percentage of non-transfected or transfected cells displaying phospho-Rab8a staining from experiments of the type depicted in (a). At least 50 cells were analyzed per condition per experiment. Bars represent mean ± s.e.m. (n=3 experiments); ****, $p < 0.0001$. **c)** HEK293T cells were transfected with the different constructs and treated with 100 nM MLi-2 for 60 min where indicated, and extracts blotted for phospho-Rab8a, total Rab8a, GFP (for LRRK2 detection), flag (for Rab7L1 detection), and GAPDH or tubulin as loading controls.

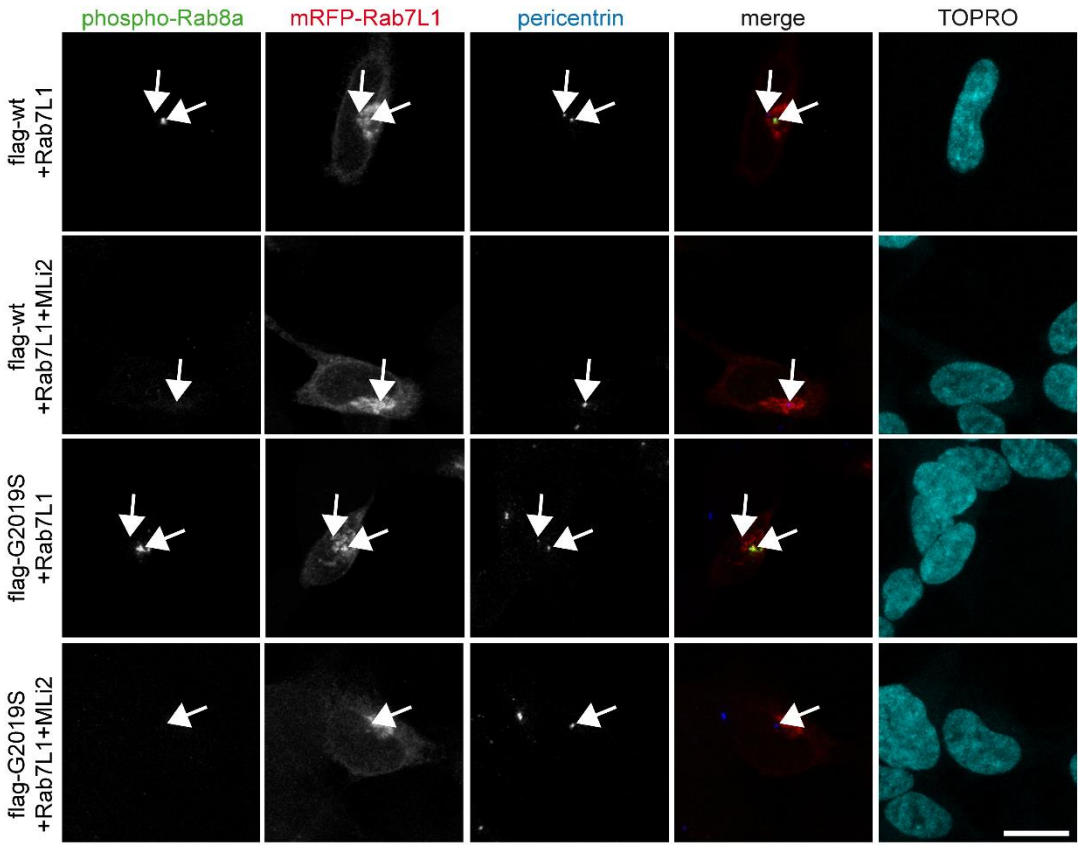

Fig. 34. Accumulation of phospho-Rab8a in SH-SY5Y cells expressing Rab7L1. Cells stably expressing flag-tagged wildtype or G2019S LRRK2 were transfected with mRFP-Rab7L1 (red), treated or not treated with 100 nM MLi-2 for 60 min prior to immunocytochemistry as indicated, and stained for phospho-Rab8a (Alexa 488-conjugated secondary antibody, green), pericentrin (Alexa 405-conjugated secondary antibody, blue), and TO-PRO-3 (far red fluorescence similar to Alexa 647, pseudo-colored in cyan). Scale bar, 10 µm.

and deficits in centrosomal functioning in the presence of wildtype as well as pathogenic LRRK2.

The Rab7L1-induced centrosomal deficits of wildtype LRRK2 require Golgi integrity and are Rab8a-mediated

To determine whether the Rab7L1-mediated recruitment of wildtype LRRK2 was required for the accumulation of pericentrosomal/centrosomal phosphorylated Rab8a, cells were treated with brefeldin A, which causes redistribution of the Golgi complex into the ER [302, 310]. Brefeldin A treatment disrupted the perinuclear localization of Rab7L1 and wildtype LRRK2, which was associated with the loss of phospho-Rab8a accumulation (Fig. 35a,b). This was paralleled by the reversal of the centrosomal cohesion deficits induced by Rab7L1 and wildtype LRRK2 (Fig. 35c,d). Therefore, the Rab7L1-mediated recruitment of wildtype LRRK2 to the Golgi complex is required for the downstream effects on centrosomal cohesion. This is in contrast to the centrosomal cohesion deficits induced by pathogenic Y1699C-mutant LRRK2, which is localized to a pericentrosomal/centrosomal area and causes centrosomal cohesion deficits also in the presence of brefeldin A (Fig. 35d) [306]. In agreement with these findings, RNAi of Rab7L1 with two different small interfering RNAs (siRNAs) did not alter the localization nor the centrosomal cohesion deficits mediated by Y1699C-mutant LRRK2 (Fig. 36a-d), suggesting that this mutant causes centrosomal defects in a manner largely independent on Rab7L1 or on Golgi integrity.

To determine whether the centrosomal cohesion deficits caused by Rab7L1 and wildtype LRRK2 were Rab8a-dependent, HEK293T cells were transiently transfected with siRNA directed against a control sequence or with two different siRNAs against Rab8a, and knockdown of protein levels confirmed by Western blotting (Fig. 37a,b). Knocking down Rab8a did not alter centrosomal cohesion in non-transfected cells, but caused a significant reversal of the cohesion deficits

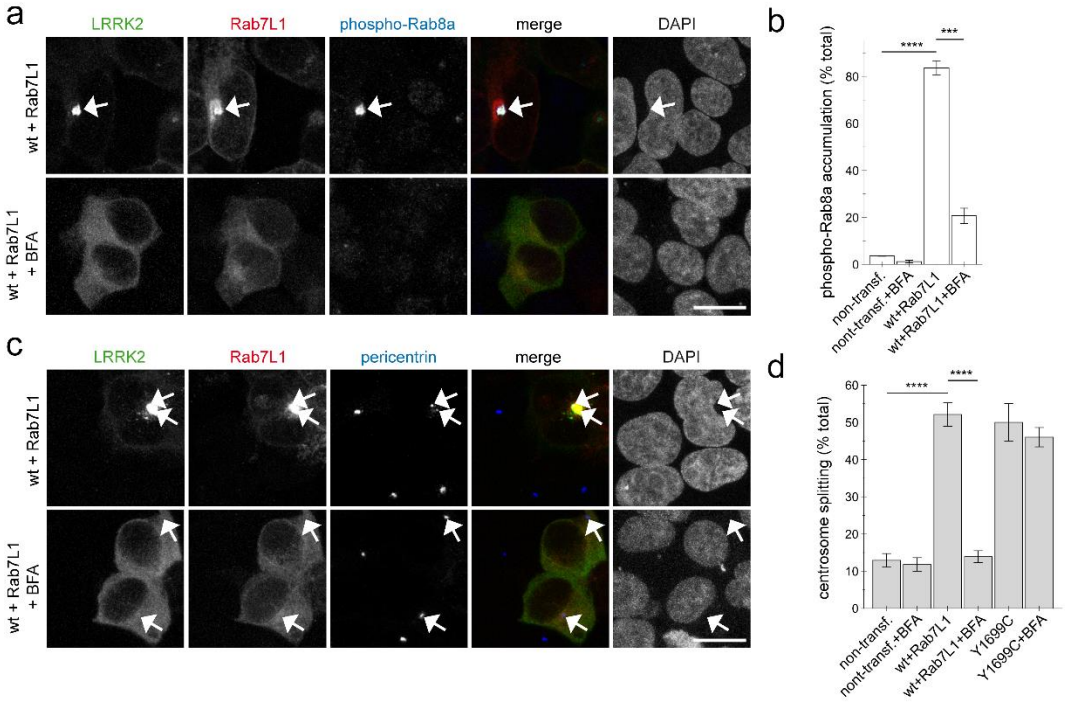

Fig. 35. Integrity of the Golgi complex is required for the Rab7L1-mediated phospho-Rab8a accumulation and centrosomal cohesion deficits of wildtype LRRK2. a) HEK293T cells were cotransfected with GFP-tagged LRRK2 (green) and mRFP-tagged Rab7L1 (red), and either treated or non-treated with brefeldin A (BFA; 5 µg/ml) for 3 h as indicated before staining with phospho-Rab8a antibody (Alexa 647-conjugated secondary antibody, pseudo-colored in blue) and DAPI (pseudo-colored in grey). Scale bar, 10 µm. **b)** Quantification of the percentage of non-transfected or transfected cells displaying phospho-Rab8a staining, in the presence or absence of brefeldin A as indicated, from experiments of the type depicted in (a). At least 50 cells were analyzed per condition per experiment. Bars represent mean ± s.e.m. (n=3 experiments); ****, $p < 0.0001$; ***, $p < 0.005$. **c)** Cells were cotransfected with GFP-tagged LRRK2 (green) and mRFP-tagged Rab7L1 (red), and either treated or non-treated with brefeldin A (BFA; 5 µg/ml) for 3 h as indicated before staining with pericentrin antibody (Alexa 647-conjugated secondary antibody, pseudo-colored in blue) and DAPI (pseudo-colored in grey). Scale bar, 10 µm. **d)** Quantification of the split centrosome phenotype in non-transfected or transfected cells as indicated, in the presence or absence of brefeldin A, from experiments of the type depicted in (c). At least 50 cells were analyzed per condition per experiment. Bars represent mean ± s.e.m. (n=3 experiments); ****, $p < 0.0001$.

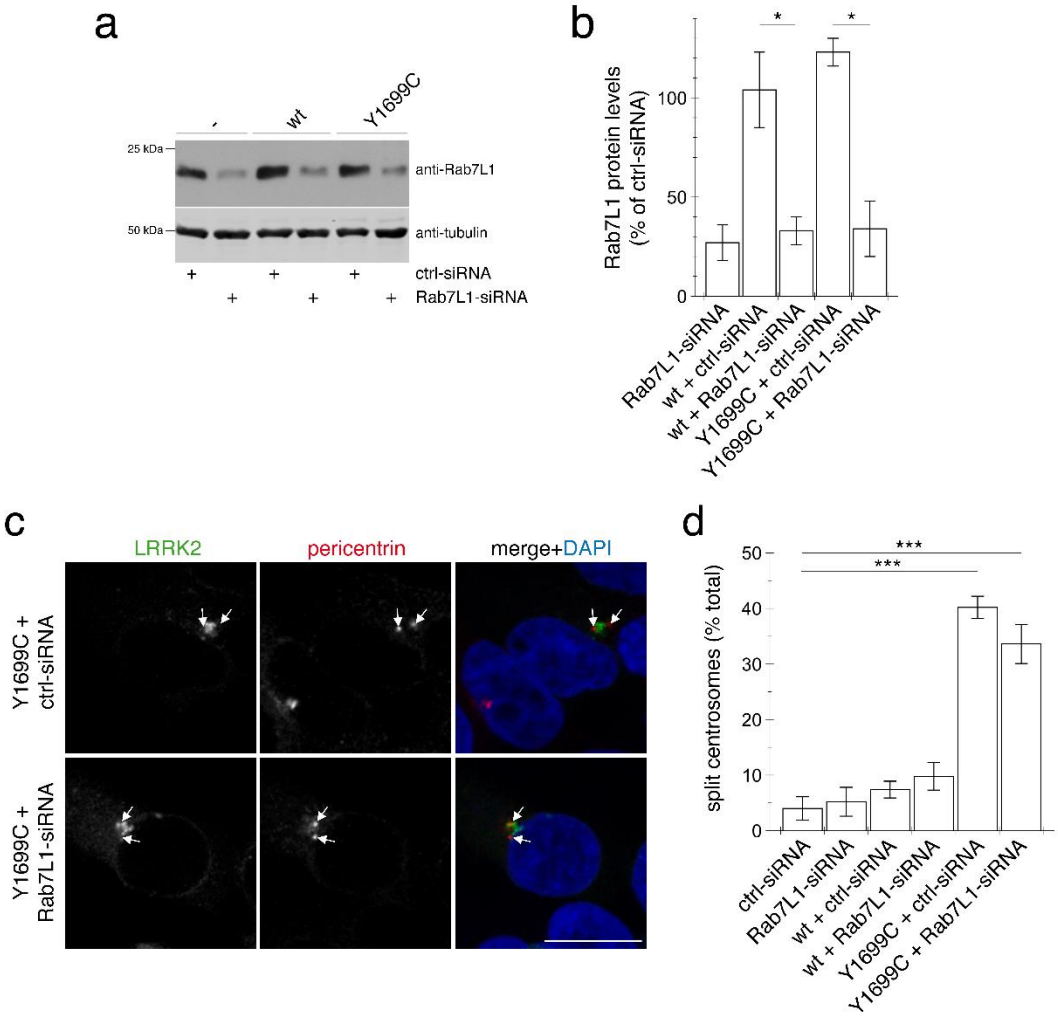

Fig. 36. Knockdown of Rab7L1 does not alter the centrosomal cohesion deficits mediated by pathogenic LRRK2. a) Representative Western blot of extracts from control cells (-), or cells transfected with wildtype (wt) or Y1699C-mutant LRRK2, along with either ctrl-siRNA or Rab7L1-siRNA as indicated, and blotted against Rab7L1 or tubulin as loading control. **b)** Quantification of the type of experiments depicted in (a), with levels of Rab7L1 normalized to tubulin and to Rab7L1 levels in the presence of ctrl-siRNA. Bars represent ± s.e.m. (n=3 experiments); *, $p < 0.05$. **c)** Example of HEK293T cells co-transfected with GFP-tagged Y1699C mutant LRRK2 (green) and either ctrl-siRNA or Rab7L1-siRNA as indicated, and stained with pericentrin antibody (Alexa 647-conjugated secondary antibody, pseudo-colored in red) and DAPI (blue). Scale bar, 10 μm. **d)** Quantification of the split centrosome phenotype in control cells transfected with either ctrl-siRNA or Rab7L1-siRNA, or in cells co-transfected with siRNA and with wildtype or mutant LRRK2. Around 100 transfected cells were analyzed per condition per experiment. Bars represent mean ± s.e.m. (n=3 experiments); ***, $p < 0.005$.

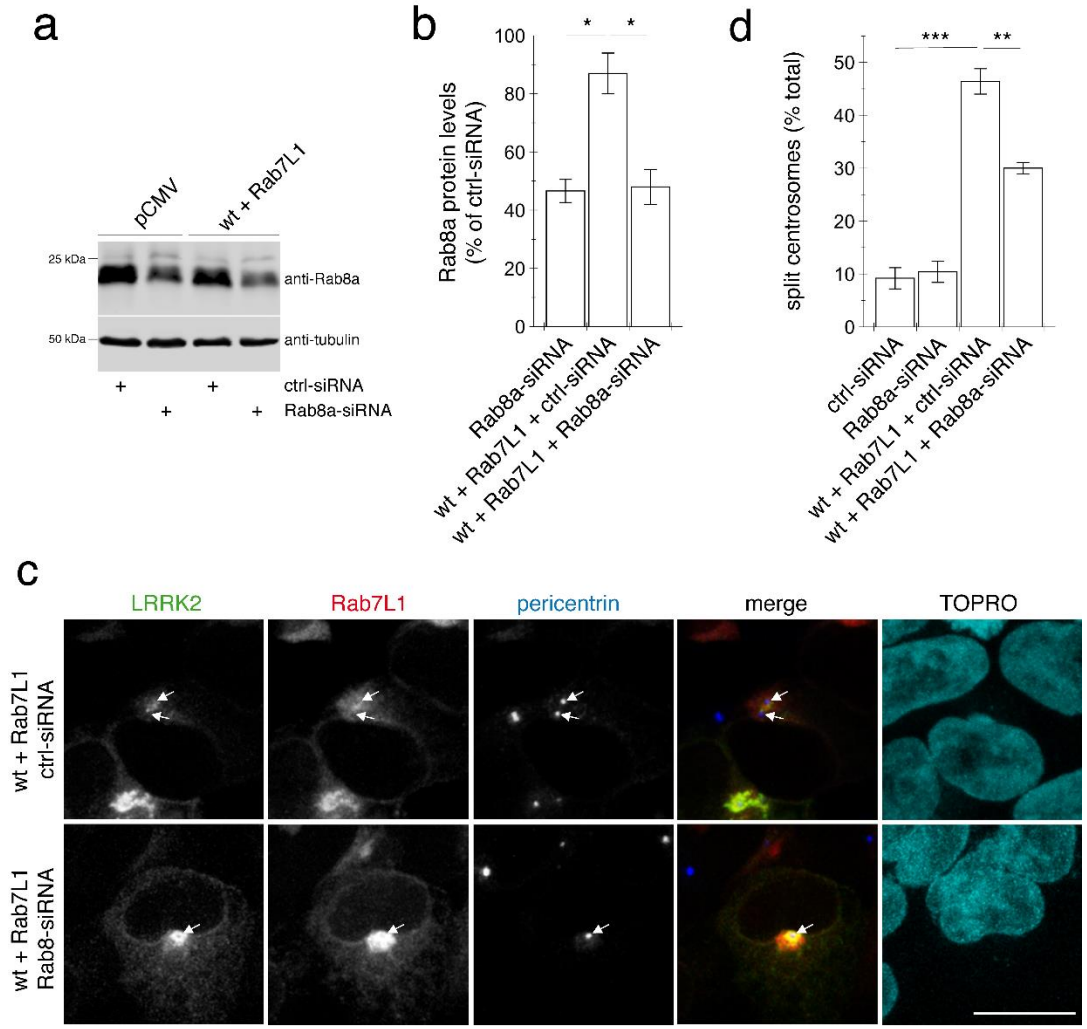

Fig. 37. Knockdown of Rab8a significantly reverses the centrosomal cohesion deficits mediated by Rab7L1 and wildtype LRRK2. a) Representative Western blot of extracts from control pCMV-transfected cells, or cells transfected with wildtype (wt) LRRK2 and Rab7L1, along with either ctrl-siRNA or Rab8a-siRNA as indicated, and blotted against Rab8a or tubulin as loading control. **b)** Quantification of the type of experiments depicted in (a), with levels of Rab8a normalized to tubulin and to Rab8a levels in the presence of ctrl-siRNA. Bars represent ± s.e.m. (n=3 experiments); *, $p < 0.05$. **c)** Example of HEK293T cells co-transfected with GFP-tagged wildtype LRRK2 (green) and mRFP-tagged Rab7L1 (red), and either with ctrl-siRNA or Rab8a-siRNA as indicated, and stained with pericentrin antibody (Alexa 405-conjugated secondary antibody, blue) and TO-PRO-3 (far red fluorescence similar to Alexa 647, pseudo-colored in cyan). Scale bar, 10 µm. **d)** Quantification of the split centrosome phenotype in control cells transfected with either ctrl-siRNA or Rab8a-siRNA, or in cells co-transfected with the respective siRNAs and with wildtype LRRK2 and Rab7L1. Around 100 transfected cells were analyzed per condition per experiment. Bars represent ± s.e.m. (n=3 experiments); ***, $p < 0.005$; **, $p < 0.01$.

induced by the co-expression of Rab7L1 and LRRK2, without interfering with the recruitment of LRRK2 to the Golgi complex (Fig. 37c,d). Therefore, and as described for pathogenic LRRK2 mutants [306], phosphorylated Rab8a seems to mediate, at least in part, the centrosomal cohesion deficits induced by Rab7L1 and wildtype LRRK2.

V. DISCUSSION

The present work provides evidence that mutant LRRK2 causes centrosomal alterations in both dividing as well as non-dividing cells. Centrosomal deficits were observed with distinct pathogenic LRRK2 mutants and in distinct cell lines, as well as in two different patient-derived cell types. The effects were reverted by various specific and structurally distinct LRRK2 kinase inhibitors, suggesting that LRRK2 causes centrosomal alterations in a kinase activity-dependent manner. Pathogenic LRRK2 expression caused centrosomal defects accompanied by an accumulation of endogenous phosphorylated Rab8a in a pericentrosomal/centrosomal area. Centrosomal deficits were significantly reverted upon RNAi of Rab8a, suggesting that they are, at least in part, mediated by Rab8a. In addition, we show that increasing the levels of Rab7L1 causes recruitment of wildtype LRRK2 to the Golgi complex, triggering accumulation of endogenous phosphorylated Rab8a around the centrosome, and concomitant cohesion deficits similar to the ones observed with pathogenic LRRK2 expression. The centrosomal defects caused by wildtype LRRK2 in the presence of increased Rab7L1 levels are also reverted by RNAi of Rab8a. Altogether, the present data indicate that such centrosomal defects may be a common phenotype for a broader spectrum of PD, namely familial LRRK2-related PD and sporadic Rab7L1-related PD.

Effects of pathogenic LRRK2 on Rab8a function and centrosomal alterations

Our data confirm previous data [75] indicating that Rab8a is phosphorylated on T72 by LRRK2 *in vitro*, and furthermore indicate that phosphorylation is largely independent on the nucleotide-bound status of Rab8a. Our experiments indicate that compared to wildtype or phosphorylation-deficient Rab8a, phospho-mimetic Rab8a mutants do not display altered nucleotide binding/dissociation. This is in contrast to published data [187] suggesting that the phospho-mimetic T72D mutant shows enhanced GTP binding, whilst the T72A phospho-deficient mutant shows decreased GTP binding, suggesting that hyperactivation of LRRK2 may increase

the amount of active, GTP-bound Rab8a. Differences in experimental approaches may account for those discrepancies. Whilst we used purified Rab8a protein and radiolabeled ^{3}H–GTP and ^{3}H–GDP to measure GTP and GDP binding capacity, and GTP and GDP dissociation rates of the different Rab8a versions, respectively, Jeong et al. used hydrolyzable GTP-agarose to isolate the different Rab8a versions from whole cell soluble extracts [187]. The latter approach is highly susceptible to the activity of many distinct and potent GTPases in total cellular extracts, and thus unsuitable for sensitive and reproducible detection of possible alterations in the nucleotide binding/hydrolysis of the different Rab8a versions.

In agreement with previous data [75], we found that phosphomimetic Rab8a displays abolished interaction with GDI1/2, and decreased interaction with Rabin8. These findings were taken to indicate that phosphorylated Rab8a may accumulate in its membraneous environment in an inactive form, unable to be activated by Rabin8, and also unable to be extracted from the membrane by GDI1/2 [75]. Indeed, when co-expressing pathogenic LRRK2 and Rab8a, most phosphorylated Rab8a was found in a Triton-soluble, but not cytosolic fraction, upon subcellular fractionation [76]. These data indicate that it is the membrane-bound form of Rab8a which is phosphorylated by LRRK2, and that the phosphorylation causes a decrease in its interaction with Rabin8, thereby causing a decrease in the amount of active, GTP-bound Rab8a, and thus a loss-of-function phenotype in terms of Rab8a-mediated membrane trafficking events.

The subcellular localization of phosphorylated Rab8a in intact cells has remained entirely unknown. Using phospho-state-specific antibodies, we were the first to show that it localizes to a centrosomal/pericentrosomal area. This may reflect membrane-bound phosphorylated Rab8a localized to the early recycling compartment, which is localized in a perinuclear/pericentrosomal area and known to be in physical contact with the centrosome [236]. Alternatively, phosphorylated Rab8a may be directly associated with the centrosome. Future biochemical studies

using purified centrosomes will be required to distinguish between those two possibilities. In either case, phosphorylated Rab8a seems to be proximal to the centrosome, a localization consistent with it directly contributing to the centrosomal deficits described here.

Our data using immunocytochemistry in HEK293T cells show that phosphorylated Rab8a accumulates in a pericentrosomal/centrosomal area in cells expressing pathogenic LRRK2, but no phospho-Rab8a accumulation could be detected in cells expressing wildtype LRRK2. This may be due to the small amount of endogenous Rab8a being phosphorylated in the presence of wildtype as compared to pathogenic LRRK2, which may not be detectable by this technology and/or by the antibodies employed. In agreement with this, when co-expressing wildtype LRRK2 with wildtype Rab8a, a phospho-Rab8a signal could be detected, which was accompanied with centrosomal deficits in a manner dependent on the LRRK2 kinase activity. These data indicate that increasing the amount of phosphorylated Rab8a by distinct means causes centrosomal deficits, whilst the presence of a basal amount of phosphorylated Rab8a has no effect on centrosomal cohesion. It remains to be determined whether such "basal" amount of phosphorylated Rab8a also accumulates in a centrosomal/pericentrosomal area under conditions of endogenous wildtype LRRK2, or whether such accumulation is only observed upon increasing phospho-Rab8a levels beyond a certain threshold, maybe related to the affinity by which it binds to its target(s) in such centrosomal/pericentrosomal area to cause the cohesion deficits.

We employed both sheep polyclonal as well as rabbit polyclonal antibodies against phospho-Rab8a. Recently, highly potent rabbit monoclonal phospho-Rab8 and Rab10 antibodies have been developed [189]. However, in our hands, these antibodies were not suitable for immunocytochemistry purposes. Therefore, studies aimed at determining the accumulation of phospho-Rab8a in an endogenous context from patient-derived samples will depend on the future development of

additional phospho-antibodies suitable for such applications. In addition, the phospho-Rab8a antibodies employed, as well as the monoclonal phospho-Rab8 antibodies generated, are not specific to Rab8a, but also crossreact with phosphorylated Rab10 and Rab35 [189]. It will be interesting to determine whether these Rab proteins, in their phosphorylated form, also contribute to the observed centrosomal cohesion deficits, and thus whether the main LRRK2 kinase substrates all impact upon the same mechanism. In either case, whilst we currently cannot exclude the contribution of these other phosphorylated Rab proteins to the centrosomal cohesion phenotype, Rab8a seems to be at least partially responsible, since pericentrosomal/centrosomal accumulation was also detected using several antibodies specific for total Rab8a, and since the resulting centrosomal cohesion deficits were at least in part reversed upon knockdown of Rab8a.

As another means to increase phosphorylated Rab8a and determine its effects on centrosomal cohesion, we used phosphomimetic Rab8a mutants. However, these mutants were localized to the cytosol rather than to a membranous compartment. Thus, they were not able to mimick the localization of phospho-Rab8a in intact cells. Consequently, they may not be able to mimick the action of phosphorylated Rab8a neither. This is evidenced by the fact that unique protein interactors of the phosphorylated form of Rab8a have only been found when using the phosphorylated protein, but not when using the phosphomimetic versions [186]. Such inability of phosphomimetic mutants to mimic the phosphorylated state of the protein may explain why overexpression of phosphomimetic Rab8a mutants does not cause centrosomal deficits, and also does not cause neurotoxicity in primary neurons nor degeneration of dopaminergic neurons *in vivo* [187]. Whilst phosphomimetic mutants are designed to mimick the phosphorylated state of a protein, both the negative charge and the size of the ionic shell produced by aspartate (D) or glutamate (E) substitutions are different from those of a phosphorylated residue at physiological pH. In addition, if the

phosphorylation site serves as a recognition signal for a binding partner, phosphomimetic mutants cannot bind as not fitting into the binding pocket [311, 312]. Therefore, and as observed here, phosphomimetic mutations often fail to reproduce the changes to a protein caused by its phosphorylation, and any data obtained with phosphomimetic Rab mutants have to be interpreted with great caution.

Whilst the biochemical studies mentioned above indicate that LRRK2 mediated phosphorylation of Rab8a may lead to a loss-of-function phenotype, our data indicate that at least in terms of the centrosomal readout described here, it rather acts in a toxic gain-of-function manner. On the one hand, knockdown of Rab8a in control cells did not cause centrosomal cohesion deficits. Conversely, pathogenic LRRK2 expression caused centrosomal defects accompanied by an accumulation of endogenous phosphorylated Rab8a in a pericentrosomal/centrosomal compartment, and increasing the amount of phosphorylated Rab8a by coexpression of wildtype LRRK2 with wildtype but not phospho-deficient Rab8a caused centrosomal cohesion deficits and centrosomal polarity defects in a kinase activity-mediated manner as well. On the other hand, RNAi of Rab8a in pathogenic LRRK2-expressing cells caused a significant reversal of centrosomal cohesion deficits. Whilst future studies will be required to address whether the centrosomal cohesion deficits remaining upon Rab8a knockdown are mediated by remnant Rab8a, by other functionally redundant Rab protein LRRK2 kinase substrates such as Rab8b or Rab10 [75], or indeed by other, non-Rab-related LRRK2 substrates, these results indicate that a significant part of the phenotype is dependent on the presence of phosphorylated Rab8a. Altogether, our data are consistent with a model whereby pathogenic LRRK2 kinase activity causes an abnormal accumulation of phosphorylated Rab8a in a pericentrosomal/centrosomal compartment with various downstream effects on centrosome functioning, in a toxic gain-of-function manner.

The mechanism(s) by which phosphorylated Rab8a causes the observed centrosomal deficits remain unknown. Interestingly, a recent proteomics study described a small subset of proteins, most prominently RILPL1/2, only interacting with Rab8a when in its phosphorylated form [186]. These poorly characterized proteins have been shown to localize to the primary cilium and centrosome, and seem to regulate ciliary protein concentration by unknown mechanisms [313]. It will be interesting to determine the possible colocalization of phosphorylated Rab8a with those proteins by immunocytochemistry, and determine whether a knockdown or knockout of these proteins causes reversal of the pathogenic LRRK2-mediated centrosomal deficits. In addition, further studies will be needed to determine how the pericentrosomal/centrosomal accumulation of phosphorylated Rab8a may lead to centrosomal deficits. Conceptually, this may occur by "mass action", for example with accumulating phospho-Rab8a displacing proteins forming a linker between duplicated centrosomes, or somehow impacting upon the access and/or balance of kinase/phosphatase pathways which regulate the dissociation of such linker proteins [244, 247]. Alternatively, phosphorylated Rab8a may somehow impair centrosomal maturation processes by impacting upon centriolar satellites, known to be crucial for such processes [314]. Finally, phosphorylated Rab8a may also impact upon centrosomal function in non-dividing cells via alterations in the subcellular positioning of the centrosome with respect to the Golgi complex, a nexus which is known to be important for cell polarity [156].

Increased Rab7L1 levels mimic the effect of pathogenic LRRK2 on Rab8a phosphorylation and centrosome cohesion

Since increased PD risk seems to correlate with increased Rab7L1 expression [45], we tested for centrosomal alterations in the context of wildtype LRRK2 and overexpressed Rab7L1. Increased Rab7L1 levels caused recruitment of LRRK2 to the Golgi apparatus. Such recruitment was independent on the

LRRK2 kinase activity, as kinase-dead mutant LRRK2 or pharmacologically kinase-inhibited LRRK2 displayed similar Rab7L1-mediated Golgi recruitment. The Rab7L1-mediated recruitment of wildtype LRRK2 caused centrosomal/pericentrosomal accumulation of phospho-Rab8a and centrosomal cohesion deficits similar to the ones caused by pathogenic LRRK2. These defects were mediated by the LRRK2 kinase activity, as reverted upon pharmacological kinase inhibition and not observed with kinase-dead mutant LRRK2. RNAi of Rab8a also rescued the centrosomal deficits caused by wildtype-LRRK2 in the presence of overexpressed Rab7L1, again indicating that phosphorylated Rab8a causes centrosomal deficits in a toxic gain-of-function manner. In addition, the centrosomal deficits caused by the Rab7L1-mediated recruitment of wildtype LRRK2 depended on Golgi integrity, as not observed when expressing Rab7L1 and wildtype LRRK2 in cells treated with brefeldin A. Thus, both the Rab7L1-mediated Golgi recruitment as well as the kinase activity of wildtype LRRK2 are required for the observed centrosomal defects. These data are in agreement with recent studies indicating that Rab7L1 not only acts to recruit LRRK2 to the Golgi complex, but also triggers its kinase activation [76, 93].

We also analyzed the effects of Rab7L1 expression on centrosomal cohesion deficits in the context of endogenous levels of wildtype LRRK2. Whilst Rab7L1 expression was without effect in HEK293T cells, it caused a significant deficit in centrosomal cohesion when expressed in control SH-SY5Y cells. Whilst further work will be required to dissect the reasons for these cell type-specific differences, they may be related to the already high expression levels of endogenous Rab7L1 in kidney [239] as compared to more rate-limiting amounts in other tissues, also reflected by higher levels of endogenous Rab7L1 in HEK293T as compared to SH-SY5Y cells, respectively. Alternatively, they may be due to differential expression of other unknown Rab proteins which may modulate the Rab7L1-mediated effects. Altogether, our present data indicate that the Golgi

recruitment of wildtype LRRK2 by Rab7L1 causes centrosomal alterations by increasing the molecular proximity of LRRK2 to its kinase substrate Rab8a, allowing for the aberrant accumulation of phosphorylated Rab8a and resulting in centrosomal cohesion deficits similar to those caused by pathogenic LRRK2, indicating that such centrosomal cohesion defects may be a common phenotype for a broader spectrum of PD.

Pathogenic LRRK2 mutants display an altered subcellular localization, with a partial centrosomal/pericentrosomal colocalization which is most pronounced for the pathogenic R1441C and Y1699C LRRK2 mutants, but also observed for the G2019S LRRK2 mutant as compared to wildtype LRRK2. The precise mechanism of such altered subcellular localization of pathogenic LRRK2 remains unclear, but it is not dependent on Golgi integrity, as still observed in the presence of brefeldin A. In agreement with these data, siRNA of Rab7L1 did not alter the pericentrosomal localization or cohesion deficits mediated by pathogenic LRRK2. Thus, whilst the Rab7L1-mediated Golgi recruitment seems to be crucial for the downstream effects on centrosomal cohesion mediated by wildtype LRRK2, pathogenic mutant LRRK2 seems to already display an altered subcellular localization allowing for subsequent effects on centrosomal cohesion via Rab8a phosphorylation. Interestingly, recent studies using fixation conditions to deplete cytosolic proteins indicate that pathogenic LRRK2 can be detected in a perinuclear region where it partially colocalizes with Rab8a [93]. Such subcellular proximity of pathogenic LRRK2 with its kinase substrate Rab8a may thus be sufficient to cause centrosomal deficits in a manner largely independent on Rab7L1.

Previous studies have reported that pathogenic LRRK2 disrupts Golgi morphology [45, 93, 150], which may be due to LRRK2-mediated Rab7L1 phosphorylation [238]. Our data suggest that the centrosomal cohesion deficits mediated by pathogenic LRRK2 are not a downstream effect of altered Golgi morphology, even though an intact Golgi is required for the Rab7L1-mediated

recruitment and concomitant downstream centrosomal defects mediated by wildtype LRRK2. Similarly, even though LRRK2 phosphorylates Rab7L1 [76, 238], the observed centrosomal cohesion deficits with pathogenic LRRK2 are not due to aberrant Rab7L1 phosphorylation, as also observed upon siRNA of Rab7L1. Rather, they correlate with the abnormal phosphorylation and centrosomal/pericentrosomal accumulation of Rab8a. Not necessarily in contrast to our data, Purlyte et al. have shown that Rab7L1 knockout reduces activation of LRRK2 kinase activity, as they observed a reduction in phospho-Rab10 and phospho-S935 LRRK2 signals, implying that Rab7L1 is needed for wildtype-LRRK2 kinase activity [93]. It may be possible that whilst Rab7L1 is needed for wildtype-LRRK2 activation, pathogenic LRRK2 shows a Rab7L1 independent kinase activity. Also, it may be possible that our siRNA knockdown is incomplete, and remnant Rab7L1 is still able to activate pathogenic LRRK2.

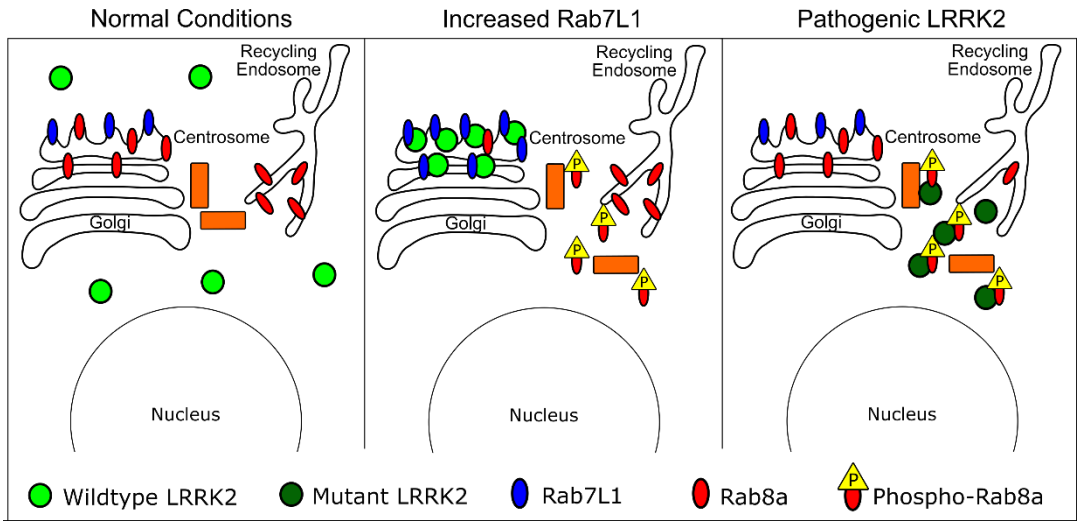

Fig. 38. Schematics of how altered Rab7L1 levels or pathogenic LRRK2 mutants cause accumulation of phospho-Rab8a and centrosomal cohesion deficits. Under normal conditions, wildtype LRRK2 is largely cytosolic, but can also be recruited to the Golgi by binding to endogenous Rab7L1 ("Normal Conditions"). Under conditions of increased Rab7L1 levels ("Increased Rab7L1"), more wildtype LRRK2 becomes recruited to the Golgi apparatus. This new localization allows LRRK2 to phosphorylate Golgi-localized Rab8a, which accumulates at/around the centrosome, resulting in centrosomal cohesion deficits. Pathogenic LRRK2 ("Pathogenic LRRK2"), by currently unknown mechanisms, displays a more pericentrosomal/centrosomal localization, which probably causes aberrant Rab8a phosphorylation from the recycling endosome that is in direct contact with the centrosome, causing centrosomal cohesion deficits in a manner independent on Rab7L1 or on Golgi integrity.

Centrosomal defects and implications for PD

The link between centrosomal alterations as described here and its relevance to PD remains unclear. Deficits in adult neurogenesis have been suggested to contribute to some of the age-dependent non-motor symptoms of PD patients [315, 316], including depression, anxiety and hyposmia, as adult neurogenesis in humans occurs in the hippocampal dentate gyrus and in the subventricular zone/olfactory bulb [317, 318]. It will be interesting to determine whether alterations in centrosomal cohesion parallel the deficits in cell growth of neuronal progenitor cells (NPCs) derived from LRRK2 PD patients *in vitro* [316], or the impairment of adult neurogenesis in mutant LRRK2-transgenic mice *in vivo* [315]. Two studies have tried to determine whether post-mortem brains from PD patients show altered adult neurogenesis with contradictory results. The initial study identified significant reduced adult neurogenesis in post-mortem brains from 4 sporadic PD patients as compared to controls [319]. However, a later study using 10 sporadic PD patients did not report differences in adult neurogenesis markers [320]. The reduced number of patients and the lack of patients' genotypes may explain the differences observed between the two studies. Therefore, studies using LRRK2-PD patients are necessary to corroborate the data obtained in mice models and patient-derived NPCs.

In addition, as centrosomal alterations are frequently associated with cancer, the changes reported here may further contribute to the reported increased cancer risk in LRRK2-PD patients [271-273]. Centrosomes are the major microtubule-nucleating centers within a cell, and proper centrosome functioning and orientation ensure appropriate microtubule-mediated vesicular trafficking. Interestingly, pathogenic LRRK2 has been linked to alterations in microtubule stability [165] and to intracellular vesicular trafficking steps including autophagy, endolysosomal and retromer-mediated trafficking pathways [45, 126, 129, 140, 145, 150, 296, 321]. Therefore, the centrosomal alterations described here may

contribute to the observed alterations in microtubule-mediated membrane trafficking pathways which have been directly related to the pathobiology of PD [322, 323].

Importantly, our data also suggest that centrosomal cohesion deficits may comprise a valid cellular biomarker readout for testing the efficacy of LRRK2 kinase inhibitors in clinical trials, as centrosomal cohesion deficits are observed in distinct peripheral cell types derived from G2019S LRRK2-PD patients as compared to healthy controls. Since increased PD risk seems to correlate with increased Rab7L1 expression [45], the finding that increased Rab7L1 also causes centrosome cohesion deficits may have implications for targeting LRRK2 kinase activity also in Rab7L1-related idiopathic PD. It will be important to determine whether centrosomal alterations can also be observed in peripheral cells from Rab7L1 risk factor patients, and from patients due to mutations in other genes, such as VPS35, recently shown to activate the LRRK2 kinase activity [324]. In either case, much further work is required to decipher whether such centrosomal alterations play a role in PD pathogenesis or merely serve as a cellular readout in patient-derived peripheral cells.

Centrosomal deficits were also observed in non-dividing cells. Differentiated SH-SY5Y cells expressing pathogenic LRRK2 displayed a deficit in cell polarity as evidenced by a significant increase in the amount of cells with abnormal positioning of the centrosome with respect to the longest neurite and a decrease in overall differentiation capability, consistent with previous reports that pathogenic LRRK2 interferes with neurite outgrowth [126, 129, 315, 325]. Mutant LRRK2 also caused deficits in cell polarity associated with an impairment in directional cell migration. Whilst both positive and negative effects of mutant LRRK2 on cell migration have been previously described [265-267], this may relate to cell type-specific differences in the position of the centrosome with respect to the leading edge of migratory cells [326]. In addition, impaired adult

neurogenesis in mutant LRRK2-expressing cells seems to be accompanied by a reduction in the number of newly generated neurons migrating to the olfactory bulb [315]. As deficits in these processes may contribute to early clinical signs of PD such as anosmia, it will be interesting to determine whether these migrational deficits are due to a lack of proper centrosome positioning and cell polarization *in vivo*. Since Rab8a has also been implicated in neurite formation and polarized membrane transport [208, 327], and since polarity deficits were also observed when co-expressing wildtype but not phospho-deficient Rab8a with wildtype LRRK2, it is tempting to speculate that the effects on neurite outgrowth and directional migration may also involve altered Rab8a-mediated processes.

Apart from our studies linking pathogenic LRRK2 to centrosomal deficits, a recent study reported a link between pathogenic LRRK2 and ciliogenesis, a centrosome-related event [186]. A deficit in ciliogenesis was observed in R1441G mutant LRRK2 knockin MEFs, which was reverted by a LRRK2 kinase inhibitor, even though no comparison was made to control cells in the absence or presence of kinase inhibitor [186]. Similarly, expression of G2019S mutant LRRK2 in 3T3 fibroblasts was shown to display ciliogenesis defects as compared to cells treated with kinase inhibitor, even though this was not compared to control cells [186], so further studies are needed to establish a possible link between pathogenic LRRK2 and ciliogenesis. In addition, expression of phospho-mimetic Rab8a mutants did not cause an effect on ciliogenesis, and these mutants were not localized to a ciliary compartment, in agreement with our data that the phospho-mimetic mutants are not properly mimicking the localization and functional status of phosphorylated Rab8a. Interestingly, the phospho-deficient Rab8a mutant was also not localized to a ciliary compartment under starvation conditions. This is in contrast to our localization studies, suggesting that at least part of phospho-deficient Rab8a is properly localized to an early recycling compartment under serum-fed conditions, all whilst not able to trigger centrosomal deficits when co-expressed with wildtype

LRRK2. Thus, careful subcellular fractionation studies are warranted to determine whether phospho-deficient Rab8a is indeed localized to a membraneous compartment similar to wildtype Rab8a, and thus able to properly act as a phospho-deficient mutant.

Whilst pathogenic LRKR2-mediated deficits in ciliogenesis require independent validation, it also remains unknown how ciliogenesis deficits may relate to PD pathogenesis. On the one hand, this may lead to the observed defects in adult neurogenesis in pathogenic LRRK2-expressing cells and animal model systems [315, 316], which at least in some neuronal subtypes can be driven by signals from non-motile primary cilia [328]. Alternatively, it may affect the pool of dopamine receptors (D1, D2 and D5) described to accumulate in neuronal cilia [278, 279], which may impact upon dopamine-mediated signalling in the striatum. Future studies will be needed to determine possible differences in the amount of ciliated cells in the substantia nigra and/or the striatum in pathogenic LRRK2-expressing rodent model systems.

Rab protein phosphorylation by LRRK2 and PD

Our work reveals a mechanistic link between pathogenic LRRK2 and altered Rab protein phosphorylation which may be relevant to PD pathogenesis. A recent study aimed to address the consequence of Rab phosphorylation in neuronal cells *in vitro* as well as *in vivo* [187]. Overexpression of phosphomimetic as well as phosphodeficient Rab8a in cortical neurons *in vitro* was found to cause a slight deficit in neurite length, without effects on neurotoxicity as assessed by TUNEL staining [187]. Again, given that phosphomimetic mutants do not seem to properly mimick the phosphorylated status of Rab8a, these data have to be interpreted with caution. The same study also revealed that both phosphodeficient as well as phosphomimetic Rab35 mutants caused pronounced neurite length deficits and neurotoxicity *in vitro*, and both caused neurodegeneration of dopaminergic neurons

in vivo upon adeno-associated virus (AAV) injected into the SNpc of adult mice [187]. Whilst further experiments will be required to determine the effects of Rab35 phosphorylation on mechanisms related to PD pathogenesis, these data again highlight the limitations of using point-mutated Rab protein constructs.

The groundbreaking studies identifying a subset of Rab proteins as LRRK2 kinase substrates were performed using MEFs [75]. Therefore, it will be crucially important to determine which Rab proteins are present and enriched in the distinct brain regions, and which are subject to LRRK2-mediated phosphorylation. Interestingly, phosphorylated Rab10 was detected in the cingulate cortex from control as well as sporadic PD patients, even though levels were highly variable and did not differ between healthy controls and sporadic PD patients [189]. It will be important to determine possible differences in the phosphorylated status of Rab8 as well as Rab10 in LRRK2-PD patients as compared to healthy controls. In addition, phosphoproteomic studies aimed at detecting the subset of Rab proteins phosphorylated by LRRK2 in distinct brain areas may yield insight into the precise subset of Rabs being present and phosphorylated by LRRK2 in PD-relevant tissue. Interestingly, if Rab proteins are confirmed to play a role in PD pathogenesis, a new possible therapeutic approach may be opened, in which targeting the activity of certain Rabs by modulating the effects of their GEFs or GAPs may complement and/or replace LRRK2 kinase inhibitor treatments. Finally, it will also be important to determine whether these Rab proteins all act upon the same intracellular pathway, or whether their phosphorylation causes distinct cellular deficits which all impinge upon cellular demise associated with PD.

VI. CONCLUSIONS / CONCLUSIONES

1. Pathogenic LRRK2 causes deficits in centrosome positioning in differentiated SH-SY5Y cells that correlates with decreased differentiation capacity and shortening of neurite length.
2. Pathogenic LRRK2-expressing SH-SY5Y cells display deficits in directed and persistent cell migration associated with cell polarity defects.
3. Pathogenic LRRK2 cause centrosomal cohesion deficits in dividing SH-SY5Y and HEK293T cells.
4. The centrosomal cohesion deficits observed upon pathogenic LRRK2 expression are dependent on LRRK2 kinase activity.
5. Centrosomal cohesion deficits are observed in two distinct peripheral cell types from LRRK2 PD patients as compared to healthy controls.
6. Pathogenic LRRK2 phosphorylate Rab8a and cause abnormal pericentrosomal/centrosomal accumulation of phosphorylated Rab8a, that is reverted upon LRRK2 kinase inhibition.
7. Centrosomal cohesion defects caused by pathogenic LRRK2 are partially reverted upon Rab8a knockdown, indicating that they are, at least, partially mediated by Rab8a.
8. Pathogenic LRRK2 phosphorylate Rab8a *in vitro* independently of the nucleotide-bound status of Rab8a.
9. Phospho-mimetic Rab8a do not display altered nucleotide binding or retention but show reduced GDI1/2 and Rabin8 interaction *in vitro*.
10. Phospho-mimetic Rab8a mutants are not properly localized in cells as compared to endogenous phopho-Rab8a, and as a consequence they do not cause centrosome splitting.
11. Mimicking sporadic PD by increasing levels of Rab7L1 cause re-localization of wildtype LRRK2 to the Rab7L1 compartment in close proximity to the centrosome.

12. Mimicking sporadic PD by increasing levels of Rab7L1 together with wildtype LRRK2 cause abnormal accumulation of phosphorylated Rab8a around the centrosome, and it is reverted upon LRRK2 kinase inhibition.
13. Mimicking sporadic PD by increasing levels of Rab7L1 together with wildtype LRRK2 cause centrosome cohesion defects comparable to those observed under pathogenic LRRK2 expression, that are also reverted upon LRRK2 kinase inhibition.
14. Centrosomal cohesion defects caused by increased levels of Rab7L1 together with wildtype LRRK2 are partially reverted upon Rab8a knockdown, indicating that they are, at least, partially mediated by Rab8a.
15. Golgi integrity is required for the effects on centrosome behavior caused by Rab7L1 and wiltype LRRK2 co-expression, but it is not needed for the centrosomal alteration caused by pathogenic LRRK2.

1. LRRK2 patogénico causa déficits en el posicionamiento del centrosoma en células SH-SY5Y diferenciadas relacionadas con una menor capacidad de diferenciación de dichas células y con un acortamiento de la longitud de las neuritas.
2. Las células SH-SY5Y que expresan LRRK2 patogénico muestran déficits en migración dirigida y constante asociados con problemas de polaridad celular.
3. LRRK2 patogénico causa defectos en la cohesión del centrosoma en células SH-SY5Y y HEK293T en división.
4. Los problemas de cohesión del centrosoma que se observan al expresar LRRK2 patogénico son dependientes de la actividad quinasa de LRRK2
5. Dos tipos diferentes de células periféricas derivadas de pacientes de Parkinson con mutaciones en LRRK2 muestran los problemas de cohesión centrosomal comparados con controles sanos.
6. LRRK2 patogénico fosforila a Rab8a y causa una acumulación de Rab8a fosforilado alrededor del centrosoma que es revertida al tratar las células con inhibidores de la actividad quinasa de LRRK2.
7. Los defectos en la cohesión centrosomal causados por LRRK2 patogénico son parcialmente revertidos al disminuir los niveles de Rab8a, indicando que son, como mínimo, parcialmente mediados por Rab8a.
8. LRRK2 patogénico fosforila a Rab8a independientemente del tipo de nucleótido unido a Rab8a *in vitro*.
9. Los constructos que mimetizan Rab8a fosforilado no muestran una capacidad alterada de unión o retención de nucleótidos, pero si muestran menos interacción con GDI1/2 y Rabin8 *in vitro*.
10. Los constructos que mimetizan Rab8a fosforilado no muestran la localización celular que Rab8a fosforilado endógeno presenta, y por lo tanto no causan separación del centrosoma.

11. El aumento de los niveles de Rab7L1 para intentar imitar la enfermedad de Parkinson esporádica provoca una relocalización de LRRK2 silvestre al compartimento donde se halla Rab7L1, que se localiza muy próximo al centrosoma.
12. El aumento conjunto de los niveles de Rab7L1 y LRRK2 silvestre causa una acumulación de Rab8a fosforilado alrededor del centrosoma que es revertida al tratar las células con inhibidores de la actividad quinasa de LRRK2.
13. El aumento conjunto de los niveles de Rab7L1 y LRRK2 silvestre provoca defectos en la cohesión centrosomal similares a los observados al expresar LRRK2 patogénico que también son revertidos al usar inhibidores de la actividad quinasa de LRRK2.
14. Los defectos de cohesión del centrosoma causado por el aumento conjunto de los niveles de Rab7L1 y LRRK2 silvestre son parcialmente revertidos al disminuir los niveles de Rab8a, lo que indica que, de nuevo, son al menos parcialmente mediados por Rab8a.
15. La integridad del aparato de Golgi es necesaria para que ocurran los efectos en el centrosoma observados por la expresión conjunta de Rab7L1 y LRRK2 silvestre, pero no es necesario para los defectos centrosomales causados por LRRK2 patogénico.

VII. REFERENCES

1. Parkinson, J. (1817). An Essay on the Shaking Palsy. London: Printed by Whittingham and Rowland for Sherwood, Neely and Jones.
2. de Lau, L.M., and Breteler, M.M. (2006). Epidemiology of Parkinson's disease. Lancet Neurol *5*, 525-535.
3. Jankovic, J. (2008). Parkinson's disease: clinical features and diagnosis. J Neurol Neurosurg Psychiatry *79*, 368-376.
4. Kalia, L.V., and Lang, A.E. (2015). Parkinson's disease. Lancet *386*, 896-912.
5. Shulman, J.M., De Jager, P.L., and Feany, M.B. (2011). Parkinson's disease: genetics and pathogenesis. Annu Rev Pathol *6*, 193-222.
6. Lewy, F. (1912). Paralysis agitans. I. Pathologische anatomie. In Handbuch der Neurologie ed. M Lewandowsky. Berlin: Springer, pp. 920–933
7. Ishizawa, T., Mattila, P., Davies, P., Wang, D., and Dickson, D.W. (2003). Colocalization of tau and alpha-synuclein epitopes in Lewy bodies. J Neuropathol Exp Neurol *62*, 389-397.
8. Sengupta, U., Guerrero-Munoz, M.J., Castillo-Carranza, D.L., Lasagna-Reeves, C.A., Gerson, J.E., Paulucci-Holthauzen, A.A., Krishnamurthy, S., Farhed, M., Jackson, G.R., and Kayed, R. (2015). Pathological interface between oligomeric alpha-synuclein and tau in synucleinopathies. Biol Psychiatry *78*, 672-683.
9. Dauer, W., and Przedborski, S. (2003). Parkinson's disease: mechanisms and models. Neuron *39*, 889-909.
10. Braak, H., Del Tredici, K., Rub, U., de Vos, R.A., Jansen Steur, E.N., and Braak, E. (2003). Staging of brain pathology related to sporadic Parkinson's disease. Neurobiol Aging *24*, 197-211.
11. Shults, C.W. (2006). Lewy bodies. Proc Natl Acad Sci U S A *103*, 1661-1668.
12. Birkmayer, W., and Hornykiewicz, O. (1961). [The L-3,4-dioxyphenylalanine (DOPA)-effect in Parkinson-akinesia]. Wien Klin Wochenschr *73*, 787-788.
13. Hornykiewicz, O. (2006). The discovery of dopamine deficiency in the parkinsonian brain. J Neural Transm Suppl, 9-15.
14. Poewe, W., Seppi, K., Tanner, C.M., Halliday, G.M., Brundin, P., Volkmann, J., Schrag, A.E., and Lang, A.E. (2017). Parkinson disease. Nat Rev Dis Primers *3*, 17013.
15. Connolly, B.S., and Lang, A.E. (2014). Pharmacological treatment of Parkinson disease: a review. JAMA *311*, 1670-1683.
16. Limousin, P., Pollak, P., Benazzouz, A., Hoffmann, D., Le Bas, J.F., Broussolle, E., Perret, J.E., and Benabid, A.L. (1995). Effect of parkinsonian signs and symptoms of bilateral subthalamic nucleus stimulation. Lancet *345*, 91-95.

17. Deuschl, G., and Agid, Y. (2013). Subthalamic neurostimulation for Parkinson's disease with early fluctuations: balancing the risks and benefits. Lancet Neurol *12*, 1025-1034.
18. Hirsch, L., Jette, N., Frolkis, A., Steeves, T., and Pringsheim, T. (2016). The Incidence of Parkinson's Disease: A Systematic Review and Meta-Analysis. Neuroepidemiology *46*, 292-300.
19. Polymeropoulos, M.H., Higgins, J.J., Golbe, L.I., Johnson, W.G., Ide, S.E., Di Iorio, G., Sanges, G., Stenroos, E.S., Pho, L.T., Schaffer, A.A., et al. (1996). Mapping of a gene for Parkinson's disease to chromosome 4q21-q23. Science *274*, 1197-1199.
20. Polymeropoulos, M.H., Lavedan, C., Leroy, E., Ide, S.E., Dehejia, A., Dutra, A., Pike, B., Root, H., Rubenstein, J., Boyer, R., et al. (1997). Mutation in the alpha-synuclein gene identified in families with Parkinson's disease. Science *276*, 2045-2047.
21. Hernandez, D.G., Reed, X., and Singleton, A.B. (2016). Genetics in Parkinson disease: Mendelian versus non-Mendelian inheritance. J Neurochem *139 Suppl 1*, 59-74.
22. Kalinderi, K., Bostantjopoulou, S., and Fidani, L. (2016). The genetic background of Parkinson's disease: current progress and future prospects. Acta Neurol Scand *134*, 314-326.
23. Spillantini, M.G., Schmidt, M.L., Lee, V.M., Trojanowski, J.Q., Jakes, R., and Goedert, M. (1997). Alpha-synuclein in Lewy bodies. Nature *388*, 839-840.
24. Gitler, A.D., Bevis, B.J., Shorter, J., Strathearn, K.E., Hamamichi, S., Su, L.J., Caldwell, K.A., Caldwell, G.A., Rochet, J.C., McCaffery, J.M., et al. (2008). The Parkinson's disease protein alpha-synuclein disrupts cellular Rab homeostasis. Proc Natl Acad Sci U S A *105*, 145-150.
25. Burre, J., Sharma, M., Tsetsenis, T., Buchman, V., Etherton, M.R., and Sudhof, T.C. (2010). Alpha-synuclein promotes SNARE-complex assembly in vivo and in vitro. Science *329*, 1663-1667.
26. Healy, D.G., Falchi, M., O'Sullivan, S.S., Bonifati, V., Durr, A., Bressman, S., Brice, A., Aasly, J., Zabetian, C.P., Goldwurm, S., et al. (2008). Phenotype, genotype, and worldwide genetic penetrance of LRRK2-associated Parkinson's disease: a case-control study. Lancet Neurol *7*, 583-590.
27. Bardien, S., Lesage, S., Brice, A., and Carr, J. (2011). Genetic characteristics of leucine-rich repeat kinase 2 (LRRK2) associated Parkinson's disease. Parkinsonism Relat Disord *17*, 501-508.
28. Satake, W., Nakabayashi, Y., Mizuta, I., Hirota, Y., Ito, C., Kubo, M., Kawaguchi, T., Tsunoda, T., Watanabe, M., Takeda, A., et al. (2009). Genome-wide association study identifies common variants at four loci as genetic risk factors for Parkinson's disease. Nat Genet *41*, 1303-1307.

29. Simon-Sanchez, J., Schulte, C., Bras, J.M., Sharma, M., Gibbs, J.R., Berg, D., Paisan-Ruiz, C., Lichtner, P., Scholz, S.W., Hernandez, D.G., et al. (2009). Genome-wide association study reveals genetic risk underlying Parkinson's disease. Nat Genet *41*, 1308-1312.
30. Kalia, L.V., Lang, A.E., Hazrati, L.N., Fujioka, S., Wszolek, Z.K., Dickson, D.W., Ross, O.A., Van Deerlin, V.M., Trojanowski, J.Q., Hurtig, H.I., et al. (2015). Clinical correlations with Lewy body pathology in LRRK2-related Parkinson disease. JAMA Neurol *72*, 100-105.
31. Zimprich, A., Benet-Pages, A., Struhal, W., Graf, E., Eck, S.H., Offman, M.N., Haubenberger, D., Spielberger, S., Schulte, E.C., Lichtner, P., et al. (2011). A mutation in VPS35, encoding a subunit of the retromer complex, causes late-onset Parkinson disease. Am J Hum Genet *89*, 168-175.
32. Vilarino-Guell, C., Wider, C., Ross, O.A., Dachsel, J.C., Kachergus, J.M., Lincoln, S.J., Soto-Ortolaza, A.I., Cobb, S.A., Wilhoite, G.J., Bacon, J.A., et al. (2011). VPS35 mutations in Parkinson disease. Am J Hum Genet *89*, 162-167.
33. Kitada, T., Asakawa, S., Hattori, N., Matsumine, H., Yamamura, Y., Minoshima, S., Yokochi, M., Mizuno, Y., and Shimizu, N. (1998). Mutations in the parkin gene cause autosomal recessive juvenile parkinsonism. Nature *392*, 605-608.
34. Periquet, M., Latouche, M., Lohmann, E., Rawal, N., De Michele, G., Ricard, S., Teive, H., Fraix, V., Vidailhet, M., Nicholl, D., et al. (2003). Parkin mutations are frequent in patients with isolated early-onset parkinsonism. Brain *126*, 1271-1278.
35. Lucking, C.B., Durr, A., Bonifati, V., Vaughan, J., De Michele, G., Gasser, T., Harhangi, B.S., Meco, G., Denefle, P., Wood, N.W., et al. (2000). Association between early-onset Parkinson's disease and mutations in the parkin gene. N Engl J Med *342*, 1560-1567.
36. Narendra, D., Tanaka, A., Suen, D.F., and Youle, R.J. (2008). Parkin is recruited selectively to impaired mitochondria and promotes their autophagy. J Cell Biol *183*, 795-803.
37. Kane, L.A., Lazarou, M., Fogel, A.I., Li, Y., Yamano, K., Sarraf, S.A., Banerjee, S., and Youle, R.J. (2014). PINK1 phosphorylates ubiquitin to activate Parkin E3 ubiquitin ligase activity. J Cell Biol *205*, 143-153.
38. Valente, E.M., Abou-Sleiman, P.M., Caputo, V., Muqit, M.M., Harvey, K., Gispert, S., Ali, Z., Del Turco, D., Bentivoglio, A.R., Healy, D.G., et al. (2004). Hereditary early-onset Parkinson's disease caused by mutations in PINK1. Science *304*, 1158-1160.
39. Kondapalli, C., Kazlauskaite, A., Zhang, N., Woodroof, H.I., Campbell, D.G., Gourlay, R., Burchell, L., Walden, H., Macartney, T.J., Deak, M., et al. (2012). PINK1 is activated by mitochondrial membrane potential

depolarization and stimulates Parkin E3 ligase activity by phosphorylating Serine 65. Open Biol *2*, 120080.

40. Mamais, A., and Cookson, M.R. (2017). Chapter 42 - Parkinson's Disease: Genetics. In Handbook of Behavioral Neuroscience, Volume 24, H. Steiner and K.Y. Tseng, eds. (Elsevier), pp. 839-855.
41. Hruska, K.S., LaMarca, M.E., Scott, C.R., and Sidransky, E. (2008). Gaucher disease: mutation and polymorphism spectrum in the glucocerebrosidase gene (GBA). Hum Mutat *29*, 567-583.
42. Smith, L., Mullin, S., and Schapira, A.H.V. (2017). Insights into the structural biology of Gaucher disease. Exp Neurol *298*, 180-190.
43. Schapira, A.H. (2015). Glucocerebrosidase and Parkinson disease: Recent advances. Mol Cell Neurosci *66*, 37-42.
44. Wang, Y., and Mandelkow, E. (2016). Tau in physiology and pathology. Nat Rev Neurosci *17*, 5-21.
45. Beilina, A., Rudenko, I.N., Kaganovich, A., Civiero, L., Chau, H., Kalia, S.K., Kalia, L.V., Lobbestael, E., Chia, R., Ndukwe, K., et al. (2014). Unbiased screen for interactors of leucine-rich repeat kinase 2 supports a common pathway for sporadic and familial Parkinson disease. Proc Natl Acad Sci U S A *111*, 2626-2631.
46. Lee, D.W., Zhao, X., Yim, Y.I., Eisenberg, E., and Greene, L.E. (2008). Essential role of cyclin-G-associated kinase (Auxilin-2) in developing and mature mice. Mol Biol Cell *19*, 2766-2776.
47. Pankratz, N., Wilk, J.B., Latourelle, J.C., DeStefano, A.L., Halter, C., Pugh, E.W., Doheny, K.F., Gusella, J.F., Nichols, W.C., Foroud, T., et al. (2009). Genomewide association study for susceptibility genes contributing to familial Parkinson disease. Hum Genet *124*, 593-605.
48. Bras, J., Guerreiro, R., and Hardy, J. (2015). SnapShot: Genetics of Parkinson's disease. Cell *160*, 570-570 e571.
49. Anglade, P., Vyas, S., Javoy-Agid, F., Herrero, M.T., Michel, P.P., Marquez, J., Mouatt-Prigent, A., Ruberg, M., Hirsch, E.C., and Agid, Y. (1997). Apoptosis and autophagy in nigral neurons of patients with Parkinson's disease. Histol Histopathol *12*, 25-31.
50. Dehay, B., Bove, J., Rodriguez-Muela, N., Perier, C., Recasens, A., Boya, P., and Vila, M. (2010). Pathogenic lysosomal depletion in Parkinson's disease. J Neurosci *30*, 12535-12544.
51. Rivero-Rios, P., Madero-Perez, J., Fernandez, B., and Hilfiker, S. (2016). Targeting the Autophagy/Lysosomal Degradation Pathway in Parkinson's Disease. Curr Neuropharmacol *14*, 238-249.
52. Manzoni, C. (2017). The LRRK2-macroautophagy axis and its relevance to Parkinson's disease. Biochem Soc Trans *45*, 155-162.

53. Schapira, A.H., Cooper, J.M., Dexter, D., Jenner, P., Clark, J.B., and Marsden, C.D. (1989). Mitochondrial complex I deficiency in Parkinson's disease. Lancet *1*, 1269.
54. Schapira, A.H., Cooper, J.M., Dexter, D., Clark, J.B., Jenner, P., and Marsden, C.D. (1990). Mitochondrial complex I deficiency in Parkinson's disease. J Neurochem *54*, 823-827.
55. Hattingen, E., Magerkurth, J., Pilatus, U., Mozer, A., Seifried, C., Steinmetz, H., Zanella, F., and Hilker, R. (2009). Phosphorus and proton magnetic resonance spectroscopy demonstrates mitochondrial dysfunction in early and advanced Parkinson's disease. Brain *132*, 3285-3297.
56. Jackson-Lewis, V., Lester, D., Kozina, E., Przedborski, S., and Smeyne, R.J. (2015). Chapter 17 - From Man to Mouse: The MPTP Model of Parkinson Disease A2 - LeDoux, Mark S. In Movement Disorders (Second Edition). (Boston: Academic Press), pp. 287-306.
57. Blesa, J., Trigo-Damas, I., Quiroga-Varela, A., and Jackson-Lewis, V.R. (2015). Oxidative stress and Parkinson's disease. Front Neuroanat *9*, 91.
58. Segura-Aguilar, J., Paris, I., Munoz, P., Ferrari, E., Zecca, L., and Zucca, F.A. (2014). Protective and toxic roles of dopamine in Parkinson's disease. J Neurochem *129*, 898-915.
59. Kordower, J.H., Chu, Y., Hauser, R.A., Freeman, T.B., and Olanow, C.W. (2008). Lewy body-like pathology in long-term embryonic nigral transplants in Parkinson's disease. Nat Med *14*, 504-506.
60. Li, J.Y., Englund, E., Holton, J.L., Soulet, D., Hagell, P., Lees, A.J., Lashley, T., Quinn, N.P., Rehncrona, S., Bjorklund, A., et al. (2008). Lewy bodies in grafted neurons in subjects with Parkinson's disease suggest host-to-graft disease propagation. Nat Med *14*, 501-503.
61. Hirsch, E.C., and Hunot, S. (2009). Neuroinflammation in Parkinson's disease: a target for neuroprotection? Lancet Neurol *8*, 382-397.
62. McGeer, P.L., Itagaki, S., Boyes, B.E., and McGeer, E.G. (1988). Reactive microglia are positive for HLA-DR in the substantia nigra of Parkinson's and Alzheimer's disease brains. Neurology *38*, 1285-1291.
63. Doorn, K.J., Moors, T., Drukarch, B., van de Berg, W., Lucassen, P.J., and van Dam, A.M. (2014). Microglial phenotypes and toll-like receptor 2 in the substantia nigra and hippocampus of incidental Lewy body disease cases and Parkinson's disease patients. Acta Neuropathol Commun *2*, 90.
64. Schapansky, J., Nardozzi, J.D., and LaVoie, M.J. (2015). The complex relationships between microglia, alpha-synuclein, and LRRK2 in Parkinson's disease. Neuroscience *302*, 74-88.
65. Sulzer, D., Alcalay, R.N., Garretti, F., Cote, L., Kanter, E., Agin-Liebes, J., Liong, C., McMurtrey, C., Hildebrand, W.H., Mao, X., et al. (2017). T cells from patients with Parkinson's disease recognize alpha-synuclein peptides. Nature *546*, 656-661.

66. Hakimi, M., Selvanantham, T., Swinton, E., Padmore, R.F., Tong, Y., Kabbach, G., Venderova, K., Girardin, S.E., Bulman, D.E., Scherzer, C.R., et al. (2011). Parkinson's disease-linked LRRK2 is expressed in circulating and tissue immune cells and upregulated following recognition of microbial structures. J Neural Transm (Vienna) *118*, 795-808.
67. Hamza, T.H., Zabetian, C.P., Tenesa, A., Laederach, A., Montimurro, J., Yearout, D., Kay, D.M., Doheny, K.F., Paschall, J., Pugh, E., et al. (2010). Common genetic variation in the HLA region is associated with late-onset sporadic Parkinson's disease. Nat Genet *42*, 781-785.
68. Funayama, M., Hasegawa, K., Kowa, H., Saito, M., Tsuji, S., and Obata, F. (2002). A new locus for Parkinson's disease (PARK8) maps to chromosome 12p11.2-q13.1. Ann Neurol *51*, 296-301.
69. Paisan-Ruiz, C., Jain, S., Evans, E.W., Gilks, W.P., Simon, J., van der Brug, M., Lopez de Munain, A., Aparicio, S., Gil, A.M., Khan, N., et al. (2004). Cloning of the gene containing mutations that cause PARK8-linked Parkinson's disease. Neuron *44*, 595-600.
70. Zimprich, A., Biskup, S., Leitner, P., Lichtner, P., Farrer, M., Lincoln, S., Kachergus, J., Hulihan, M., Uitti, R.J., Calne, D.B., et al. (2004). Mutations in LRRK2 cause autosomal-dominant parkinsonism with pleomorphic pathology. Neuron *44*, 601-607.
71. Kay, D.M., Kramer, P., Higgins, D., Zabetian, C.P., and Payami, H. (2005). Escaping Parkinson's disease: a neurologically healthy octogenarian with the LRRK2 G2019S mutation. Mov Disord *20*, 1077-1078.
72. Troiano, A.R., Elbaz, A., Lohmann, E., Belarbi, S., Vidailhet, M., Bonnet, A.M., Lesage, S., Pollak, P., Cazeneuve, C., Borg, M., et al. (2010). Low disease risk in relatives of north african lrrk2 Parkinson disease patients. Neurology *75*, 1118-1119.
73. Marder, K., Wang, Y., Alcalay, R.N., Mejia-Santana, H., Tang, M.X., Lee, A., Raymond, D., Mirelman, A., Saunders-Pullman, R., Clark, L., et al. (2015). Age-specific penetrance of LRRK2 G2019S in the Michael J. Fox Ashkenazi Jewish LRRK2 Consortium. Neurology *85*, 89-95.
74. Guaitoli, G., Gilsbach, B.K., Raimondi, F., and Gloeckner, C.J. (2016). First model of dimeric LRRK2: the challenge of unrevealing the structure of a multidomain Parkinson's-associated protein. Biochem Soc Trans *44*, 1635-1641.
75. Steger, M., Tonelli, F., Ito, G., Davies, P., Trost, M., Vetter, M., Wachter, S., Lorentzen, E., Duddy, G., Wilson, S., et al. (2016). Phosphoproteomics reveals that Parkinson's disease kinase LRRK2 regulates a subset of Rab GTPases. Elife *5*.
76. Liu, Z., Bryant, N., Kumaran, R., Beilina, A., Abeliovich, A., Cookson, M.R., and West, A.B. (2018). LRRK2 phosphorylates membrane-bound

Rabs and is activated by GTP-bound Rab7L1 to promote recruitment to the trans-Golgi network. Hum Mol Genet *27*, 385-395.

77. Smith, W.W., Pei, Z., Jiang, H., Dawson, V.L., Dawson, T.M., and Ross, C.A. (2006). Kinase activity of mutant LRRK2 mediates neuronal toxicity. Nat Neurosci *9*, 1231-1233.
78. Greggio, E., Jain, S., Kingsbury, A., Bandopadhyay, R., Lewis, P., Kaganovich, A., van der Brug, M.P., Beilina, A., Blackinton, J., Thomas, K.J., et al. (2006). Kinase activity is required for the toxic effects of mutant LRRK2/dardarin. Neurobiol Dis *23*, 329-341.
79. Rivero-Rios, P., Gomez-Suaga, P., Fernandez, B., Madero-Perez, J., Schwab, A.J., Ebert, A.D., and Hilfiker, S. (2015). Alterations in late endocytic trafficking related to the pathobiology of LRRK2-linked Parkinson's disease. Biochem Soc Trans *43*, 390-395.
80. West, A.B. (2017). Achieving neuroprotection with LRRK2 kinase inhibitors in Parkinson disease. Exp Neurol *298*, 236-245.
81. Baptista, M., Merchant, K., Bharghava, S., Bryce, D., Ellis, M., Estrada, A., Fell, M., Fuji, R., Galatsis, P., Hill, S., Hirst, W., Houle, C., Kennedy, M., Liu, X., Maddess, M., Markgraf, C., Mei, H., Needle, E., Steyn, S., Yi, Z., Yu, H., Fiske, B., Sherer, T. (2015). LRRK2 kinase inhibitors of different structural classes induce abnormal accumulation of lamellar bodies in type II pneumocytes in non-human primates but are reversible and without pulmonary functional consequences. 45th International Society for Neuroscience Meeting 763.702.
82. Fuji, R.N., Flagella, M., Baca, M., Baptista, M.A., Brodbeck, J., Chan, B.K., Fiske, B.K., Honigberg, L., Jubb, A.M., Katavolos, P., et al. (2015). Effect of selective LRRK2 kinase inhibition on nonhuman primate lung. Sci Transl Med *7*, 273ra215.
83. Herzig, M.C., Kolly, C., Persohn, E., Theil, D., Schweizer, T., Hafner, T., Stemmelen, C., Troxler, T.J., Schmid, P., Danner, S., et al. (2011). LRRK2 protein levels are determined by kinase function and are crucial for kidney and lung homeostasis in mice. Hum Mol Genet *20*, 4209-4223.
84. Ito, G., Okai, T., Fujino, G., Takeda, K., Ichijo, H., Katada, T., and Iwatsubo, T. (2007). GTP binding is essential to the protein kinase activity of LRRK2, a causative gene product for familial Parkinson's disease. Biochemistry *46*, 1380-1388.
85. Gomez-Suaga, P., Fdez, E., Fernandez, B., Martinez-Salvador, M., Blanca Ramirez, M., Madero-Perez, J., Rivero-Rios, P., Fuentes, J.M., and Hilfiker, S. (2014). Novel insights into the neurobiology underlying LRRK2-linked Parkinson's disease. Neuropharmacology *85*, 45-56.
86. West, A.B., Moore, D.J., Choi, C., Andrabi, S.A., Li, X., Dikeman, D., Biskup, S., Zhang, Z., Lim, K.L., Dawson, V.L., et al. (2007). Parkinson's

disease-associated mutations in LRRK2 link enhanced GTP-binding and kinase activities to neuronal toxicity. Hum Mol Genet *16*, 223-232.

87. Liao, J., Wu, C.X., Burlak, C., Zhang, S., Sahm, H., Wang, M., Zhang, Z.Y., Vogel, K.W., Federici, M., Riddle, S.M., et al. (2014). Parkinson disease-associated mutation R1441H in LRRK2 prolongs the "active state" of its GTPase domain. Proc Natl Acad Sci U S A *111*, 4055-4060.
88. Blanca Ramirez, M., Lara Ordonez, A.J., Fdez, E., Madero-Perez, J., Gonnelli, A., Drouyer, M., Chartier-Harlin, M.C., Taymans, J.M., Bubacco, L., Greggio, E., et al. (2017). GTP binding regulates cellular localization of Parkinson's disease-associated LRRK2. Hum Mol Genet *26*, 2747-2767.
89. Lewis, P.A., Greggio, E., Beilina, A., Jain, S., Baker, A., and Cookson, M.R. (2007). The R1441C mutation of LRRK2 disrupts GTP hydrolysis. Biochem Biophys Res Commun *357*, 668-671.
90. Guo, L., Gandhi, P.N., Wang, W., Petersen, R.B., Wilson-Delfosse, A.L., and Chen, S.G. (2007). The Parkinson's disease-associated protein, leucine-rich repeat kinase 2 (LRRK2), is an authentic GTPase that stimulates kinase activity. Exp Cell Res *313*, 3658-3670.
91. Daniels, V., Vancraenenbroeck, R., Law, B.M., Greggio, E., Lobbestael, E., Gao, F., De Maeyer, M., Cookson, M.R., Harvey, K., Baekelandt, V., et al. (2011). Insight into the mode of action of the LRRK2 Y1699C pathogenic mutant. J Neurochem *116*, 304-315.
92. Greggio, E., and Cookson, M.R. (2009). Leucine-rich repeat kinase 2 mutations and Parkinson's disease: three questions. ASN Neuro *1*.
93. Purlyte, E., Dhekne, H.S., Sarhan, A.R., Gomez, R., Lis, P., Wightman, M., Martinez, T.N., Tonelli, F., Pfeffer, S.R., and Alessi, D.R. (2018). Rab29 activation of the Parkinson's disease-associated LRRK2 kinase. EMBO J *37*, 1-18.
94. Sheng, Z., Zhang, S., Bustos, D., Kleinheinz, T., Le Pichon, C.E., Dominguez, S.L., Solanoy, H.O., Drummond, J., Zhang, X., Ding, X., et al. (2012). Ser1292 autophosphorylation is an indicator of LRRK2 kinase activity and contributes to the cellular effects of PD mutations. Sci Transl Med *4*, 164ra161.
95. Ito, G., Fujimoto, T., Kamikawaji, S., Kuwahara, T., and Iwatsubo, T. (2014). Lack of correlation between the kinase activity of LRRK2 harboring kinase-modifying mutations and its phosphorylation at Ser910, 935, and Ser955. PLoS One *9*, e97988.
96. Reynolds, A., Doggett, E.A., Riddle, S.M., Lebakken, C.S., and Nichols, R.J. (2014). LRRK2 kinase activity and biology are not uniformly predicted by its autophosphorylation and cellular phosphorylation site status. Front Mol Neurosci *7*, 54.
97. De Wit, T., Baekelandt, V., and Lobbestael, E. (2018). LRRK2 Phosphorylation: Behind the Scenes. Neuroscientist, 1073858418756309.

98. Biskup, S., Moore, D.J., Rea, A., Lorenz-Deperieux, B., Coombes, C.E., Dawson, V.L., Dawson, T.M., and West, A.B. (2007). Dynamic and redundant regulation of LRRK2 and LRRK1 expression. BMC Neurosci *8*, 102.
99. Maekawa, T., Kubo, M., Yokoyama, I., Ohta, E., and Obata, F. (2010). Age-dependent and cell-population-restricted LRRK2 expression in normal mouse spleen. Biochem Biophys Res Commun *392*, 431-435.
100. Miklossy, J., Arai, T., Guo, J.P., Klegeris, A., Yu, S., McGeer, E.G., and McGeer, P.L. (2006). LRRK2 expression in normal and pathologic human brain and in human cell lines. J Neuropathol Exp Neurol *65*, 953-963.
101. Galter, D., Westerlund, M., Carmine, A., Lindqvist, E., Sydow, O., and Olson, L. (2006). LRRK2 expression linked to dopamine-innervated areas. Ann Neurol *59*, 714-719.
102. Melrose, H., Lincoln, S., Tyndall, G., Dickson, D., and Farrer, M. (2006). Anatomical localization of leucine-rich repeat kinase 2 in mouse brain. Neuroscience *139*, 791-794.
103. Sharma, S., Bandopadhyay, R., Lashley, T., Renton, A.E., Kingsbury, A.E., Kumaran, R., Kallis, C., Vilarino-Guell, C., O'Sullivan, S.S., Lees, A.J., et al. (2011). LRRK2 expression in idiopathic and G2019S positive Parkinson's disease subjects: a morphological and quantitative study. Neuropathol Appl Neurobiol *37*, 777-790.
104. West, A.B., Cowell, R.M., Daher, J.P., Moehle, M.S., Hinkle, K.M., Melrose, H.L., Standaert, D.G., and Volpicelli-Daley, L.A. (2014). Differential LRRK2 expression in the cortex, striatum, and substantia nigra in transgenic and nontransgenic rodents. J Comp Neurol *522*, 2465-2480.
105. Trabzuni, D., Ryten, M., Emmett, W., Ramasamy, A., Lackner, K.J., Zeller, T., Walker, R., Smith, C., Lewis, P.A., Mamais, A., et al. (2013). Fine-mapping, gene expression and splicing analysis of the disease associated LRRK2 locus. PLoS One *8*, e70724.
106. Higashi, S., Moore, D.J., Colebrooke, R.E., Biskup, S., Dawson, V.L., Arai, H., Dawson, T.M., and Emson, P.C. (2007). Expression and localization of Parkinson's disease-associated leucine-rich repeat kinase 2 in the mouse brain. J Neurochem *100*, 368-381.
107. Gardet, A., Benita, Y., Li, C., Sands, B.E., Ballester, I., Stevens, C., Korzenik, J.R., Rioux, J.D., Daly, M.J., Xavier, R.J., et al. (2010). LRRK2 is involved in the IFN-gamma response and host response to pathogens. J Immunol *185*, 5577-5585.
108. Barrett, J.C., Hansoul, S., Nicolae, D.L., Cho, J.H., Duerr, R.H., Rioux, J.D., Brant, S.R., Silverberg, M.S., Taylor, K.D., Barmada, M.M., et al. (2008). Genome-wide association defines more than 30 distinct susceptibility loci for Crohn's disease. Nat Genet *40*, 955-962.

109. Franke, A., McGovern, D.P., Barrett, J.C., Wang, K., Radford-Smith, G.L., Ahmad, T., Lees, C.W., Balschun, T., Lee, J., Roberts, R., et al. (2010). Genome-wide meta-analysis increases to 71 the number of confirmed Crohn's disease susceptibility loci. Nat Genet *42*, 1118-1125.
110. Zhang, Y.M., Zhou, X.J., Cheng, F.J., Qi, Y.Y., Hou, P., Zhao, M.H., and Zhang, H. (2017). Autophagy-related gene LRRK2 is likely a susceptibility gene for systemic lupus erythematosus in northern Han Chinese. Oncotarget *8*, 13754-13761.
111. Zhang, F.R., Huang, W., Chen, S.M., Sun, L.D., Liu, H., Li, Y., Cui, Y., Yan, X.X., Yang, H.T., Yang, R.D., et al. (2009). Genomewide association study of leprosy. N Engl J Med *361*, 2609-2618.
112. Blesa, J., and Przedborski, S. (2014). Parkinson's disease: animal models and dopaminergic cell vulnerability. Front Neuroanat *8*, 155.
113. Tong, Y., Pisani, A., Martella, G., Karouani, M., Yamaguchi, H., Pothos, E.N., and Shen, J. (2009). R1441C mutation in LRRK2 impairs dopaminergic neurotransmission in mice. Proc Natl Acad Sci U S A *106*, 14622-14627.
114. Yue, M., Hinkle, K.M., Davies, P., Trushina, E., Fiesel, F.C., Christenson, T.A., Schroeder, A.S., Zhang, L., Bowles, E., Behrouz, B., et al. (2015). Progressive dopaminergic alterations and mitochondrial abnormalities in LRRK2 G2019S knock-in mice. Neurobiol Dis *78*, 172-195.
115. Ramonet, D., Daher, J.P., Lin, B.M., Stafa, K., Kim, J., Banerjee, R., Westerlund, M., Pletnikova, O., Glauser, L., Yang, L., et al. (2011). Dopaminergic neuronal loss, reduced neurite complexity and autophagic abnormalities in transgenic mice expressing G2019S mutant LRRK2. PLoS One *6*, e18568.
116. Chen, C.Y., Weng, Y.H., Chien, K.Y., Lin, K.J., Yeh, T.H., Cheng, Y.P., Lu, C.S., and Wang, H.L. (2012). (G2019S) LRRK2 activates MKK4-JNK pathway and causes degeneration of SN dopaminergic neurons in a transgenic mouse model of PD. Cell Death Differ *19*, 1623-1633.
117. Zhou, H., Huang, C., Tong, J., Hong, W.C., Liu, Y.J., and Xia, X.G. (2011). Temporal expression of mutant LRRK2 in adult rats impairs dopamine reuptake. Int J Biol Sci *7*, 753-761.
118. Li, Y., Liu, W., Oo, T.F., Wang, L., Tang, Y., Jackson-Lewis, V., Zhou, C., Geghman, K., Bogdanov, M., Przedborski, S., et al. (2009). Mutant LRRK2(R1441G) BAC transgenic mice recapitulate cardinal features of Parkinson's disease. Nat Neurosci *12*, 826-828.
119. Xiong, Y., Neifert, S., Karuppagounder, S.S., Liu, Q., Stankowski, J.N., Lee, B.D., Ko, H.S., Lee, Y., Grima, J.C., Mao, X., et al. (2018). Robust kinase- and age-dependent dopaminergic and norepinephrine neurodegeneration in LRRK2 G2019S transgenic mice. Proc Natl Acad Sci U S A *115*, 1635-1640.

120. Lee, B.D., Shin, J.H., VanKampen, J., Petrucelli, L., West, A.B., Ko, H.S., Lee, Y.I., Maguire-Zeiss, K.A., Bowers, W.J., Federoff, H.J., et al. (2010). Inhibitors of leucine-rich repeat kinase-2 protect against models of Parkinson's disease. Nat Med *16*, 998-1000.
121. Dusonchet, J., Kochubey, O., Stafa, K., Young, S.M., Jr., Zufferey, R., Moore, D.J., Schneider, B.L., and Aebischer, P. (2011). A rat model of progressive nigral neurodegeneration induced by the Parkinson's disease-associated G2019S mutation in LRRK2. J Neurosci *31*, 907-912.
122. Tsika, E., Nguyen, A.P., Dusonchet, J., Colin, P., Schneider, B.L., and Moore, D.J. (2015). Adenoviral-mediated expression of G2019S LRRK2 induces striatal pathology in a kinase-dependent manner in a rat model of Parkinson's disease. Neurobiol Dis *77*, 49-61.
123. Park, I.H., Arora, N., Huo, H., Maherali, N., Ahfeldt, T., Shimamura, A., Lensch, M.W., Cowan, C., Hochedlinger, K., and Daley, G.Q. (2008). Disease-specific induced pluripotent stem cells. Cell *134*, 877-886.
124. Soldner, F., Hockemeyer, D., Beard, C., Gao, Q., Bell, G.W., Cook, E.G., Hargus, G., Blak, A., Cooper, O., Mitalipova, M., et al. (2009). Parkinson's disease patient-derived induced pluripotent stem cells free of viral reprogramming factors. Cell *136*, 964-977.
125. Nguyen, H.N., Byers, B., Cord, B., Shcheglovitov, A., Byrne, J., Gujar, P., Kee, K., Schule, B., Dolmetsch, R.E., Langston, W., et al. (2011). LRRK2 mutant iPSC-derived DA neurons demonstrate increased susceptibility to oxidative stress. Cell Stem Cell *8*, 267-280.
126. Sanchez-Danes, A., Richaud-Patin, Y., Carballo-Carbajal, I., Jimenez-Delgado, S., Caig, C., Mora, S., Di Guglielmo, C., Ezquerra, M., Patel, B., Giralt, A., et al. (2012). Disease-specific phenotypes in dopamine neurons from human iPS-based models of genetic and sporadic Parkinson's disease. EMBO Mol Med *4*, 380-395.
127. Plowey, E.D., Cherra, S.J., 3rd, Liu, Y.J., and Chu, C.T. (2008). Role of autophagy in G2019S-LRRK2-associated neurite shortening in differentiated SH-SY5Y cells. J Neurochem *105*, 1048-1056.
128. Galvin, J.E., Uryu, K., Lee, V.M., and Trojanowski, J.Q. (1999). Axon pathology in Parkinson's disease and Lewy body dementia hippocampus contains alpha-, beta-, and gamma-synuclein. Proc Natl Acad Sci U S A *96*, 13450-13455.
129. MacLeod, D., Dowman, J., Hammond, R., Leete, T., Inoue, K., and Abeliovich, A. (2006). The familial Parkinsonism gene LRRK2 regulates neurite process morphology. Neuron *52*, 587-593.
130. Reinhardt, P., Schmid, B., Burbulla, L.F., Schondorf, D.C., Wagner, L., Glatza, M., Hoing, S., Hargus, G., Heck, S.A., Dhingra, A., et al. (2013). Genetic correction of a LRRK2 mutation in human iPSCs links

parkinsonian neurodegeneration to ERK-dependent changes in gene expression. Cell Stem Cell *12*, 354-367.

131. Glick, D., Barth, S., and Macleod, K.F. (2010). Autophagy: cellular and molecular mechanisms. J Pathol *221*, 3-12.
132. Tong, Y., Yamaguchi, H., Giaime, E., Boyle, S., Kopan, R., Kelleher, R.J., 3rd, and Shen, J. (2010). Loss of leucine-rich repeat kinase 2 causes impairment of protein degradation pathways, accumulation of alpha-synuclein, and apoptotic cell death in aged mice. Proc Natl Acad Sci U S A *107*, 9879-9884.
133. Tong, Y., Giaime, E., Yamaguchi, H., Ichimura, T., Liu, Y., Si, H., Cai, H., Bonventre, J.V., and Shen, J. (2012). Loss of leucine-rich repeat kinase 2 causes age-dependent bi-phasic alterations of the autophagy pathway. Mol Neurodegener *7*, 2.
134. Hinkle, K.M., Yue, M., Behrouz, B., Dachsel, J.C., Lincoln, S.J., Bowles, E.E., Beevers, J.E., Dugger, B., Winner, B., Prots, I., et al. (2012). LRRK2 knockout mice have an intact dopaminergic system but display alterations in exploratory and motor co-ordination behaviors. Mol Neurodegener *7*, 25.
135. Manzoni, C., Mamais, A., Dihanich, S., Abeti, R., Soutar, M.P.M., Plun-Favreau, H., Giunti, P., Tooze, S.A., Bandopadhyay, R., and Lewis, P.A. (2013). Inhibition of LRRK2 kinase activity stimulates macroautophagy. Biochim Biophys Acta *1833*, 2900-2910.
136. Saez-Atienzar, S., Bonet-Ponce, L., Blesa, J.R., Romero, F.J., Murphy, M.P., Jordan, J., and Galindo, M.F. (2014). The LRRK2 inhibitor GSK2578215A induces protective autophagy in SH-SY5Y cells: involvement of Drp-1-mediated mitochondrial fission and mitochondrial-derived ROS signaling. Cell Death Dis *5*, e1368.
137. Schapansky, J., Nardozzi, J.D., Felizia, F., and LaVoie, M.J. (2014). Membrane recruitment of endogenous LRRK2 precedes its potent regulation of autophagy. Hum Mol Genet *23*, 4201-4214.
138. Bravo-San Pedro, J.M., Niso-Santano, M., Gomez-Sanchez, R., Pizarro-Estrella, E., Aiastui-Pujana, A., Gorostidi, A., Climent, V., Lopez de Maturana, R., Sanchez-Pernaute, R., Lopez de Munain, A., et al. (2013). The LRRK2 G2019S mutant exacerbates basal autophagy through activation of the MEK/ERK pathway. Cell Mol Life Sci *70*, 121-136.
139. Manzoni, C., Mamais, A., Dihanich, S., McGoldrick, P., Devine, M.J., Zerle, J., Kara, E., Taanman, J.W., Healy, D.G., Marti-Masso, J.F., et al. (2013). Pathogenic Parkinson's disease mutations across the functional domains of LRRK2 alter the autophagic/lysosomal response to starvation. Biochem Biophys Res Commun *441*, 862-866.
140. Gomez-Suaga, P., Luzon-Toro, B., Churamani, D., Zhang, L., Bloor-Young, D., Patel, S., Woodman, P.G., Churchill, G.C., and Hilfiker, S. (2012). Leucine-rich repeat kinase 2 regulates autophagy through a

calcium-dependent pathway involving NAADP. Hum Mol Genet *21*, 511-525.

141. Henry, A.G., Aghamohammadzadeh, S., Samaroo, H., Chen, Y., Mou, K., Needle, E., and Hirst, W.D. (2015). Pathogenic LRRK2 mutations, through increased kinase activity, produce enlarged lysosomes with reduced degradative capacity and increase ATP13A2 expression. Hum Mol Genet *24*, 6013-6028.
142. Doherty, G.J., and McMahon, H.T. (2009). Mechanisms of endocytosis. Annu Rev Biochem *78*, 857-902.
143. Shin, N., Jeong, H., Kwon, J., Heo, H.Y., Kwon, J.J., Yun, H.J., Kim, C.H., Han, B.S., Tong, Y., Shen, J., et al. (2008). LRRK2 regulates synaptic vesicle endocytosis. Exp Cell Res *314*, 2055-2065.
144. Dodson, M.W., Zhang, T., Jiang, C., Chen, S., and Guo, M. (2012). Roles of the Drosophila LRRK2 homolog in Rab7-dependent lysosomal positioning. Hum Mol Genet *21*, 1350-1363.
145. Gomez-Suaga, P., Rivero-Rios, P., Fdez, E., Blanca Ramirez, M., Ferrer, I., Aiastui, A., Lopez De Munain, A., and Hilfiker, S. (2014). LRRK2 delays degradative receptor trafficking by impeding late endosomal budding through decreasing Rab7 activity. Hum Mol Genet *23*, 6779-6796.
146. Burd, C., and Cullen, P.J. (2014). Retromer: a master conductor of endosome sorting. Cold Spring Harb Perspect Biol *6*.
147. Williams, E.T., Chen, X., and Moore, D.J. (2017). VPS35, the Retromer Complex and Parkinson's Disease. J Parkinsons Dis *7*, 219-233.
148. McMillan, K.J., Korswagen, H.C., and Cullen, P.J. (2017). The emerging role of retromer in neuroprotection. Curr Opin Cell Biol *47*, 72-82.
149. Linhart, R., Wong, S.A., Cao, J., Tran, M., Huynh, A., Ardrey, C., Park, J.M., Hsu, C., Taha, S., Peterson, R., et al. (2014). Vacuolar protein sorting 35 (Vps35) rescues locomotor deficits and shortened lifespan in Drosophila expressing a Parkinson's disease mutant of Leucine-Rich Repeat Kinase 2 (LRRK2). Mol Neurodegener *9*, 23.
150. MacLeod, D.A., Rhinn, H., Kuwahara, T., Zolin, A., Di Paolo, G., McCabe, B.D., Marder, K.S., Honig, L.S., Clark, L.N., Small, S.A., et al. (2013). RAB7L1 interacts with LRRK2 to modify intraneuronal protein sorting and Parkinson's disease risk. Neuron *77*, 425-439.
151. Dodson, M.W., Leung, L.K., Lone, M., Lizzio, M.A., and Guo, M. (2014). Novel ethyl methanesulfonate (EMS)-induced null alleles of the Drosophila homolog of LRRK2 reveal a crucial role in endolysosomal functions and autophagy in vivo. Dis Model Mech *7*, 1351-1363.
152. Wang, S., Ma, Z., Xu, X., Wang, Z., Sun, L., Zhou, Y., Lin, X., Hong, W., and Wang, T. (2014). A role of Rab29 in the integrity of the trans-Golgi network and retrograde trafficking of mannose-6-phosphate receptor. PLoS ONE *9*, e96242.

153. Barbero, P., Bittova, L., and Pfeffer, S.R. (2002). Visualization of Rab9-mediated vesicle transport from endosomes to the trans-Golgi in living cells. J Cell Biol *156*, 511-518.
154. Wilson, C., Venditti, R., Rega, L.R., Colanzi, A., D'Angelo, G., and De Matteis, M.A. (2011). The Golgi apparatus: an organelle with multiple complex functions. Biochem J *433*, 1-9.
155. De Matteis, M.A., and Luini, A. (2008). Exiting the Golgi complex. Nat Rev Mol Cell Biol *9*, 273-284.
156. Rios, R.M. (2014). The centrosome-Golgi apparatus nexus. Philos Trans R Soc Lond B Biol Sci *369*.
157. Yadav, S., and Linstedt, A.D. (2011). Golgi positioning. Cold Spring Harb Perspect Biol *3*.
158. Chabin-Brion, K., Marceiller, J., Perez, F., Settegrana, C., Drechou, A., Durand, G., and Pous, C. (2001). The Golgi complex is a microtubule-organizing organelle. Mol Biol Cell *12*, 2047-2060.
159. Ori-McKenney, K.M., Jan, L.Y., and Jan, Y.N. (2012). Golgi outposts shape dendrite morphology by functioning as sites of acentrosomal microtubule nucleation in neurons. Neuron *76*, 921-930.
160. Hatano, T., Kubo, S., Imai, S., Maeda, M., Ishikawa, K., Mizuno, Y., and Hattori, N. (2007). Leucine-rich repeat kinase 2 associates with lipid rafts. Hum Mol Genet *16*, 678-690.
161. Biskup, S., Moore, D.J., Celsi, F., Higashi, S., West, A.B., Andrabi, S.A., Kurkinen, K., Yu, S.W., Savitt, J.M., Waldvogel, H.J., et al. (2006). Localization of LRRK2 to membranous and vesicular structures in mammalian brain. Ann Neurol *60*, 557-569.
162. Gloeckner, C.J., Kinkl, N., Schumacher, A., Braun, R.J., O'Neill, E., Meitinger, T., Kolch, W., Prokisch, H., and Ueffing, M. (2006). The Parkinson disease causing LRRK2 mutation I2020T is associated with increased kinase activity. Hum Mol Genet *15*, 223-232.
163. Lin, X., Parisiadou, L., Gu, X.L., Wang, L., Shim, H., Sun, L., Xie, C., Long, C.X., Yang, W.J., Ding, J., et al. (2009). Leucine-rich repeat kinase 2 regulates the progression of neuropathology induced by Parkinson's-disease-related mutant alpha-synuclein. Neuron *64*, 807-827.
164. Fletcher, D.A., and Mullins, R.D. (2010). Cell mechanics and the cytoskeleton. Nature *463*, 485-492.
165. Pellegrini, L., Wetzel, A., Granno, S., Heaton, G., and Harvey, K. (2017). Back to the tubule: microtubule dynamics in Parkinson's disease. Cell Mol Life Sci *74*, 409-434.
166. Iqbal, K., Liu, F., and Gong, C.X. (2016). Tau and neurodegenerative disease: the story so far. Nat Rev Neurol *12*, 15-27.

167. Ballatore, C., Lee, V.M., and Trojanowski, J.Q. (2007). Tau-mediated neurodegeneration in Alzheimer's disease and related disorders. Nat Rev Neurosci *8*, 663-672.
168. Ujiie, S., Hatano, T., Kubo, S., Imai, S., Sato, S., Uchihara, T., Yagishita, S., Hasegawa, K., Kowa, H., Sakai, F., et al. (2012). LRRK2 I2020T mutation is associated with tau pathology. Parkinsonism Relat Disord *18*, 819-823.
169. Wszolek, Z.K., Pfeiffer, R.F., Tsuboi, Y., Uitti, R.J., McComb, R.D., Stoessl, A.J., Strongosky, A.J., Zimprich, A., Muller-Myhsok, B., Farrer, M.J., et al. (2004). Autosomal dominant parkinsonism associated with variable synuclein and tau pathology. Neurology *62*, 1619-1622.
170. Wills, J., Jones, J., Haggerty, T., Duka, V., Joyce, J.N., and Sidhu, A. (2010). Elevated tauopathy and alpha-synuclein pathology in postmortem Parkinson's disease brains with and without dementia. Exp Neurol *225*, 210-218.
171. Kawakami, F., Yabata, T., Ohta, E., Maekawa, T., Shimada, N., Suzuki, M., Maruyama, H., Ichikawa, T., and Obata, F. (2012). LRRK2 phosphorylates tubulin-associated tau but not the free molecule: LRRK2-mediated regulation of the tau-tubulin association and neurite outgrowth. PLoS One *7*, e30834.
172. Bailey, R.M., Covy, J.P., Melrose, H.L., Rousseau, L., Watkinson, R., Knight, J., Miles, S., Farrer, M.J., Dickson, D.W., Giasson, B.I., et al. (2013). LRRK2 phosphorylates novel tau epitopes and promotes tauopathy. Acta Neuropathol *126*, 809-827.
173. Shanley, M.R., Hawley, D., Leung, S., Zaidi, N.F., Dave, R., Schlosser, K.A., Bandopadhyay, R., Gerber, S.A., and Liu, M. (2015). LRRK2 Facilitates tau Phosphorylation through Strong Interaction with tau and cdk5. Biochemistry *54*, 5198-5208.
174. Meixner, A., Boldt, K., Van Troys, M., Askenazi, M., Gloeckner, C.J., Bauer, M., Marto, J.A., Ampe, C., Kinkl, N., and Ueffing, M. (2011). A QUICK screen for Lrrk2 interaction partners--leucine-rich repeat kinase 2 is involved in actin cytoskeleton dynamics. Mol Cell Proteomics *10*, M110 001172.
175. Gandhi, P.N., Wang, X., Zhu, X., Chen, S.G., and Wilson-Delfosse, A.L. (2008). The Roc domain of leucine-rich repeat kinase 2 is sufficient for interaction with microtubules. J Neurosci Res *86*, 1711-1720.
176. Kett, L.R., Boassa, D., Ho, C.C., Rideout, H.J., Hu, J., Terada, M., Ellisman, M., and Dauer, W.T. (2012). LRRK2 Parkinson disease mutations enhance its microtubule association. Hum Mol Genet *21*, 890-899.
177. Gillardon, F. (2009). Leucine-rich repeat kinase 2 phosphorylates brain tubulin-beta isoforms and modulates microtubule stability--a point of

convergence in parkinsonian neurodegeneration? J Neurochem *110*, 1514-1522.
178. Law, B.M., Spain, V.A., Leinster, V.H., Chia, R., Beilina, A., Cho, H.J., Taymans, J.M., Urban, M.K., Sancho, R.M., Blanca Ramirez, M., et al. (2014). A direct interaction between leucine-rich repeat kinase 2 and specific beta-tubulin isoforms regulates tubulin acetylation. J Biol Chem *289*, 895-908.
179. Godena, V.K., Brookes-Hocking, N., Moller, A., Shaw, G., Oswald, M., Sancho, R.M., Miller, C.C., Whitworth, A.J., and De Vos, K.J. (2014). Increasing microtubule acetylation rescues axonal transport and locomotor deficits caused by LRRK2 Roc-COR domain mutations. Nat Commun *5*, 5245.
180. Manzoni, C., Denny, P., Lovering, R.C., and Lewis, P.A. (2015). Computational analysis of the LRRK2 interactome. PeerJ *3*, e778.
181. Waschbusch, D., Michels, H., Strassheim, S., Ossendorf, E., Kessler, D., Gloeckner, C.J., and Barnekow, A. (2014). LRRK2 transport is regulated by its novel interacting partner Rab32. PLoS One *9*, e111632.
182. Wasmeier, C., Romao, M., Plowright, L., Bennett, D.C., Raposo, G., and Seabra, M.C. (2006). Rab38 and Rab32 control post-Golgi trafficking of melanogenic enzymes. J Cell Biol *175*, 271-281.
183. Nichols, R.J., Dzamko, N., Morrice, N.A., Campbell, D.G., Deak, M., Ordureau, A., Macartney, T., Tong, Y., Shen, J., Prescott, A.R., et al. (2010). 14-3-3 binding to LRRK2 is disrupted by multiple Parkinson's disease-associated mutations and regulates cytoplasmic localization. Biochem J *430*, 393-404.
184. Dzamko, N., Deak, M., Hentati, F., Reith, A.D., Prescott, A.R., Alessi, D.R., and Nichols, R.J. (2010). Inhibition of LRRK2 kinase activity leads to dephosphorylation of Ser(910)/Ser(935), disruption of 14-3-3 binding and altered cytoplasmic localization. Biochem J *430*, 405-413.
185. Morrison, D.K. (2009). The 14-3-3 proteins: integrators of diverse signaling cues that impact cell fate and cancer development. Trends Cell Biol *19*, 16-23.
186. Steger, M., Diez, F., Dhekne, H.S., Lis, P., Nirujogi, R.S., Karayel, O., Tonelli, F., Martinez, T.N., Lorentzen, E., Pfeffer, S.R., et al. (2017). Systematic proteomic analysis of LRRK2-mediated Rab GTPase phosphorylation establishes a connection to ciliogenesis. Elife *6*.
187. Jeong, G.R., Jang, E.H., Bae, J.R., Jun, S., Kang, H.C., Park, C.H., Shin, J.H., Yamamoto, Y., Tanaka-Yamamoto, K., Dawson, V.L., et al. (2018). Dysregulated phosphorylation of Rab GTPases by LRRK2 induces neurodegeneration. Mol Neurodegener *13*, 8.
188. Thirstrup, K., Dachsel, J.C., Oppermann, F.S., Williamson, D.S., Smith, G.P., Fog, K., and Christensen, K.V. (2017). Selective LRRK2 kinase

inhibition reduces phosphorylation of endogenous Rab10 and Rab12 in human peripheral mononuclear blood cells. Sci Rep *7*, 10300.

189. Lis, P., Burel, S., Steger, M., Mann, M., Brown, F., Diez, F., Tonelli, F., Holton, J.L., Ho, P.W., Ho, S.L., et al. (2018). Development of phospho-specific Rab protein antibodies to monitor in vivo activity of the LRRK2 Parkinson's disease kinase. Biochem J *475*, 1-22.
190. Fan, Y., Howden, A.J.M., Sarhan, A.R., Lis, P., Ito, G., Martinez, T.N., Brockmann, K., Gasser, T., Alessi, D.R., and Sammler, E.M. (2018). Interrogating Parkinson's disease LRRK2 kinase pathway activity by assessing Rab10 phosphorylation in human neutrophils. Biochem J *475*, 23-44.
191. Stenmark, H. (2009). Rab GTPases as coordinators of vesicle traffic. Nat Rev Mol Cell Biol *10*, 513-525.
192. Rojas, A.M., Fuentes, G., Rausell, A., and Valencia, A. (2012). The Ras protein superfamily: evolutionary tree and role of conserved amino acids. J Cell Biol *196*, 189-201.
193. Wandinger-Ness, A., and Zerial, M. (2014). Rab proteins and the compartmentalization of the endosomal system. Cold Spring Harb Perspect Biol *6*, a022616.
194. Zhen, Y., and Stenmark, H. (2015). Cellular functions of Rab GTPases at a glance. J Cell Sci *128*, 3171-3176.
195. Hutagalung, A.H., and Novick, P.J. (2011). Role of Rab GTPases in membrane traffic and cell physiology. Physiol Rev *91*, 119-149.
196. Seabra, M.C., and Wasmeier, C. (2004). Controlling the location and activation of Rab GTPases. Curr Opin Cell Biol *16*, 451-457.
197. Pfeffer, S., and Aivazian, D. (2004). Targeting Rab GTPases to distinct membrane compartments. Nat Rev Mol Cell Biol *5*, 886-896.
198. Muller, M.P., and Goody, R.S. (2018). Molecular control of Rab activity by GEFs, GAPs and GDI. Small GTPases *9*, 5-21.
199. Fukuda, M. (2011). TBC proteins: GAPs for mammalian small GTPase Rab? Biosci Rep *31*, 159-168.
200. Mignogna, M.L., Giannandrea, M., Gurgone, A., Fanelli, F., Raimondi, F., Mapelli, L., Bassani, S., Fang, H., Van Anken, E., Alessio, M., et al. (2015). The intellectual disability protein RAB39B selectively regulates GluA2 trafficking to determine synaptic AMPAR composition. Nat Commun *6*, 6504.
201. Wilson, G.R., Sim, J.C., McLean, C., Giannandrea, M., Galea, C.A., Riseley, J.R., Stephenson, S.E., Fitzpatrick, E., Haas, S.A., Pope, K., et al. (2014). Mutations in RAB39B cause X-linked intellectual disability and early-onset Parkinson disease with alpha-synuclein pathology. Am J Hum Genet *95*, 729-735.

202. Mata, I.F., Jang, Y., Kim, C.H., Hanna, D.S., Dorschner, M.O., Samii, A., Agarwal, P., Roberts, J.W., Klepitskaya, O., Shprecher, D.R., et al. (2015). The RAB39B p.G192R mutation causes X-linked dominant Parkinson's disease. Mol Neurodegener *10*, 50.
203. Shi, C.H., Zhang, S.Y., Yang, Z.H., Yang, J., Shang, D.D., Mao, C.Y., Liu, H., Hou, H.M., Shi, M.M., Wu, J., et al. (2016). A novel RAB39B gene mutation in X-linked juvenile parkinsonism with basal ganglia calcification. Mov Disord *31*, 1905-1909.
204. Lesage, S., Bras, J., Cormier-Dequaire, F., Condroyer, C., Nicolas, A., Darwent, L., Guerreiro, R., Majounie, E., Federoff, M., Heutink, P., et al. (2015). Loss-of-function mutations in RAB39B are associated with typical early-onset Parkinson disease. Neurol Genet *1*, e9.
205. Goncalves, S.A., Macedo, D., Raquel, H., Simoes, P.D., Giorgini, F., Ramalho, J.S., Barral, D.C., Ferreira Moita, L., and Outeiro, T.F. (2016). shRNA-Based Screen Identifies Endocytic Recycling Pathway Components That Act as Genetic Modifiers of Alpha-Synuclein Aggregation, Secretion and Toxicity. PLoS Genet *12*, e1005995.
206. Chiu, C.C., Yeh, T.H., Lai, S.C., Weng, Y.H., Huang, Y.C., Cheng, Y.C., Chen, R.S., Huang, Y.Z., Hung, J., Chen, C.C., et al. (2016). Increased Rab35 expression is a potential biomarker and implicated in the pathogenesis of Parkinson's disease. Oncotarget *7*, 54215-54227.
207. Chutna, O., Goncalves, S., Villar-Pique, A., Guerreiro, P., Marijanovic, Z., Mendes, T., Ramalho, J., Emmanouilidou, E., Ventura, S., Klucken, J., et al. (2014). The small GTPase Rab11 co-localizes with alpha-synuclein in intracellular inclusions and modulates its aggregation, secretion and toxicity. Hum Mol Genet *23*, 6732-6745.
208. Hattula, K., Furuhjelm, J., Arffman, A., and Peranen, J. (2002). A Rab8-specific GDP/GTP exchange factor is involved in actin remodeling and polarized membrane transport. Mol Biol Cell *13*, 3268-3280.
209. Yoshimura, S., Gerondopoulos, A., Linford, A., Rigden, D.J., and Barr, F.A. (2010). Family-wide characterization of the DENN domain Rab GDP-GTP exchange factors. J Cell Biol *191*, 367-381.
210. Itzen, A., Pylypenko, O., Goody, R.S., Alexandrov, K., and Rak, A. (2006). Nucleotide exchange via local protein unfolding--structure of Rab8 in complex with MSS4. EMBO J *25*, 1445-1455.
211. Sellier, C., Campanari, M.L., Julie Corbier, C., Gaucherot, A., Kolb-Cheynel, I., Oulad-Abdelghani, M., Ruffenach, F., Page, A., Ciura, S., Kabashi, E., et al. (2016). Loss of C9ORF72 impairs autophagy and synergizes with polyQ Ataxin-2 to induce motor neuron dysfunction and cell death. EMBO J *35*, 1276-1297.

212. Bryant, D.M., Datta, A., Rodriguez-Fraticelli, A.E., Peranen, J., Martin-Belmonte, F., and Mostov, K.E. (2010). A molecular network for de novo generation of the apical surface and lumen. Nat Cell Biol *12*, 1035-1045.
213. Knodler, A., Feng, S., Zhang, J., Zhang, X., Das, A., Peranen, J., and Guo, W. (2010). Coordination of Rab8 and Rab11 in primary ciliogenesis. Proc Natl Acad Sci U S A *107*, 6346-6351.
214. Chiba, S., Amagai, Y., Homma, Y., Fukuda, M., and Mizuno, K. (2013). NDR2-mediated Rabin8 phosphorylation is crucial for ciliogenesis by switching binding specificity from phosphatidylserine to Sec15. EMBO J *32*, 874-885.
215. Wang, J., Ren, J., Wu, B., Feng, S., Cai, G., Tuluc, F., Peranen, J., and Guo, W. (2015). Activation of Rab8 guanine nucleotide exchange factor Rabin8 by ERK1/2 in response to EGF signaling. Proc Natl Acad Sci U S A *112*, 148-153.
216. Furusawa, K., Asada, A., Urrutia, P., Gonzalez-Billault, C., Fukuda, M., and Hisanaga, S.I. (2017). Cdk5 Regulation of the GRAB-Mediated Rab8-Rab11 Cascade in Axon Outgrowth. J Neurosci *37*, 790-806.
217. Nuoffer, C., Wu, S.K., Dascher, C., and Balch, W.E. (1997). Mss4 does not function as an exchange factor for Rab in endoplasmic reticulum to Golgi transport. Mol Biol Cell *8*, 1305-1316.
218. DeJesus-Hernandez, M., Mackenzie, I.R., Boeve, B.F., Boxer, A.L., Baker, M., Rutherford, N.J., Nicholson, A.M., Finch, N.A., Flynn, H., Adamson, J., et al. (2011). Expanded GGGGCC hexanucleotide repeat in noncoding region of C9ORF72 causes chromosome 9p-linked FTD and ALS. Neuron *72*, 245-256.
219. Renton, A.E., Majounie, E., Waite, A., Simon-Sanchez, J., Rollinson, S., Gibbs, J.R., Schymick, J.C., Laaksovirta, H., van Swieten, J.C., Myllykangas, L., et al. (2011). A hexanucleotide repeat expansion in C9ORF72 is the cause of chromosome 9p21-linked ALS-FTD. Neuron *72*, 257-268.
220. Aoki, Y., Manzano, R., Lee, Y., Dafinca, R., Aoki, M., Douglas, A.G.L., Varela, M.A., Sathyaprakash, C., Scaber, J., Barbagallo, P., et al. (2017). C9orf72 and RAB7L1 regulate vesicle trafficking in amyotrophic lateral sclerosis and frontotemporal dementia. Brain *140*, 887-897.
221. Goldenring, J.R. (2015). Recycling endosomes. Curr Opin Cell Biol *35*, 117-122.
222. McCaffrey, M.W., Bielli, A., Cantalupo, G., Mora, S., Roberti, V., Santillo, M., Drummond, F., and Bucci, C. (2001). Rab4 affects both recycling and degradative endosomal trafficking. FEBS Lett *495*, 21-30.
223. Hattula, K., Furuhjelm, J., Tikkanen, J., Tanhuanpaa, K., Laakkonen, P., and Peranen, J. (2006). Characterization of the Rab8-specific membrane traffic route linked to protrusion formation. J Cell Sci *119*, 4866-4877.

224. Ullrich, O., Reinsch, S., Urbe, S., Zerial, M., and Parton, R.G. (1996). Rab11 regulates recycling through the pericentriolar recycling endosome. J Cell Biol *135*, 913-924.
225. Ang, A.L., Folsch, H., Koivisto, U.M., Pypaert, M., and Mellman, I. (2003). The Rab8 GTPase selectively regulates AP-1B-dependent basolateral transport in polarized Madin-Darby canine kidney cells. J Cell Biol *163*, 339-350.
226. Sato, T., Mushiake, S., Kato, Y., Sato, K., Sato, M., Takeda, N., Ozono, K., Miki, K., Kubo, Y., Tsuji, A., et al. (2007). The Rab8 GTPase regulates apical protein localization in intestinal cells. Nature *448*, 366-369.
227. Ang, A.L., Taguchi, T., Francis, S., Folsch, H., Murrells, L.J., Pypaert, M., Warren, G., and Mellman, I. (2004). Recycling endosomes can serve as intermediates during transport from the Golgi to the plasma membrane of MDCK cells. J Cell Biol *167*, 531-543.
228. Grigoriev, I., Yu, K.L., Martinez-Sanchez, E., Serra-Marques, A., Smal, I., Meijering, E., Demmers, J., Peranen, J., Pasterkamp, R.J., van der Sluijs, P., et al. (2011). Rab6, Rab8, and MICAL3 cooperate in controlling docking and fusion of exocytotic carriers. Curr Biol *21*, 967-974.
229. Shibata, S., Kawanai, T., Hara, T., Yamamoto, A., Chaya, T., Tokuhara, Y., Tsuji, C., Sakai, M., Tachibana, T., and Inagaki, S. (2016). ARHGEF10 directs the localization of Rab8 to Rab6-positive executive vesicles. J Cell Sci *129*, 3620-3634.
230. Gerges, N.Z., Backos, D.S., and Esteban, J.A. (2004). Local control of AMPA receptor trafficking at the postsynaptic terminal by a small GTPase of the Rab family. J Biol Chem *279*, 43870-43878.
231. Zhu, H., Xue, C., Xu, X., Guo, Y., Li, X., Lu, J., Ju, S., Wang, Y., Cao, Z., and Gu, X. (2016). Rab8a/Rab11a regulate intercellular communications between neural cells via tunneling nanotubes. Cell Death Dis *7*, e2523.
232. Yoshimura, S., Egerer, J., Fuchs, E., Haas, A.K., and Barr, F.A. (2007). Functional dissection of Rab GTPases involved in primary cilium formation. J Cell Biol *178*, 363-369.
233. Nachury, M.V., Loktev, A.V., Zhang, Q., Westlake, C.J., Peranen, J., Merdes, A., Slusarski, D.C., Scheller, R.H., Bazan, J.F., Sheffield, V.C., et al. (2007). A core complex of BBS proteins cooperates with the GTPase Rab8 to promote ciliary membrane biogenesis. Cell *129*, 1201-1213.
234. Westlake, C.J., Baye, L.M., Nachury, M.V., Wright, K.J., Ervin, K.E., Phu, L., Chalouni, C., Beck, J.S., Kirkpatrick, D.S., Slusarski, D.C., et al. (2011). Primary cilia membrane assembly is initiated by Rab11 and transport protein particle II (TRAPPII) complex-dependent trafficking of Rabin8 to the centrosome. Proc Natl Acad Sci U S A *108*, 2759-2764.
235. Sato, T., Iwano, T., Kunii, M., Matsuda, S., Mizuguchi, R., Jung, Y., Hagiwara, H., Yoshihara, Y., Yuzaki, M., Harada, R., et al. (2014). Rab8a

and Rab8b are essential for several apical transport pathways but insufficient for ciliogenesis. J Cell Sci *127*, 422-431.

236. Hehnly, H., Chen, C.T., Powers, C.M., Liu, H.L., and Doxsey, S. (2012). The centrosome regulates the Rab11- dependent recycling endosome pathway at appendages of the mother centriole. Curr Biol *22*, 1944-1950.
237. Feng, M., Hu, X., Li, N., Hu, F., Chang, F., Xu, H.F., and Liu, Y.J. (2017). Distinctive roles of Rac1 and Rab29 in LRRK2 mediatedmembrane trafficking and neurite outgrowth. J Biomed Res.
238. Fujimoto, T., Kuwahara, T., Eguchi, T., Sakurai, M., Komori, T., and Iwatsubo, T. (2018). Parkinson's disease-associated mutant LRRK2 phosphorylates Rab7L1 and modifies trans-Golgi morphology. Biochem Biophys Res Commun *495*, 1708-1715.
239. Massmann, S., Schurmann, A., and Joost, H.G. (1997). Cloning of two splicing variants of the novel Ras-related GTPase Rab29 which is predominantly expressed in kidney. Biochim Biophys Acta *1352*, 48-55.
240. Kuwahara, T., Inoue, K., D'Agati, V.D., Fujimoto, T., Eguchi, T., Saha, S., Wolozin, B., Iwatsubo, T., and Abeliovich, A. (2016). LRRK2 and RAB7L1 coordinately regulate axonal morphology and lysosome integrity in diverse cellular contexts. Sci Rep *6*, 29945.
241. Spano, S., Liu, X., and Galan, J.E. (2011). Proteolytic targeting of Rab29 by an effector protein distinguishes the intracellular compartments of human-adapted and broad-host Salmonella. Proc Natl Acad Sci U S A *108*, 18418-18423.
242. Onnis, A., Finetti, F., Patrussi, L., Gottardo, M., Cassioli, C., Spano, S., and Baldari, C.T. (2015). The small GTPase Rab29 is a common regulator of immune synapse assembly and ciliogenesis. Cell Death Differ *22*, 1687-1699.
243. Doxsey, S.J., Stein, P., Evans, L., Calarco, P.D., and Kirschner, M. (1994). Pericentrin, a highly conserved centrosome protein involved in microtubule organization. Cell *76*, 639-650.
244. Fu, J., Hagan, I.M., and Glover, D.M. (2015). The centrosome and its duplication cycle. Cold Spring Harb Perspect Biol *7*, a015800.
245. Doxsey, S. (2001). Re-evaluating centrosome function. Nat Rev Mol Cell Biol *2*, 688-698.
246. Vertii, A., Hehnly, H., and Doxsey, S. (2016). The Centrosome, a Multitalented Renaissance Organelle. Cold Spring Harb Perspect Biol *8*.
247. Agircan, F.G., Schiebel, E., and Mardin, B.R. (2014). Separate to operate: control of centrosome positioning and separation. Philos Trans R Soc Lond B Biol Sci *369*.
248. Nigg, E.A. (2002). Centrosome aberrations: cause or consequence of cancer progression? Nat Rev Cancer *2*, 815-825.

249. Yang, J., Adamian, M., and Li, T. (2006). Rootletin interacts with C-Nap1 and may function as a physical linker between the pair of centrioles/basal bodies in cells. Mol Biol Cell *17*, 1033-1040.
250. Fry, A.M., Mayor, T., Meraldi, P., Stierhof, Y.D., Tanaka, K., and Nigg, E.A. (1998). C-Nap1, a novel centrosomal coiled-coil protein and candidate substrate of the cell cycle-regulated protein kinase Nek2. J Cell Biol *141*, 1563-1574.
251. Helps, N.R., Luo, X., Barker, H.M., and Cohen, P.T. (2000). NIMA-related kinase 2 (Nek2), a cell-cycle-regulated protein kinase localized to centrosomes, is complexed to protein phosphatase 1. Biochem J *349*, 509-518.
252. Mayor, T., Stierhof, Y.D., Tanaka, K., Fry, A.M., and Nigg, E.A. (2000). The centrosomal protein C-Nap1 is required for cell cycle-regulated centrosome cohesion. J Cell Biol *151*, 837-846.
253. Bahe, S., Stierhof, Y.D., Wilkinson, C.J., Leiss, F., and Nigg, E.A. (2005). Rootletin forms centriole-associated filaments and functions in centrosome cohesion. J Cell Biol *171*, 27-33.
254. Faragher, A.J., and Fry, A.M. (2003). Nek2A kinase stimulates centrosome disjunction and is required for formation of bipolar mitotic spindles. Mol Biol Cell *14*, 2876-2889.
255. Mardin, B.R., Lange, C., Baxter, J.E., Hardy, T., Scholz, S.R., Fry, A.M., and Schiebel, E. (2010). Components of the Hippo pathway cooperate with Nek2 kinase to regulate centrosome disjunction. Nat Cell Biol *12*, 1166-1176.
256. Smith, E., Hegarat, N., Vesely, C., Roseboom, I., Larch, C., Streicher, H., Straatman, K., Flynn, H., Skehel, M., Hirota, T., et al. (2011). Differential control of Eg5-dependent centrosome separation by Plk1 and Cdk1. EMBO J *30*, 2233-2245.
257. Raaijmakers, J.A., van Heesbeen, R.G., Meaders, J.L., Geers, E.F., Fernandez-Garcia, B., Medema, R.H., and Tanenbaum, M.E. (2012). Nuclear envelope-associated dynein drives prophase centrosome separation and enables Eg5-independent bipolar spindle formation. EMBO J *31*, 4179-4190.
258. Wang, G., Jiang, Q., and Zhang, C. (2014). The role of mitotic kinases in coupling the centrosome cycle with the assembly of the mitotic spindle. J Cell Sci *127*, 4111-4122.
259. Teixido-Travesa, N., Roig, J., and Luders, J. (2012). The where, when and how of microtubule nucleation - one ring to rule them all. J Cell Sci *125*, 4445-4456.
260. Mogensen, M.M., Malik, A., Piel, M., Bouckson-Castaing, V., and Bornens, M. (2000). Microtubule minus-end anchorage at centrosomal and

non-centrosomal sites: the role of ninein. J Cell Sci *113 (Pt 17)*, 3013-3023.
261. Bornens, M. (2012). The centrosome in cells and organisms. Science *335*, 422-426.
262. Elric, J., and Etienne-Manneville, S. (2014). Centrosome positioning in polarized cells: common themes and variations. Exp Cell Res *328*, 240-248.
263. de Anda, F.C., Pollarolo, G., Da Silva, J.S., Camoletto, P.G., Feiguin, F., and Dotti, C.G. (2005). Centrosome localization determines neuronal polarity. Nature *436*, 704-708.
264. Luxton, G.W., and Gundersen, G.G. (2011). Orientation and function of the nuclear-centrosomal axis during cell migration. Curr Opin Cell Biol *23*, 579-588.
265. Caesar, M., Zach, S., Carlson, C.B., Brockmann, K., Gasser, T., and Gillardon, F. (2013). Leucine-rich repeat kinase 2 functionally interacts with microtubules and kinase-dependently modulates cell migration. Neurobiol Dis *54*, 280-288.
266. Choi, I., Kim, B., Byun, J.W., Baik, S.H., Huh, Y.H., Kim, J.H., Mook-Jung, I., Song, W.K., Shin, J.H., Seo, H., et al. (2015). LRRK2 G2019S mutation attenuates microglial motility by inhibiting focal adhesion kinase. Nat Commun *6*, 8255.
267. Moehle, M.S., Daher, J.P., Hull, T.D., Boddu, R., Abdelmotilib, H.A., Mobley, J., Kannarkat, G.T., Tansey, M.G., and West, A.B. (2015). The G2019S LRRK2 mutation increases myeloid cell chemotactic responses and enhances LRRK2 binding to actin-regulatory proteins. Hum Mol Genet *24*, 4250-4267.
268. Conduit, P.T., Wainman, A., and Raff, J.W. (2015). Centrosome function and assembly in animal cells. Nat Rev Mol Cell Biol *16*, 611-624.
269. Godinho, S.A., and Pellman, D. (2014). Causes and consequences of centrosome abnormalities in cancer. Philos Trans R Soc Lond B Biol Sci *369*.
270. Gonczy, P. (2015). Centrosomes and cancer: revisiting a long-standing relationship. Nat Rev Cancer *15*, 639-652.
271. Saunders-Pullman, R., Barrett, M.J., Stanley, K.M., Luciano, M.S., Shanker, V., Severt, L., Hunt, A., Raymond, D., Ozelius, L.J., and Bressman, S.B. (2010). LRRK2 G2019S mutations are associated with an increased cancer risk in Parkinson disease. Mov Disord *25*, 2536-2541.
272. Inzelberg, R., Cohen, O.S., Aharon-Peretz, J., Schlesinger, I., Gershoni-Baruch, R., Djaldetti, R., Nitsan, Z., Ephraty, L., Tunkel, O., Kozlova, E., et al. (2012). The LRRK2 G2019S mutation is associated with Parkinson disease and concomitant non-skin cancers. Neurology *78*, 781-786.
273. Agalliu, I., San Luciano, M., Mirelman, A., Giladi, N., Waro, B., Aasly, J., Inzelberg, R., Hassin-Baer, S., Friedman, E., Ruiz-Martinez, J., et al.

(2015). Higher frequency of certain cancers in LRRK2 G2019S mutation carriers with Parkinson disease: a pooled analysis. JAMA Neurol *72*, 58-65.
274. Satir, P., Pedersen, L.B., and Christensen, S.T. (2010). The primary cilium at a glance. J Cell Sci *123*, 499-503.
275. Wheway, G., Nazlamova, L., and Hancock, J.T. (2018). Signaling through the Primary Cilium. Front Cell Dev Biol *6*, 8.
276. Reiter, J.F., and Leroux, M.R. (2017). Genes and molecular pathways underpinning ciliopathies. Nat Rev Mol Cell Biol *18*, 533-547.
277. Garcia-Gonzalo, F.R., and Reiter, J.F. (2017). Open Sesame: How Transition Fibers and the Transition Zone Control Ciliary Composition. Cold Spring Harb Perspect Biol *9*.
278. Marley, A., and von Zastrow, M. (2010). DISC1 regulates primary cilia that display specific dopamine receptors. PLoS One *5*, e10902.
279. Domire, J.S., Green, J.A., Lee, K.G., Johnson, A.D., Askwith, C.C., and Mykytyn, K. (2011). Dopamine receptor 1 localizes to neuronal cilia in a dynamic process that requires the Bardet-Biedl syndrome proteins. Cell Mol Life Sci *68*, 2951-2960.
280. Sancho, R.M., Law, B.M., and Harvey, K. (2009). Mutations in the LRRK2 Roc-COR tandem domain link Parkinson's disease to Wnt signalling pathways. Hum Mol Genet *18*, 3955-3968.
281. Berwick, D.C., and Harvey, K. (2012). LRRK2 functions as a Wnt signaling scaffold, bridging cytosolic proteins and membrane-localized LRP6. Hum Mol Genet *21*, 4966-4979.
282. Berwick, D.C., Javaheri, B., Wetzel, A., Hopkinson, M., Nixon-Abell, J., Granno, S., Pitsillides, A.A., and Harvey, K. (2017). Pathogenic LRRK2 variants are gain-of-function mutations that enhance LRRK2-mediated repression of beta-catenin signaling. Mol Neurodegener *12*, 9.
283. Reyniers, L., Del Giudice, M.G., Civiero, L., Belluzzi, E., Lobbestael, E., Beilina, A., Arrigoni, G., Derua, R., Waelkens, E., Li, Y., et al. (2014). Differential protein-protein interactions of LRRK1 and LRRK2 indicate roles in distinct cellular signaling pathways. J Neurochem *131*, 239-250.
284. Vancraenenbroeck, R., De Raeymaecker, J., Lobbestael, E., Gao, F., De Maeyer, M., Voet, A., Baekelandt, V., and Taymans, J.M. (2014). In silico, in vitro and cellular analysis with a kinome-wide inhibitor panel correlates cellular LRRK2 dephosphorylation to inhibitor activity on LRRK2. Front Mol Neurosci *7*, 51.
285. Louie, L.G., and King, M.C. (1991). A novel approach to establishing permanent lymphoblastoid cell lines: Epstein-Barr virus transformation of cryopreserved lymphocytes. Am J Hum Genet *48*, 637-638.
286. Lindqvist, A., van Zon, W., Karlsson Rosenthal, C., and Wolthuis, R.M. (2007). Cyclin B1-Cdk1 activation continues after centrosome separation to control mitotic progression. PLoS Biol *5*, e123.

287. Abbi, S., Ueda, H., Zheng, C., Cooper, L.A., Zhao, J., Christopher, R., and Guan, J.L. (2002). Regulation of focal adhesion kinase by a novel protein inhibitor FIP200. Mol Biol Cell *13*, 3178-3191.
288. Etienne-Manneville, S., and Hall, A. (2001). Integrin-mediated activation of Cdc42 controls cell polarity in migrating astrocytes through PKCzeta. Cell *106*, 489-498.
289. Taymans, J.M., Vancraenenbroeck, R., Ollikainen, P., Beilina, A., Lobbestael, E., De Maeyer, M., Baekelandt, V., and Cookson, M.R. (2011). LRRK2 kinase activity is dependent on LRRK2 GTP binding capacity but independent of LRRK2 GTP binding. PLoS ONE *6*, e23207.
290. Sutterlin, C., and Colanzi, A. (2010). The Golgi and the centrosome: building a functional partnership. J Cell Biol *188*, 621-628.
291. Delaval, B., and Doxsey, S.J. (2010). Pericentrin in cellular function and disease. J Cell Biol *188*, 181-190.
292. Hurtado, L., Caballero, C., Gavilan, M.P., Cardenas, J., Bornens, M., and Rios, R.M. (2011). Disconnecting the Golgi ribbon from the centrosome prevents directional cell migration and ciliogenesis. J Cell Biol *193*, 917-933.
293. Nigg, E.A., and Stearns, T. (2011). The centrosome cycle: Centriole biogenesis, duplication and inherent asymmetries. Nat Cell Biol *13*, 1154-1160.
294. Deng, X., Dzamko, N., Prescott, A., Davies, P., Liu, Q., Yang, Q., Lee, J.D., Patricelli, M.P., Nomanbhoy, T.K., Alessi, D.R., et al. (2011). Characterization of a selective inhibitor of the Parkinson's disease kinase LRRK2. Nat Chem Biol *7*, 203-205.
295. Reith, A.D., Bamborough, P., Jandu, K., Andreotti, D., Mensah, L., Dossang, P., Choi, H.G., Deng, X., Zhang, J., Alessi, D.R., et al. (2012). GSK2578215A; a potent and highly selective 2-arylmethyloxy-5-substitutent-N-arylbenzamide LRRK2 kinase inhibitor. Bioorg Med Chem Lett *22*, 5625-5629.
296. Alegre-Abarrategui, J., Christian, H., Lufino, M.M., Mutihac, R., Venda, L.L., Ansorge, O., and Wade-Martins, R. (2009). LRRK2 regulates autophagic activity and localizes to specific membrane microdomains in a novel human genomic reporter cellular model. Hum Mol Genet *18*, 4022-4034.
297. Papkovskaia, T.D., Chau, K.Y., Inesta-Vaquera, F., Papkovsky, D.B., Healy, D.G., Nishio, K., Staddon, J., Duchen, M.R., Hardy, J., Schapira, A.H., et al. (2012). G2019S leucine-rich repeat kinase 2 causes uncoupling protein-mediated mitochondrial depolarization. Hum Mol Genet *21*, 4201-4213.
298. Fell, M.J., Mirescu, C., Basu, K., Cheewatrakoolpong, B., DeMong, D.E., Ellis, J.M., Hyde, L.A., Lin, Y., Markgraf, C.G., Mei, H., et al. (2015).

MLi-2, a Potent, Selective, and Centrally Active Compound for Exploring the Therapeutic Potential and Safety of LRRK2 Kinase Inhibition. J Pharmacol Exp Ther *355*, 397-409.

299. Shisheva, A., Chinni, S.R., and DeMarco, C. (1999). General role of GDP dissociation inhibitor 2 in membrane release of Rab proteins: modulations of its functional interactions by in vitro and in vivo structural modifications. Biochemistry *38*, 11711-11721.
300. Jakobsen, L., Vanselow, K., Skogs, M., Toyoda, Y., Lundberg, E., Poser, I., Falkenby, L.G., Bennetzen, M., Westendorf, J., Nigg, E.A., et al. (2011). Novel asymmetrically localizing components of human centrosomes identified by complementary proteomics methods. EMBO J *30*, 1520-1535.
301. Gundersen, G.G., and Worman, H.J. (2013). Nuclear positioning. Cell *152*, 1376-1389.
302. Copeland, S.J., Thurston, S.F., and Copeland, J.W. (2016). Actin- and microtubule-dependent regulation of Golgi morphology by FHDC1. Mol Biol Cell *27*, 260-276.
303. Li, X., Wang, Q.J., Pan, N., Lee, S., Zhao, Y., Chait, B.T., and Yue, Z. (2011). Phosphorylation-dependent 14-3-3 binding to LRRK2 is impaired by common mutations of familial Parkinson's disease. PLoS ONE *6*, e17153.
304. Doggett, E.A., Zhao, J., Mork, C.N., Hu, D., and Nichols, R.J. (2012). Phosphorylation of LRRK2 serines 955 and 973 is disrupted by Parkinson's disease mutations and LRRK2 pharmacological inhibition. J Neurochem *120*, 37-45.
305. Lobbestael, E., Zhao, J., Rudenko, I.N., Beylina, A., Gao, F., Wetter, J., Beullens, M., Bollen, M., Cookson, M.R., Baekelandt, V., et al. (2013). Identification of protein phosphatase 1 as a regulator of the LRRK2 phosphorylation cycle. Biochem J *456*, 119-128.
306. Madero-Perez, J., Fdez, E., Fernandez, B., Lara Ordonez, A.J., Blanca Ramirez, M., Gomez-Suaga, P., Waschbusch, D., Lobbestael, E., Baekelandt, V., Nairn, A.C., et al. (2018). Parkinson disease-associated mutations in LRRK2 cause centrosomal defects via Rab8a phosphorylation. Mol Neurodegener *13*, 3.
307. Huotari, J., and Helenius, A. (2011). Endosome maturation. EMBO J *30*, 3481-3500.
308. Guerra, F., and Bucci, C. (2016). Multiple Roles of the Small GTPase Rab7. Cells *5*.
309. Kucera, A., Bakke, O., and Progida, C. (2016). The multiple roles of Rab9 in the endolysosomal system. Commun Integr Biol *9*, e1204498.
310. Lippincott-Schwartz, J., Yuan, L.C., Bonifacino, J.S., and Klausner, R.D. (1989). Rapid redistribution of Golgi proteins into the ER in cells treated

with brefeldin A: evidence for membrane cycling from Golgi to ER. Cell *56*, 801-813.
311. Dephoure, N., Gould, K.L., Gygi, S.P., and Kellogg, D.R. (2013). Mapping and analysis of phosphorylation sites: a quick guide for cell biologists. Mol Biol Cell *24*, 535-542.
312. Hunter, T. (2012). Why nature chose phosphate to modify proteins. Philos Trans R Soc Lond B Biol Sci *367*, 2513-2516.
313. Schaub, J.R., and Stearns, T. (2013). The Rilp-like proteins Rilpl1 and Rilpl2 regulate ciliary membrane content. Mol Biol Cell *24*, 453-464.
314. Tollenaere, M.A., Mailand, N., and Bekker-Jensen, S. (2015). Centriolar satellites: key mediators of centrosome functions. Cell Mol Life Sci *72*, 11-23.
315. Winner, B., Melrose, H.L., Zhao, C., Hinkle, K.M., Yue, M., Kent, C., Braithwaite, A.T., Ogholikhan, S., Aigner, R., Winkler, J., et al. (2011). Adult neurogenesis and neurite outgrowth are impaired in LRRK2 G2019S mice. Neurobiol Dis *41*, 706-716.
316. Liu, G.H., Qu, J., Suzuki, K., Nivet, E., Li, M., Montserrat, N., Yi, F., Xu, X., Ruiz, S., Zhang, W., et al. (2012). Progressive degeneration of human neural stem cells caused by pathogenic LRRK2. Nature *491*, 603-607.
317. Eriksson, P.S., Perfilieva, E., Bjork-Eriksson, T., Alborn, A.M., Nordborg, C., Peterson, D.A., and Gage, F.H. (1998). Neurogenesis in the adult human hippocampus. Nat Med *4*, 1313-1317.
318. Curtis, M.A., Kam, M., Nannmark, U., Anderson, M.F., Axell, M.Z., Wikkelso, C., Holtas, S., van Roon-Mom, W.M., Bjork-Eriksson, T., Nordborg, C., et al. (2007). Human neuroblasts migrate to the olfactory bulb via a lateral ventricular extension. Science *315*, 1243-1249.
319. Hoglinger, G.U., Rizk, P., Muriel, M.P., Duyckaerts, C., Oertel, W.H., Caille, I., and Hirsch, E.C. (2004). Dopamine depletion impairs precursor cell proliferation in Parkinson disease. Nat Neurosci *7*, 726-735.
320. van den Berge, S.A., van Strien, M.E., Korecka, J.A., Dijkstra, A.A., Sluijs, J.A., Kooijman, L., Eggers, R., De Filippis, L., Vescovi, A.L., Verhaagen, J., et al. (2011). The proliferative capacity of the subventricular zone is maintained in the parkinsonian brain. Brain *134*, 3249-3263.
321. Soukup, S.F., Kuenen, S., Vanhauwaert, R., Manetsberger, J., Hernandez-Diaz, S., Swerts, J., Schoovaerts, N., Vilain, S., Gounko, N.V., Vints, K., et al. (2016). A LRRK2-Dependent EndophilinA Phosphoswitch Is Critical for Macroautophagy at Presynaptic Terminals. Neuron *92*, 829-844.
322. Abeliovich, A., and Gitler, A.D. (2016). Defects in trafficking bridge Parkinson's disease pathology and genetics. Nature *539*, 207-216.
323. Roosen, D.A., and Cookson, M.R. (2016). LRRK2 at the interface of autophagosomes, endosomes and lysosomes. Mol Neurodegener *11*, 73.

324. Mir, R., Tonelli, F., Lis, P., Macartney, T., Polinski, N.K., Martinez, T.N., Chou, M.Y., Howden, A.J.M., Konig, T., Hotzy, C., et al. (2018). The Parkinson's disease VPS35[D620N] mutation enhances LRRK2 mediated Rab protein phosphorylation in mouse and human. Biochem J.
325. Sepulveda, B., Mesias, R., Li, X., Yue, Z., and Benson, D.L. (2013). Short- and long-term effects of LRRK2 on axon and dendrite growth. PLoS ONE *8*, e61986.
326. Pouthas, F., Girard, P., Lecaudey, V., Ly, T.B., Gilmour, D., Boulin, C., Pepperkok, R., and Reynaud, E.G. (2008). In migrating cells, the Golgi complex and the position of the centrosome depend on geometrical constraints of the substratum. J Cell Sci *121*, 2406-2414.
327. Villarroel-Campos, D., Gastaldi, L., Conde, C., Caceres, A., and Gonzalez-Billault, C. (2014). Rab-mediated trafficking role in neurite formation. J Neurochem *129*, 240-248.
328. Whitfield, J.F., and Chakravarthy, B.R. (2009). The neuronal primary cilium: driver of neurogenesis and memory formation in the hippocampal dentate gyrus? Cell Signal *21*, 1351-1355.

VIII. LIST OF PUBLICATIONS

Research articles included in this thesis

I. Parkinson disease-associated mutations in LRRK2 cause centrosomal defects via Rab8a phosphorylation
Madero-Pérez J, Fdez E, Fernández B, Lara Ordóñez AJ, Blanca Ramírez M, Gómez-Suaga P, Waschbüsch D, Lobbestael E, Baekelandt V, Nairn AC, Ruiz-Martínez J, Aiastui A, López de Munain A, Lis P, Comptdaer T, Taymans JM, Chartier-Harlin MC, Beilina A, Gonnelli A, Cookson MR, Greggio E, Hilfiker S.
Molecular Neurodegeneration. 2018. 13:3.
Impact factor: 6.78 Quartile: Q1

II. Rab7L1-mediated relocalization of LRRK2 to the Golgi complex causes centrosomal deficits via Rab8a
Madero-Pérez, J., Fernández, B., Lara Ordóñez, A.J., Lobbestael, E., Baekelandt, V. and Hilfiker, S.
Under review in *Neurobiology of Disease*.

Review articles directly related to this thesis

III. Cellular effects mediated by pathogenic LRRK2: homing in on Rab-mediated processes
Madero-Pérez, J., Fdez, E., Fernández, B., Lara Ordóñez, A.J., Blanca Ramírez, M., Romo-Lozano, M., Rivero-Ríos, P. and Hilfiker, S.
Biochemical Society Transactions. 2017. 45 (1): 147-154.
Impact factor: 2.765 Quartile: Q2

Other articles not directly related to this thesis

IV. Pathogenic LRRK2 alters endolysosomal trafficking through impairing Rab8a function.
Rivero-Ríos, P., **Madero-Pérez, J**., Thomas, A., Biosa, A., Greggio, E. and Hilfiker, S.
Under review in *Molecular Neurobiology*

V. GTP binding regulates cellular localization of Parkinson's disease-associated LRRK2.
Blanca Ramírez, M., Lara Ordóñez, A.J., Fdez, E., **Madero-Pérez, J.**, Gonnelli, A., Drouyer, M., Chartier-Harlin, MC., Taymans, JM., Bubacco, L., Greggio, E. and Hilfiker, S.
Human Molecular Genetics. 2017 26(14):2747-2767.

VI. LRRK2 and Parkinson´s disease: from lack of structure to gain of function.
Ramírez, M.B., **Madero-Pérez, J**., Rivero-Ríos, P., Martínez-Salvador, M., Lara Ordóñez, A.J., Fernández, B., Fdez, E. and Hilfiker, S.
Current Protein & Peptide Science. 2017. 18(7):677-686.

VII. Targeting the Autophagy/Lysosomal Degradation Pathway in Parkinson´s Disease.
Rivero-Ríos, P., **Madero-Pérez, J.**, Fernández, B. and Hilfiker, S.
Current Neuropharmacology. 2016. 14(3): 238-249

VIII. Alterations in late endocytic trafficking related to the pathobiology of LRRK2-linked Parkinson's disease.
Rivero-Ríos, P., Gómez-Suaga, P., Fernández, B., **Madero-Pérez, J.**, Schwab, A.J., Ebert, A.D. and Hilfiker, S.
Biochemical Society Transactions. 2015. 43: 390-395.

IX. Novel insights into the neurobiology underlying LRRK2-linked Parkinson's disease.
Gómez-Suaga, P., Fdez, E., Fernández, B., Martínez-Salvador, M., Blanca Ramírez, M., **Madero-Pérez, J.**, Rivero-Ríos, P., Fuentes, J.M. and Hilfiker, S.
Neuropharmacology.2014.85:45-56